Investigation of Aerodynamic Effect of Rooftop Cargo Compartment for Locally Modified Intercity Bus Both Numerically and Experimentally

By

Addis Tefera Tirfe

A Thesis Submitted to

The Department of Mechanical Systems and Vehicle Engineering

School of Mechanical, Chemical and Materials Engineering

Presented in Partial Fulfillment of the Requirement for Master of Science in Automotive Engineering

Office of Graduate Studies

Adama Science and Technology University

October, 2021

Adama, Ethiopia

Investigation of Aerodynamic Effect of Rooftop Cargo Compartment for Locally Modified Intercity Bus Both Numerically and Experimentally

By

Addis Tefera Tirfe

Advisor: Dr. Addisu Bekele (Associate Professor)

Co-Advisor: Mr. Mekonnen Liben (Assistant Professor)

A Thesis Submitted to

The Department of Mechanical Systems and Vehicle Engineering

School of Mechanical, Chemical and Materials Engineering

Presented in Partial Fulfillment of the Requirement for Master of Science in Automotive Engineering

Office of Graduate Studies

Adama Science and Technology University

October, 2021

Adama, Ethiopia

DECLARATION

I hereby declare that this Master Thesis entitled **"**Investigation of Aerodynamic Effect of Rooftop Cargo Compartment for Locally Modified Intercity Bus both Numerically and Experimentally" is my original work. That is, it has not been submitted for the award of any academic degree, diploma or certificate in any other university. All sources of materials that are used for this thesis have been duly acknowledged through citation.

Addis Tefera Tirfe		
Name of the student	Signature	Date

RECOMMENDATION

We, the advisors of this thesis, hereby certify that we have read the revised version of the thesis entitled "Investigation of Aerodynamic Effect of Rooftop Cargo Compartment for Locally Modified Intercity Bus both Numerically and Experimentally" prepared under our guidance by Addis Tefera submitted in partial fulfillment of the requirements for Master of Science in automotive engineering. Therefore, we recommend the submission of revised version of the thesis to the department following the applicable procedures.

Dr. Addisu Bekele		
Major Advisor	Signature	Date
Mr. Mekonnen Liben		
Co-Advisor	Signature	Date

APPROVAL PAGE

We, the advisors of the thesis entitled "Investigation of Aerodynamic Effect of Rooftop Cargo Compartment for Locally Modified Intercity Bus both Numerically and Experimentally" and developed by Addis Tefera, hereby certify that the recommendation and suggestions made by the board of examiners are appropriately incorporated into the final version of the thesis.

______________________	______________________	______________________
Major Advisor	Signature	Date
______________________	______________________	______________________
Co-advisor	Signature	Date

We, the undersigned, members of the Board of Examiners of the thesis by Addis Tefera have read and evaluated the thesis entitled "Investigation of Aerodynamic Effect of Rooftop Cargo Compartment for Locally Modified Intercity Bus both Numerically and Experimentally" and examined the candidate during open defense. This is, therefore, to certify that the thesis is accepted for partial fulfilment of the requirement of Master of Science in Automotive Engineering.

______________________	______________________	______________________
Chairperson	Signature	Date
______________________	______________________	______________________
Internal Examiner	Signature	Date
______________________	______________________	______________________
External Examiner	Signature	Date

Finally, approval and acceptance of the thesis is contingent upon submission of its final copy to the Office of Postgraduate Studies (OPGS) through the Department Graduate Council (DGC) and School Graduate Committee (SGC).

______________________	______________________	______________________
Department Head	Signature	Date
______________________	______________________	______________________
School Dean	Signature	Date
______________________	______________________	______________________
Office of Postgraduate Studies, Dean	Signature	Date

ACKNOWLEDGMENT

First and foremost I would like to express my sincere gratitude to my teacher and advisor Dr. Addisu Bekele (Associate Professor) for his incredible contribution in shaping the foundation of this thesis. He has taught me the methodology to carry out the research and to present the research work as clear as possible. It was a great privilege and honor to work under his guidance. I would also like to thank my teacher and co-advisor Mr. Mekonnen Liben (Assistant Professor) for his incredible guidance throughout this research and I am extremely grateful for what he has offered. Finally, I would like to thank my teacher Dr. Ramesh Babu, my friends and my families for your significant contribution, help, support and advice.

TABLE OF CONTENTS

LIST OF TABLES

LIST OF FIGURES

ACRONYMS

ABS………………………..Acrylonitrile Butadiene Styrene

AFC………………………..Active Flow Control

ANSYS……………………Analysis of Systems

CAD………………………Computer-Aided Design

CATIA…………………......Computer Aided Three Dimensional Interactive Application

CFD………………………..Computational Fluid Dynamics

DNS………………………..Direct Numerical Simulation

GHG………………………Green House Gas

HVAC……………………..Heating, Ventilation and Air Conditioning

LES………………………...Large Eddy Simulation

PFC………………………..Passive Flow Control

RANS……………………..Reynolds Averaged Navier - Stokes Simulation

RHS………………………Rectangular Hollow Sections

SST………………………..Shear Stress Transport

UNEP……………………..United Nations Environment Program

VG………………………...Vortex Generator

NOMENCLATURE

A………………………………….Projected Area (m^2)

C_d ………………………………...Drag Coefficient

C_l …………………………………Lift Coefficient

D………………………………….Aerodynamic Drag (N)

E_{ACC} ………………………………Energy Required by Vehicle Accessories (J)

F_{TR} ………………………………..Tractive Force (N)

$F_{D\text{-}Bas}$ ……………………………...Drag Force of the Baseline Bus (N)

$F_{D\text{-}Mod}$ ……………………………Drag Force of the Modified Bus (N)

g …………………………………..Acceleration Due to Gravity (m/s^2)

k …………………………………..Fuel Dependent Constant

L …………………………………..Lift (N)

m ………………………………….Vehicle Mass (kg)

$\dot{m}_{fuel}$……………………….........Mass Flow Rate (m^3/s)

P_{sav} ………………………………...Power Saved (W)

Q_{LHV} ……………………………….Lower Heating Value (J/kg)

R …………………………………..Rolling Resistance (N)

S …………………………………...Total Distance Travelled (m)

W …………………………………..Weight (N)

V_{bus} ………………………………..Speed of the Bus (m/s)

ϴ …………………………………...Inclination Angle of the Road (^{0})

ρ_{fuel} ………………………………...Density of Fuel (kg/m^3)

η_d …………………………………..Energy Average Drive Train Efficiency

η_b …………………………………..Average Engine Efficiency

η_{engine} ………………………………Thermal Efficiency of the Engine

ABSTRACT

Buses are the foremost important mode of mass transportation but they are inefficient in terms of fuel consumption. Thus to decrease the fuel consumption, improvement with in the aerodynamics of the bus shape is needed. This thesis mainly concerned about locally modified ISUZU buses which served as an intercity bus. These buses help the country in terms of transportation and knowledge transfer but they are inefficient in terms of fuel consumption because of their body design and other add-on devices. One of the add-on devices which spoil the aerodynamic profile of this bus is the roof rack which is used to load the passengers' luggage. Most modern intercity buses have a separate luggage hold mounted below the passenger compartment. But, these locally modified buses are low floor buses in which it is very difficult to design a luggage compartment under the body. Therefore, using roof racks is the only alternative to transport the luggage. Unfortunately, the luggage loaded on the roof rack increased the aerodynamic drag; hence the fuel efficiency is affected. Therefore, in this thesis aerodynamically efficient rooftop luggage compartment is designed for locally modified intercity bus. The Aerodynamic analysis is carried out numerically using Computational Fluid Dynamics (CFD) and experimentally by wind tunnel testing. The CFD analysis is done on ANSYS Fluent using a scaled-down Isuzu Bus model which is modeled using CATIA V5. The experiment is carried out in Adama Science and Technology University using HM 170 open wind tunnel. According to the numerical result, the modified bus improved the drag coefficient by 34%, 34.5% and 34%, when compared to the clean roof baseline bus, the baseline bus without roof rack and the loaded baseline bus respectively, whereas the drag force is improved by 12%, 14% and 32% respectively. When comparing the modified bus with the loaded baseline bus the power requirement at 80 km/hr, 100 km/hr and 120 km/hr is reduced by 7655.23W, 14825.07W and 25741W respectively. In addition to that, the fuel consumption is improved by 2.15 L/hr, 4.17 L/hr and 7.24 L/hr respectively. The experimental result showed that, the drag coefficient of the modified bus is 0.487, 0.468, 0.461 and 0.452 at a speed of 5.6m/s, 11.2m/s, 16.8m/s and 22.4m/s respectively. The drag coefficient of the experimental result deviates from the numerical result by 8.64%, 7.83%, 7.45 and 6.35% respectively. However, according to many researches the percentage of the deviation is permissible.

Key words: Aerodynamic drag, Computational Fluid Dynamics, Fuel Consumption, Local Bus, Luggage Compartment, wind tunnel

CHAPTER ONE

INTRODUCTION

1.1 Background of the Study

Ethiopia has signed the United Nations Framework Convention on Climate Change in Rio de Janeiro, in 1994. According to the terms of the responsibilities of the convention, Ethiopia has submitted initial communication in 2001 and it is working to contribute to efforts in reduction of global Green House Gas (GHG) emissions by promoting green economic development strategy. It is well known that reduction of GHG emissions requires reduction of fossil fuel consumptions. Hence, Ethiopia is working with United Nations Environment Program (UNEP) to increase vehicle fuel efficiency by identifying and implementing relevant policy package (According to Final Report on Pilot Global Fuel Economy Initiative Study in Ethiopia, 2012).

Reducing the aerodynamic drag offers an inexpensive solution to improve fuel efficiency and shape optimization for low drag become an essential part of the overall vehicle design process (Wickern et al., 2011). Buses are the foremost important mode of mass transportation. Buses are inefficient in term of fuel consumption, thus to decrease the fuel consumption of buses, improvement within the aerodynamics of bus shapes will augment the value (Roy et al., 2018). It becomes essential to thoroughly design a bus for its aerodynamics, because it directly relates to fuel economy. About 60 to 70 percent of the drag of a bus is attributed to pressure loads acting on the vehicle frontal part of the body, making it the principal area for drag reduction strategies (Patten et al., 2012). By far the most efficient method of reducing fore body drag is to minimize flow separation by combining the rounding of the forward corners with the tapering of the fore body. Additionally, underbody aerodynamics is becoming increasingly important, in the quest to reduce fuel consumption of surface vehicles (Patten et al., 2012).

This thesis is mainly concerned about locally modified ISUZU bus in which its body is manufactured in Ethiopia. Now a day, there are many bus body manufacturers who modify ISUZU truck vehicles into buses in which it helps the country in terms of transportation and knowledge transfer. Many government and private organizations are using these buses as a service and public transport. Most of these buses also served as an intercity bus.

This locally built ISUZU buses are inefficient in terms of fuel consumption because of their body design and other add-on devices. One of the add-on devices which spoil the aerodynamic profile of the bus is the roof rack which is used to load luggage. When people are traveling across the country sometimes they will consider using roof racks especially if their motor vehicle is not large enough to transport the luggage in the trunk. Technically speaking, anything you install in the exterior of your vehicle is going to spoil the aerodynamic profile over the body. Installing a roof rack will increase the aerodynamic drag by obstructing the air flowing over the body.

Figure 1.1: Loaded locally modified bus (Dreamstime.com)

The roof rack is one of the most common and popular accessories on vehicles (Reynolds, 2014). Installation of a roof rack can increase aerodynamic drag by increasing both the drag coefficient (C_d) and the projected frontal area (A). Lenner (1998) investigated on-road impacts of roof racks for a 1992 Volvo 940 midsize sedan. The vehicle was equipped with an unloaded roof rack and driven at 43.5 mph, 49.7 mph and 55.9 mph. Fuel consumption increased 2.6%, 2% and 1.1% compared with a clean roof. When the roof rack was loaded with a ski box, fuel consumption increased 10%, 11% and 12.3% compared with the clean-roof conditions.

Thus, the aim of this thesis is to design aerodynamically efficient rooftop cargo compartment and conduct an experimental investigation for locally modified intercity bus. This is addressed by designing an appropriate rooftop cargo compartment which is efficient in-terms of aerodynamic drag reduction by using CATIA V5 software. Then, the physics of fluid flow around the bus and the rooftop cargo compartment is simulated by using CFD (Fluent). Finally, experimental validation is carried out in a wind tunnel to validate the results obtained from the software by using a scale model of the new modified bus.

1.2 Statement of the Problem

Now a day, there are many bus body manufacturers in Ethiopia who modifies ISUZU truck vehicles into buses in which it helps the country in terms of transportation and knowledge transfer. Most of these buses are serving as an intercity bus. This locally built ISUZU buses are inefficient in terms of fuel consumption because of their body design and other add-on devices. Therefore, it becomes essential to redesign the bus for its aerodynamics, as it directly relates to the fuel economy and pollution. As it is known Cargo compartment is the essential part of an intercity bus. Most of modern buses have a separate luggage hold mounted below the passenger compartment. But these locally modified buses are low floor buses in which it is very difficult to design a luggage compartment under the body. Therefore, using roof racks is the only alternative to transport the luggage. Unfortunately, roof rack will increase the aerodynamic drag; hence the fuel efficiency is affected. Therefore, in this thesis aerodynamically efficient rooftop cargo compartment for locally modified intercity buses is designed to reduce fuel consumption.

1.3 Objectives

1.3.1 General Objective

The general objective of this research is to investigate aerodynamic effect of rooftop cargo compartment for locally modified intercity bus and analyze its aerodynamic performance both numerically and experimentally.

1.3.2 Specific Objectives

The main objective of this research is achieved through the following specific objectives:

- ✓ Study the existing problem of the vehicle
- ✓ Design an aerodynamically efficient rooftop cargo compartment
- ✓ Model the existing bus and the new one with the rooftop cargo compartment
- ✓ Analyze the aerodynamic performance of the existing and modified models at various speeds using CFD tool.
- ✓ Manufacture a scaled down model of modified bus and conduct an experimental test in a wind tunnel to validate the numerical study.
- ✓ Determining energy saving.

1.4 Significance of the Study

The final outcome of this thesis is to give a better contribution to ISUZU bus body manufacturers in terms of aerodynamic performance. The modification of bus reduces fuel consumption, reduces emission of harmful exhaust gases and protects the luggage from adverse weather. Additionally, the designed rooftop luggage compartment provides enough space to accommodate the luggage of the entire passengers. It also encourages the air to flow smoothly over the roof of the bus in which it avoids the flow separation occurred on the top of the bus and reduces the wake formation.

1.5 Scope of the Thesis Work

The scope of the work includes modeling of the bus using CATIA software and analyzing it using CFD for its aerodynamic performance. Experimentation in a wind tunnel using scaled down model also included for validation of the numerical results.

1.6 Limitations

Aerodynamic analysis is carried out in two ways these are experimentally using wind-tunnel and numerically using CFD software. To perform the numerical analysis, it is necessary to use a high-performance computer in order to obtain accurate results. However, one of the limitations is the performance of the computer in which the numerical analysis is conducted. Because of this limitation a scale down model is used and the mesh is forced to be as optimized as possible to be compatible to fluent software.

Apart from the simplifications undertaken on the geometry to reduce cell number, other important simplifications were done to the model. Thus, to reduce the number of cells some parts such as windscreen wipers, mud flaps, cooling system and roof rack are excluded while designing the models.

1.7 Organization of the Study

This thesis consists seven chapters. The first chapter is an introduction to the study. It includes the background of the study, statement of the problem, objectives, significant of the study, scopes, limitation and structure of the thesis. Chapter two focuses on different kinds of literature that emphasize on study of bus aerodynamics and computational fluid dynamics analysis. Chapter three describes materials and methods used to complete this work. Chapter four presented design and numerical analysis of the baseline bus and the modified bus. Chapter five discussed the experimental evaluation. Chapter six presented results and discussions of computational analysis and experimental validation. The aerodynamic performances, drag reduction, power saving and fuel consumption are presented in form of tables and graphs for quantitative and qualitative discussions. Finally, conclusion and recommendation is included in chapter seven.

CHAPTER TWO
LITERATURE REVIEW

2.1 Vehicle Aerodynamics

Aerodynamics is a branch of dynamics which study the motion of air when it interacts with a moving object. Automotive aerodynamics is the field of study of aerodynamics of road vehicles. The main objectives of vehicle aerodynamics are:

- ✓ Avoidance of flow separation
- ✓ Reducing drag and wind noise
- ✓ Producing down force to improve traction and cornering abilities
- ✓ Minimizing noise emission and preventing undesired lift forces and other causes of aerodynamic instability at high speed.
- ✓ Enhancement of performance and fuel economy

2.2 Vehicle Attributes Affected by Aerodynamics

2.2.1 Performance and Fuel Economy

Fuel economy and global warming are the current key situations for low drag. At any instant, the tractive force required at the vehicle's driving wheels is (Sovran & Bohn, 1981):

$$\mathrm{F_{TR}} = \mathrm{R} + \mathrm{D} + \mathrm{M}\frac{dV}{dt} + \mathrm{Mg}\sin\theta \qquad \text{Equ (2.1)}$$

Where, F_{TR} = Tractive force

R = Rolling resistance

D = Aerodynamic drag

M = Vehicle mass

g = Acceleration due to gravity

Ө = Inclination angle of the road.

The corresponding tractive power is given as:

$$\mathrm{P_{TR}} = \mathrm{F_{TR}V} \qquad \text{Equ (2.2)}$$

The tractive energy required for propulsion during any given driving period is:

$$\mathrm{E_{TR}} = \int_0^{\mathrm{T}} \mathrm{P_{TR}}\, dt \qquad \text{Equ (2.3)}$$

Therefore, the main reason that fuel is consumed is to provide this tractive energy. For writing an equation for instantaneous fuel consumption, the following fundamental equation for the average fuel consumed per unit distance traveled can be obtained (Sovran 1983):

$$\tilde{g} = \frac{k}{\eta_b \eta_d S}[E_{TR} + E_{ACC}] + g_u \qquad \text{Equ (2.4)}$$

Where k is a fuel-dependent constant, η_b is the average engine efficiency during propulsion, η_d is the average drivetrain efficiency, S is the total distance traveled, E_{ACC} is the energy required by vehicle accessories, and g_u is the fuel consumption during idling and braking.

Aerodynamic drag is responsible for part of E_{TR}. Therefore, total fuel consumption of a vehicle depends on relative magnitude of the aerodynamic drag. The benefits of reduced drag are actually reduced fuel consumption, increased acceleration capability, and increased top speed.

2.2.2 Handling

The resultant aerodynamic force has components in all six degrees of freedom (Figure 2.1). In principle, they all influence a vehicle's dynamics. Traditionally, test engineers distinguish between vehicle behaviors in still air (handling), and its behavior in the presence of a crosswind (crosswind sensitivity).

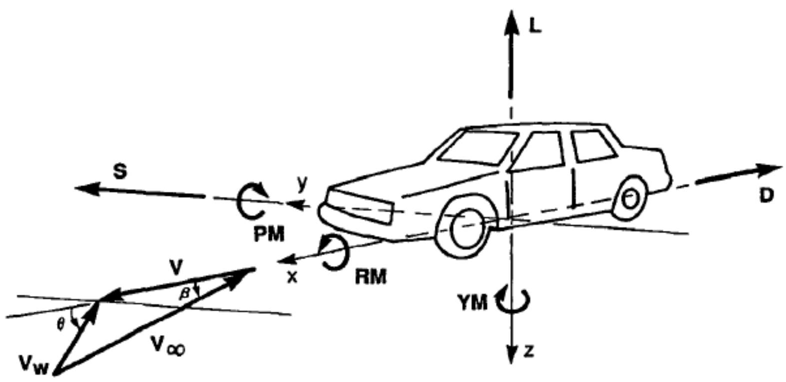

Figure 2.1: Aerodynamic forces and moments acting on a vehicle

The flow over a vehicle which is moving through still air is symmetric about the vehicle's plane of symmetry. In these condition Lift, pitching moment and drag are the only aerodynamic components. Unless special measures are taken, the vertical force on a bluff body close to the ground is positive and it tends to lift the vehicle. As a result it reduces the load on the tires which is disadvantageous to handling (Hucho, 1993).

2.2.3 Crosswind Sensitivity

In a crosswind the flow around a vehicle becomes asymmetric and as a result, side force, yawing moment and rolling moment are produced. Also, the components of drag, lift, and pitching moment are altered, and they are increased. From both experience and numerical simulations of vehicle dynamics, it is known that only two of these components are significant to a vehicle's behavior in crosswind, these are yawing moment and side force. The yawing moment tends to twist the vehicle further away from the wind. As a result, the yawing moment, and the side force are increased even further (Hucho, 1993).

2.2.4 Functional

The flow over a vehicle not only produces aerodynamic forces and moments, but also many other effects that can be summarized under the term functionals (Hucho, 1993). . These functional effects are:

- ✓ **Forces on body parts**: Vehicle bodies are made up of large and comparatively flat panels, and these have to withstand considerable aerodynamic loading. Hoods, doors, and frameless windows have to be tight under all conditions (Hucho, 1993).
- ✓ **Wind noise**: the more that the formerly dominant noise sources (i.e. engine and tires) have been attenuated, the more that wind noise has become objectionable inside vehicles. Passenger cars and buses are of particular concern (Hucho, 1993).

2.3 Aerodynamic Forces

2.3.1 Drag

Aerodynamic drag is a force that opposes the vehicles direction of movement. The main contributor to vehicle drag is the high pressure acting on the front of the vehicle, surface friction and the relatively negative pressure left behind the vehicle (Lucas, 2014). The equation which is used to calculate aerodynamic drag is as followed.

$$D = \frac{1}{2}\rho A V^2 C_d \qquad \text{Equ(2.5)}$$

Aerodynamic drag consists of two main components. These are skin friction drag and pressure drag. Pressure drag accounts for more than 80% of the total drag and it is highly dependent on vehicle geometry due to boundary layer separation from rear window surface and formation of wake region behind the vehicle. The location of separation determines the size of wake region and consequently, it determines the value of aerodynamic drag (Sudin, 2014).

2.3.2 Lift

Lift is force acting perpendicular to the motion of the vehicle. In vehicles negative lift it sought after to force the vehicle into the ground, this force acting on the vehicle helps increase vehicle grip which leads to faster cornering speed (Joseph, 2006). The formula to mathematically calculate aerodynamic lift is similar to the drag formula although the drag coefficient is replaced with a lift coefficient and is as followed.

$$L = \frac{1}{2}\rho A V^2 C_L \qquad \text{Equ}(2.6)$$

Where L = Lift (N)

C_L = Lift Coefficient

A = Frontal Area of the vehicle (m^2)

2.4 Vehicles Aerodynamic Drag Reduction Methods

Based upon the consumption of energy to control the flow, vehicle aerodynamic drag reduction methods are classified in to two. These are:

- ✓ Active Flow control methods
- ✓ Passive Flow control methods

2.4.1 Active Flow Control

Active control is performed by using actuators that require power generally taken from the vehicle. The system includes visible part like mobile walls, circular holes or slots distributed on the vehicle surface where the flow has got to be controlled. AFC requires mechanical, electromagnetic, electric, piezoelectric or acoustic systems placed within the hollow parts of the vehicle (Sudin, 2014). In order to reduce their impacts on consumption and habitable volume their weights and their overall dimensions must be smallest as possible. The adopted solutions generally contains suction or blowing systems through circular or rectangular slots and the suction or blowing are often continuous or intermittent (Sudin, 2014).

- ✓ **Active flow control with air jets**

Bideaux et al. (2011) conducted an experimental study to regulate the flow separation on car window of a generic vehicle shape of Ahmed body with a scale of 0.7 and a slope angle of 35°. In the experiment the rear a part of Ahmed body was modified by changing the sharp edge between roof and car window with smooth curved surfaces.

The model was equipped with a strip of pulsed jets at the top of the roof to regulate the flow at a velocity of 30 m/s based on a periodical blowing. Their result showed that a maximum of 20 % drag reduction was obtained. The result confirms that the aerodynamic drag of the vehicle can be improved by applying pulsed jets.

- ✓ **Active flow control with steady blowing**

Heinemann et al. (2012) carried out a research by applying steady blowing on a car model to observe its influence on the drag and lift forces. It is supplied through continuous slots at positions above and under the rear window of the vehicle. They found that the reduction of rear axle lift was possible with active flow control with small reduction in drag performance. From there result, the rear axle lift is reduced by about 5% with C_D changes around 1%.

- ✓ **Active flow control with suction**

Harinaldi et al. (2012) conducted a study on a van which was modeled with a modified form of Ahmed's body. There model was provided with suction on the rear side to examine the pressure field modifications that may occur. From the result it is seen that the appliance of suction within the rear a part of the van reduces the wake and the vortex formation. Finally, the aerodynamic drag is reduced by 13.86% for the computational approach and 16.32% for the experimental.

2.4.2 Passive Flow Control

Passive control systems consists the utilization of more or less discrete obstacles, added around or on the roof of the vehicle. They can be declined in two groups consistent with their influence on the flow control. The first group consist obstacles positioned on the surface of the geometry. The second group consists of the obstacles positioned upstream or downstream of the geometry to be controlled (Kourta, 2009). Some of passive flow control methods are:

- ✓ **Vortex Generator (VG)**

VG is an aerodynamic surface which is a little vane that makes a vortex. VG widely utilized in the aerospace industry, mainly to regulate the boundary layer transition and to delay flow separations. A different kind of VG is used on race cars for manipulating the flow over and under the vehicle, mainly to urge down force (which is required for better performance) (Akojwar, 2016).

- ✓ **Spoiler**

A spoiler is a tool which is used to reduce unfavorable air movement around the vehicle. It can be divided into front spoilers and rear spoilers. A front spoiler is mainly used to direct air flow away from the tires to the underbody and it is connected with the bumper. A rear spoiler is commonly mounted on the trunk lid of a vehicle and it has measurable effect on aerodynamic drag reduction and vehicle stability (Wong, 2011). The added spoiler adds more downward pressure to the back end of the vehicle by reducing the turbulence at the rear of the vehicle and reduces lift acted on the rear trunk (Zakem, 2008).

- ✓ **Underbody diffuser**

The automotive underbody diffuser is an expansion device which is used to speed up the air flowing underneath a vehicle. This increases the down force by reducing the pressure below the vehicle (Unni, 2017).

2.5 Bus Aerodynamics

Buses are the foremost important mode of mass transportation everywhere the planet. Buses are inefficient in term of fuel consumption, thus to decrease the fuel consumption of buses, improvement within the aerodynamics of bus shapes will augment the value (Roy et al., 2018).

It becomes essential to thoroughly design a bus for its aerodynamics, because it directly relates to the fuel economy and resisting forces. More precisely the reduction of their coefficient of drag becomes the foremost topics of the automotive research. Aerodynamics being the assistance to create a body shape that maximizes the down force, the negative lifts and minimizes the force that opposes the forward movement and also the drag forces (Gophane et al., 2014). The aerodynamically efficient design of the bus reduces the drag force and improves the fuel efficiency (Damissie et al., 2017).

Drag related problems were first examined in the aeronautical industry after that the automotive industry also realized that it could affect fuel consumption reduction. For ground vehicles, drag related problems are specific due to external effects, such as road inclination and wind. However, the examined velocity regime is tighter than the airplanes because the speed is limited to 50–130 km/h. This limit also gives us several more simplifications, as the air can be incompressible and isothermal due to low velocity (Szodrai, 2020).

2.6 Intercity Bus Add-On Devices

2.6.1 Roof rack

When people are traveling across the country sometimes they will consider using roof racks specifically if their motor vehicle is not large enough to transport the luggage in the trunk. Depending on the luggage, a roof rack with a cover may be a convenient option. This is particularly common when traveling with a lot of luggage. There are several benefits to this type of roof racks which include, keeping whatever you have stored within it relatively dry if you travel through adverse weather (although the majority of these racks are not 100% weatherproof). These are generally easy to install although you may need a small step ladder when loading and unloading to get ensure you get all items in and out.

Technically speaking, anything you install in the exterior of your vehicle is going to spoil the aerodynamic profile over the body. Installing a roof rack will increase the aerodynamic drag; in the sense prove to be an obstruction to the air flowing over the body. In order to overcome this, the engine has to produce an increased power, to move further, hence the fuel efficiency is effected, Speaking of car's performance, aerodynamically it will be affected.

2.6.2 Roof Rack Categorization

We divided the many configurations of roof racks into three categories. These categories reflect their gross aerodynamic impacts. The categories are defined as follows (Chen, 2016):

1. Bare roof or roof with built-in rails. In most cases, the built-in rails are installed by the vehicle manufacturer and are part of a package. We assume this type of rack does not significantly influence vehicle fuel consumption.
2. Unloaded cross roof racks. In this configuration, cross pieces are present to adapt the pre-existing roof rack to the specific application, such as carrying bicycles or skis. Additional hardware may be present to facilitate attachment. By "unloaded", we mean the hardware is present for a specific application but no bicycles, skis, etc. are actually being carried.
3. Loaded cross roof racks. In this configuration, bicycles or other equipment are actually on the roof rack and being transported. Previous studies have found high fuel consumption in this configuration, especially at higher speeds

2.6.3 Fuel Consumption Impact of Loaded Roof Rack

The roof rack is one of the most common and popular accessories on vehicles (Reynolds, 2014). Installation of a roof rack can increase aerodynamic drag by increasing both the drag coefficient (C_d) and the projected frontal area (A). Previous studies found that, for a vehicle moving at 100km/h, aerodynamic drag typically accounts for 75–80% of the total resistance, which is directly related to vehicle fuel consumption (Hucho, 1998; Juhala, 2014). Therefore, a roof rack (and the loads installed on it) will lead to significant fuel consumption on the vehicle.

Lenner (1998) investigated on-road impacts of roof racks for a 1992 Volvo 940 midsize sedan. The vehicle was equipped with an unloaded roof rack and driven at 43.5 mph, 49.7 mph and 55.9 mph. Fuel consumption increased 2.6%, 2% and 1.1% compared with a clean roof. When the roof rack was loaded with a ski box, fuel consumption increased 10%, 11% and 12.3% compared with the clean-roof conditions.

Chowdhury et al. (2012) measured drag forces of passenger car add-ons through a series of wind tunnel tests. At high driving speeds (>80 km/h), the unloaded and loaded roof rack resulted in 10–22% and 13–28% increases in aerodynamic drag depending on cross-wind effects and speeds.

Fuel consumption for unloaded racks in non-highway driving conditions as it is developed by Thomas et al. (2014) is 8% for passenger cars and 2.4% for passenger trucks. About 70% (18 observations out of 26) of consumer-reported data estimated loaded cross roof rack fuel consumption is between 20% and 30%. These observations seem to match results from Thomas et al. (2014) which is 24.8% fuel consumption increase at 70mph constant-speed highway driving for passenger cars. Thomas et al. (2014) also reported 11.7% fuel consumption for a passenger truck under the same conditions.

Lenner (1998) found fuel consumption increased 12.3% for a sedan with a roof rack and ski box traveling at 55.9 mph. An extrapolation of Lenner's result from 55.9 mph to 70mph, gives a fuel consumption increase of about 20%. This is close to other studies as well as consumer-reported data. Therefore it is adopted 24.8% as the fuel consumption impacts for passenger cars and 11.7% for passenger trucks driving on highways. These values from Thomas et al. (2014) are the most recent and based on the most comprehensive study.

Earlier studies found 1.1–2.6% fuel consumption increases for a sedan traveling at 43.5–55.9 mph with an unloaded cross roof rack (Lenner, 1998). Roof racks increase air resistance and increased overall fuel consumption by approximately 1% (Chen et al. 2016). Due increased wind resistance, roof racks may add sound on the highway.

2.7 Aerodynamic Drag Reduction on Intercity Bus

Intercity buses travel long distances at higher speeds usually in a stretch. The significant increase of road transport combined with the increasing environmental issues and fuel prices has renewed the interest in bus design. Reducing the aerodynamic drag has a large positive influence on the fuel economy and reduction of harmful exhaust gases (Taherian et al., 2014).

The drag which affects the fuel consumption can be minimized by designing the bus with proper aerodynamic characteristics and also with implementation of lightweight materials for the body frame, which would decrease not only the fuel consumption but also the vehicle weight (Mohammad et al., 2019). Aerodynamic drag can be classified as skin friction drag and pressure drag. It is observed through an assessment that the pressure drag or form drag or parasite drag has the 80% contribution in the total aerodynamic drag due to the geometry of vehicles that leads to form the boundary layer separation and formation of wake region behind the vehicles (Wood, 2004).

Moreover, buses aerodynamic performances have been enhanced through experimental and numerical approaches with extensive investigations. Among these researches, it is seen that the methods of reducing drag and shape optimization are considered to be an inexpensive way to improve the fuel efficiency (Wickern et al., 2011). Muthuvel et al. (2013) modified the outer surface and structure of a bus aerodynamically in order to reduce the effect of drag force of the vehicle which in turn results in reduction of fuel consumption of the vehicle. The effectiveness of their new concept design was proved by an Experimental and numerical tests which was conducted in a Wind Tunnel. It is evident from their test result, that a considerable reduction in drag force of about 30%-34% from the existing bus to the new concept and 6 to 7 liters of fuel is consumed for the every 100km.

Reducing the aerodynamic drag offers an inexpensive solution to improve fuel efficiency and thus shape optimization for low drag become an essential part of the overall vehicle design process (Wickern et al., 2011). It has been found that 40% of the drag force is concentrated at the rear of the geometry (Perera et al., 2008).

Roy et al. (2018) redesigned an intercity bus with enhanced exterior styling, reduced aerodynamic drag and increased comfort for the passengers. Principles of product design were used to analyze the styling and comfort. The benchmarked high floor bus was redesigned with low - floor for reduced aerodynamic drag. The exterior was redesigned with emphasis on improvised aerodynamic performance and appealing looks. The interior was modified to meet aspirations of the commuters. The results of the redesigned exterior body showed a reduction of about 45% in coefficient of drag and overall aerodynamic drag reduction by 60% due to combined effect of reduced coefficient of drag and frontal area.

Damissie & Ramesh (2017) modified the outer surface of the bus aerodynamically in order to reduce the effect of drag force of the bus which in turn results in reduction of fuel consumption of the bus. Their study was conducted for three wind speeds. Numerical tests have been conducted in CFD to prove the effectiveness of the new concept design. It is evident from the test result, that there is a considerable reduction in drag force of about 39.4% from the existing bus to the new concepts and 22.8% (5 to 6 liters) of fuel can be saved for the every 100 Km.

Prasad et al. (2011) redesigned an intercity bus with enhanced exterior styling and reduced aerodynamic drag. The exterior of the chosen bus is redesigned with emphasis on improvised aerodynamic performance and appealing looks. The interior was modified to meet aspirations of the commuters. The results of the redesigned exterior body showed a reduction of C_d from 0.581 to 0.41 at a speed of 100 km/hr and overall aerodynamic drag reduction by about 30% due to combined effect of reduced Cd and frontal area.

Alam et al. (2010) conducted an experiment on aerodynamic drag generated by various vehicle add-ons under a range of vehicle operating speeds. Most modern passenger cars use various add-ons including roof-rack, , bicycle rack, advertising signboard, police and ambulance siren, portable ladder and taxi signs for commercial and professional reasons. Any add-ons causes extra drag to the total system hence the extra fuel cost. The primary objectives of the study were to experimentally measure the aerodynamic drag generated by various vehicle add-ons under a range of vehicle operating speeds. The vehicle add-ons have significant effects on aerodynamic drag as they can generate 5 to 30% more aerodynamic drag depending on yaw angles. The average fuel consumption considerably increases due to vehicle add-ons, especially for the bluff body type vehicle add-ons.

2.8 Aerodynamic Drag Reduction Devices for Buses

A typical highway bus exhibits a number of aerodynamic advantages as the body comes lower to the ground effectively incorporating side skirts; and a flat front end eliminates the multiple aerodynamic discontinuities typically caused by radiator-hood, hood-windscreen and windscreen-fairing locations. Consequently, a stock long haul highway coach may have a CD as low as 0.384. For a given percent-reduction in drag coefficient, the net percent-reduction in fuel consumption is larger for a bus than it is for a tractor-trailer (Patten et al., 2012). The dominant contribution to the aerodynamic drag of an intercity bus is the pressure differential between the forward- and rearward-facing surfaces of the body, with a minimal contribution from skin friction.

About 60 to 70 percent of the total wind-averaged drag of a bus is attributed to pressure loads acting on the vehicle frontal part of the body, making it the principal area for drag reduction strategies (Patten et al., 2012). By far the most efficient method of reducing fore body drag is to minimize flow separation by combining the rounding of the forward corners (sides and top) with the tapering of the fore body.

Underbody aerodynamics is becoming increasingly important, in the quest to reduce fuel consumption of surface vehicles. Wind tunnel tests showed a drag reduction reaching about $\Delta CD \approx -0.012$, as a result of the underbody panels. In addition, it was found that streamlining the wheels with hub covers further reduced CD by 0.022. The objectives of underbody modifications can be summarized into three fundamental sub objectives:

- ✓ To shield forward-facing surfaces from high-speed flow;
- ✓ To mitigate wakes behind underbody elements, in order to attenuate suction pressures on rearward-facing surfaces; and
- ✓ To maximize the air velocity exiting at the rear of the vehicle underside, in order to energize the vehicle wakes, thereby reducing the magnitude of the negative base pressure.

Finally, an area of possible aerodynamic benefit is by re-profiling the roofline. As coach buses do not have the same cargo capacity constraints, it is believed that the rear roofline could be modified with minimal impact to passenger comfort.

2.9 Computational Fluid Dynamics (CFD)

Computational Fluid Dynamic (CFD) is the branch of fluid dynamics providing a cost-effective mean of simulating real flows by the numerical solution of the governing equation. The differential equation governing the system is converted to a set of the algebraic equation at discrete points and then solved using digital computer. For such a complex interaction, CFD analysis is probably the only efficient tool in order to assess specific design parameterization of a generic car shape. Aerodynamic evaluation of airflow over an object can be performed using analytical method or CFD approach (Lanfrit, 2005).

On one hand the analytical method of solving airflow over an object can be done only for simple flows over simple geometries like laminar flow over a flat plate. If airflow gets complex as inflows over a bluff body, the flow becomes turbulent and it is impossible to solve Navier-Stokes and continuity equations analytically, in that case CFD is useful (Vipul and Chopade, 2018).

The CFD (Computational Fluid Dynamics) analysis is used to find different parameters in the automobile industry. This analysis is used to understand the fuel consumption, stability of the vehicle and passenger comfort. The airflow over ground vehicle is analyzed and coefficient of drag is calculated using CFD/ ANSYS Fluent (Rehan and Sudhakar, 2014). With the increase in computational power, CFD has become a valuable tool for performing the different cases in vehicle motion simulation and predicting the drag coefficients.

2.9.1 Turbulence Modeling

The CFD prediction for turbulent flow is highly dependent upon the quality of the turbulence modeling. This is even more important for the flow around ground vehicles, whose salient flow features include three-dimensional boundary layers with strong streamline curvature, separation and strong (Lanfrit, 2005). There are three major approaches in order to capture turbulent flow. These are:

- ✓ **DNS (Direct Numerical Simulation):** Numerically solving the full unsteady Navier-Stokes equations. It resolves the whole spectrum of scales but the cost is too prohibitive. Not practical for industrial flows.

- ✓ **LES (Large Eddy Simulation):** It solves the filtered N-S equations and some turbulence is directly resolved. It is less expensive than DNS, but the efforts and computational resources needed are still too large for most practical applications
- ✓ **RANS (Reynolds Averaged Navier - Stokes Simulation):** It solves time-averaged Navier **-** Stokes equations and all turbulent motion is modeled. For most problems the time-averaged flow (and level of turbulence) is all that is needed. This is the most widely used approach for industrial flows.

2.9.2 RANS (Reynolds Averaged Navier - Stokes Simulation) Models

Spalart-Allmaras: Economical for large meshes. Good for mildly complex external/internal flows and boundary layer flows under pressure gradient (e.g. airfoils, wings, airplane fuselages, missiles, ship hulls). It performs poorly for 3D flows, free shear flows, flows with strong separation.

Standard k–ε: It is widely used despite the known limitations of the model. It performs poorly for complex flows involving severe pressure gradient, separation, and strong streamline curvature. It is Suitable for initial iterations, initial screening of alternative designs, and parametric studies.

Realizable k–ε: Suitable for complex shear flows involving rapid strain, moderate swirl, vortices, and locally transitional flows (e.g. boundary layer separation, massive separation, and vortex shedding behind bluff bodies, stall in wide-angle diffusers, room ventilation).

RNG k–ε: Offers largely the same benefits and has similar applications as Realizable. It is possibly harder to converge than Realizable.

Standard k–ω: Superior performance for wall-bounded boundary layer, free shear, and low Reynolds number flows compared to models from the k-e family. Suitable for complex boundary layer flows under adverse pressure gradient and separation (external aerodynamics and turbo machinery). Separation can be predicted to be excessive and early.

SST k–ω: Offers similar benefits as standard k–ω. Not overly sensitive to inlet boundary conditions like the standard k–ω. Provides more accurate prediction of flow separation than other RANS models.

RSM: Physically the most sound RANS model. Avoids isotropic eddy viscosity assumption. More CPU time and memory required. Tougher to converge due to close coupling of equations. Suitable for complex 3D flows with strong streamline curvature, strong swirl/rotation (e.g. curved duct, rotating flow passages, swirl combustors with very large inlet swirl, cyclones).

According to ANSYS Fluent manual The Realizable k-e or SST k-w models are recommended choices for standard cases. Where highly accurate resolution of boundary layers is critical, such as applications involving flow separation or finely resolved heat transfer profiles, SST k-w is preferred.

2.10 Previous Investigations on Related Topics

There are several researches which are intended in improving the aerodynamic performance of locally modified ISUZU buses. Some of these researches are discussed as follows:

Damissie & Ramesh (2017) carried out numerical study to improve the outer surface of Yutong cross-country bus in order reduce drag force of the bus which in turn results in reduction of fuel consumption of the bus. Their study was conducted for three wind speeds. The numerical analysis is conducted using CFD to prove the effectiveness of the new concept design. It is evident from the test result, that there is a considerable reduction in drag force of about 39.4% from the existing bus to the new concepts and 22.8% (5 to 6 liters) of fuel can be saved for the every 100 Km.

Bahiru (2020) improved the frontal body shape of the locally built FSR ISUZU bus to reduce of aerodynamic resistance. The study includes modeling, meshing and estimating drag force reduction, emission reduction and fuel saving of FSR ISUZU bus. The modified shapes are analyzed and simulated using CFD to find the best performing shape. The CFD analysis is done on three different models. The first model is made with only front tapering angle of 15^0. The second model had front tapering angle of 20^0, bottom fairing and smoothing surface with curved devices. The last model had front tapering angle of 25^0 as well as it had top and bottom fairing.

The results from the simulation showed that drag coefficient has reduced from 0.5451 for the baseline model to 0.4141 for the third model. Thus, the drag coefficient is improved by 24.03 % at an average speed of 80 Kmph. Subsequently the drag force has reduced from 581.07 N to 441.43 N and the power requirement is reduced by 3447.56 W (17.87 % reduction). Therefore, the study indicates that the modifications made on the frontal body shape improved the aerodynamic performance of the bus.

Natnael (2019) conducted numerical and experimental study to improve the outer body shape of the existing Isuzu Midi Bus aerodynamically, in order to reduce the overall aerodynamic drag force which in turn results in reduction of fuel consumption and carbon dioxide emission. The numerical analysis was performed using Computational Fluid Dynamic /ANSYS Fluent and the experiment was conducted in a Wind Tunnel to validate the numerical results. The baseline model of the bus was modeled with Solid Works with a scale of 1:20 and analyzed at various speeds. Later modifications and addition of rear spoiler were made to the base design in order to reduce the coefficient of drag and lift. Four models such as model I, model II, model III, and model IV were prepared. The results showed that the aerodynamic shape improvement in model IV reduced the drag coefficient by 54.35% which has resulted in the percentage reduction in fuel consumption of 32.61% and exhaust gas emission 9.7%.

Dawit (2017) redesigned locally built Isuzu passenger bus for obtaining better aerodynamic design. The redesign was done using CATIA and the aerodynamic simulation was carried out using CFD software. The work depicts how the modification could reduce the drag and the lift forces acting on the vehicle including the effect of variation of different parameters such as floor panel height, diffuser angle as well as modifying the edges for a bus body over the resisting forces. The results showed that a maximum of 5.17 Liter/hour fuel and 52.1ton/year CO_2 emission reduction can be saved at 120 km/h cruising speed. It was also found that as radius of the Bus edge increases the coefficient of drag decreases as compare to the result.

2.11 Research Gap

As it is discussed above, all of the researches which are intended in improving aerodynamic performance of locally built ISUZU buses followed the same procedure to achieve their objectives. The main objective of the researches were redesigning the frontal area of the existing bus to a more streamlined shape and avoiding add-on devices which affect the air flow. One of the add-on device which is eliminated during redesigning the existing bus is the roof rack. However, the roof rack is very necessary for locally modified intercity buses as there is no enough space to accommodate the luggage of the entire passengers in underbody compartments. Therefore, the designs were suitable for city buses as additional luggage compartment is not that necessary. Unfortunately, the loaded luggage on the roof rack increases the projected area and the drag coefficient of the existing bus. Therefore, in order to address the problem there has to be an alternative approach to provide additional luggage compartment and to improve the aerodynamic performance of the bus.

CHAPTER THREE
MATERIALS AND METHODS

3.1 Introduction

Aerodynamics analysis is mainly carried out in two ways such as numerically using Computational Fluid Dynamics (CFD) and experimentally by wind tunnel testing. The CFD analysis is done using ANSYS Fluent and to do that a scaled-down model of the Isuzu Bus is designed and constructed using CATIA V5. Once the CAD model of the bus is designed, it is imported into the Computational Fluid Dynamics (CFD) ANSYS Fluent. ANSYS Fluent is utilized to perform external fluid flow simulations in order to predict the aerodynamic performance of each bus model. The experiment is carried out in Adama Science and Technology University using HM 170 open wind tunnel. The HM 170 demonstration wind tunnel was developed for experimentation and demonstration purposes in the fields of aerodynamics and fluid mechanics. It is a subsonic, open wind tunnel with a square measurement-section profile (Gerätebau, 2012).

3.2 Methods

In order to address the general and specific objectives of this work a well-designed methodology was followed. Various steps which are included in the methodology are listed below.

(a) Literature review

Latest literatures and research works about bus aerodynamics and the effect of the loaded luggage on the roof rack on performance and fuel consumption of intercity buses is surveyed.

(b) Data collection

In order to do the Numerical analysis the necessary data about the existing bus is collected by using primary or secondary data collection methods. The data is collected from:

i. Anta PLC
ii. Intercity bus station (Lamberet Menaharya)

i. Anta metal Engineering PLC

Anta PLC is one of the known bus body builder in Ethiopia and obtained its license in grade 4 vehicles body manufacturing. The survey mainly focused on the following points:

- ✓ Whether there is any national standard code for bus body building and design in Ethiopia.
- ✓ Types of buses that the company build
- ✓ To know all the necessary dimension of the bus
- ✓ Material used to build the bus body
- ✓ Performance of the buses

ii. Intercity bus station (Lamberet Menaharya)

To design the roof top cargo compartment it is very necessary to know the actual trends at the station. The survey at the station mainly focused on the following points:

- ✓ Fuel consumption of the bus when it is driven without luggage and with luggage
- ✓ The maximum speed in which the bus is driven
- ✓ The approximate dimension of the luggage loaded on the roof rack
- ✓ Luggage holding capacity of the bus
- ✓ Whether there is a regulation regarding the loaded luggage
- ✓ Types of luggage bags which are usually used by passengers

(c) Design

After reviewing the literatures, design of aerodynamically efficient rooftop cargo compartment was carried out using CATIA V5 software.

(d) Numerical Analysis

The numerical analysis of the baseline model and the modified model was carried out using ANSYS.

(e) Conduct Experiment and Compare with the Baseline Bus

Finally, experimental investigation was carried out in a wind tunnel to validate the results obtained from the software by using a scale down model of the new modified bus.

(f) Determining energy saving

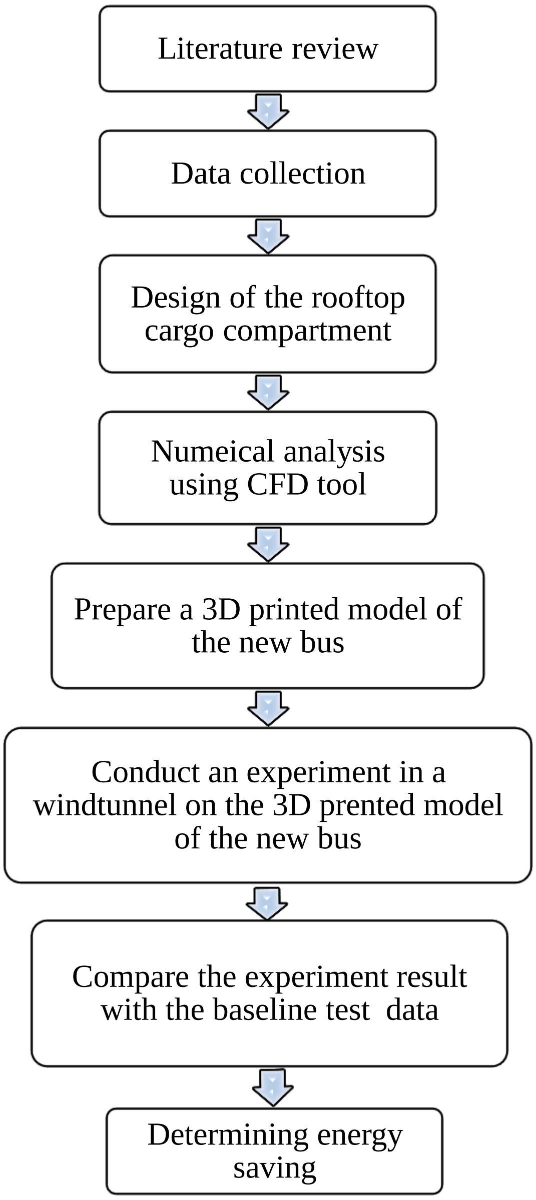

Figure 3.1: Block diagram of the research methodology

3.3 Materials

To conduct the experiment a 3D printed scale model of the new bus and a wind tunnel is required. The dimension which is used to make a scale model is obtained from the design that is made by CATIA V5 software.

Materials used in this study are:

- ✓ **CATIA V5:** It is used to construct the baseline model of the Isuzu Bus and the modified models
- ✓ **ANSYS Fluent:** It is used to simulate the flow around the bus models as well as calculate the drag and lift coefficients.
- ✓ **Prusa i3 MK3S:** It is a 3D Printer which is used to print the scale down model of the modified bus.
- ✓ **HM 170 Educational Wind Tunnel:** It is a subsonic, open wind tunnel with a square measurement-section in which the experiment is carried out.

3.3.1 Material Selection

The materials used to construct the structure of the luggage compartment and the panel is RHS steel and ABS sheet respectively.

- ✓ **Rectangular Hollow Section:** Rectangular hollow sections are commonly used in welded frames, columns and as beams providing various benefits to a range of construction and mechanical applications. Rectangular hollow sections (RHS) are a popular choice for mechanical, structural and construction applications. Its Property is given in the appendix Table B-1.

- ✓ **ABS (Acrylonitrile Butadiene Styrene):** ABS stands for Acrylonitrile Butadiene Styrene. ABS is an impact-resistant engineering thermoplastic & amorphous polymer. ABS is made up of three monomers: acrylonitrile, butadiene and styrene. Its Property is given in the appendix Table B-2.

3.4 Survey Findings

3.4.1 Anta PLC

Anta PLC was founded in accordance with the law of the country by legal name of Anta trading PLC. Anta obtained its license in grade 4 vehicles body manufacturing with investment capital of 150,000,000.00 (one hundred fifty million). It is the first of its kind and well-known company in the country specializing in vehicles part manufacturing business. Its head quarter is situated in Addis Ababa, near Kality industry zone. The survey is mainly focused on knowing the following points:

- ✓ The standard of the bus
- ✓ Dimension of the bus
- ✓ Dimension of the available luggage compartments and its holding capacity

I. Standard of the Bus

The company follows the standard developed by ministry of transport. The standard includes the main dimension like length, width and height of the bus depending on the size of the vehicle frame. Additionally the standard includes the space between the passenger seats. The bus body builders use RHS steel and sheet metal to construct the body of the bus.

II. Dimension of the Bus

The dimension of the bus may vary depending on the length of the frame but almost all bus body builders use the same dimension for the same frame.

Table 3.1: Dimension of the existing bus (Anta PLC)

Parameter	Dimension (m)
Length	7.2
Width	2.1
Height	2.2
Wheel base	3.85
Front overhang	1.2
Rear overhang	2.15

III. Luggage Compartment of the Bus

The bus has three underbody luggage compartments in which one of them is located at the rear of the bus whereas the other two are located at the sides of the bus and the main one is the roof rack. If the existing bus is used as a cross country bus the available underbody luggage compartments of the bus are not enough to transport the luggage. Therefore, the only alternative is to use the roof rack.

Dimension of the luggage compartment

Side luggage compartment

Length: 0.70 m, Height: 0.50 m, Depth: 0.30 m

Rear luggage compartment

Length: 2 m, Height: 0.70 m, Depth: 0.70 m

Dimension of the roof rack

Length: 3 m, Width: 1.5 m, Height: 0.35 m

Figure 3.2: The existing bus (Anta PLC)

3.4.2 Intercity Bus Station (Lamberet Menaharya)

To design the roof top cargo compartment it is very necessary to know the actual trends at the station. The survey at the station mainly focused on knowing:

- ✓ The maximum speed in which the bus is driven
- ✓ Fuel consumption of the existing bus when unloaded and loaded
- ✓ Types of luggage bags which are usually used by passengers

I. Speed

For cross country buses it is allowed to be driven up to 100 km/hr. During the survey most of the drivers said that they drive from 60 km/hr up to 120 km/hr.

Figure 3.3: Existing bus at the station (Lamberet Menaharya)

II. Fuel Consumption

According to the survey it is conformed that fuel consumption of the bus increased when the bus is loaded. At the station five bus drivers were willing for the interview and their response is summarized in the table given below. Almost all of the drivers knew the fuel consumption in terms of its total cost, then for ease of calculation it is converted to kilometer per liter. The price of diesel fuel is taken as 23 br/L for calculation.

Table 3.2: Fuel consumption of loaded and unloaded buses (Lamberet Menaharya)

Respondent	Starting place	Destination	Distance traveled (km)	Total cost (Birr)		Fuel consumption (km/L)	
				Loaded	Not loaded	Loaded	Not loaded
1	A.A	Debre Birhan	130	1200	1000	2.5	3.02
2	A.A	Mehal Meda	295	2500	2000	2.7	3.39
3	A.A	Dese	384	3300	2700	2.67	3.27
4	A.A	Agere Mariyam	379	3000	2500	2.9	3.48
5	A.A	Jiru	195	1700	1400	2.6	3.2

CHAPTER FOUR

MODELING AND ANALYSIS OF LOCAL BUS

4.1 Introduction

In order to do the Numerical analysis all the necessary data about the existing bus is collected from Anta PLC and Intercity bus station (Lamberet Menaharya). Then, based on the survey result the geometry of a scale down bus is considered for the analysis in order to have a minimum number of cells and to reduce computational time. The Geometry of the bus is created using CATIA V5 and the entire analysis and the post-processing is performed in ANSYS Workbench. The detailed process involved in geometry creation, mesh generation and the strategy used for optimization are explained in the subsequent sections.

4.2 Bench Marking the Baseline Model

The CFD analysis is conducted on a 1:10 scale bus model and three cases were carried out to evaluate the impact of luggage loaded on the roof rack on the aerodynamic performance of the existing bus. The cases are:

- ✓ Bus model without roof rack
- ✓ Bus model with the roof rack
- ✓ Bus model loaded with luggage: In order to know the effect of the luggage loaded on aerodynamic performance of the bus it is necessary to know the average height of the luggage. From the field survey and various gathered data the average height of the luggage is taken as 70 cm.

Case 1: The Existing Bus model without roof rack

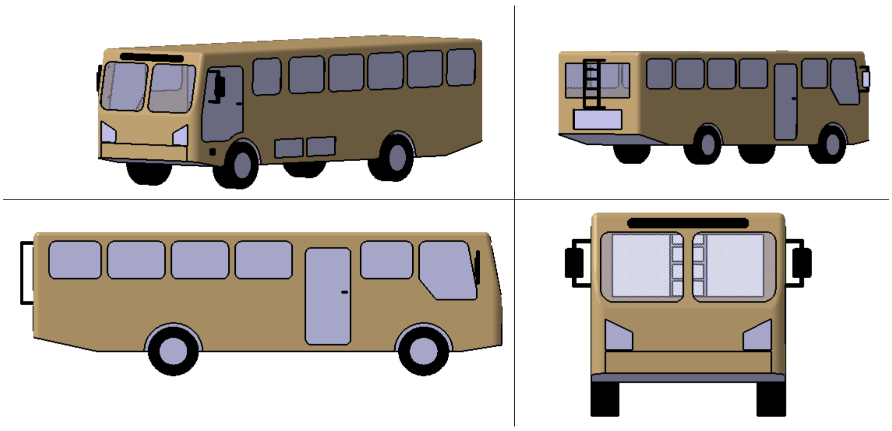

Figure 4.1: Different views of the existing bus model without roof rack

Case 2: The Existing Bus model with roof rack

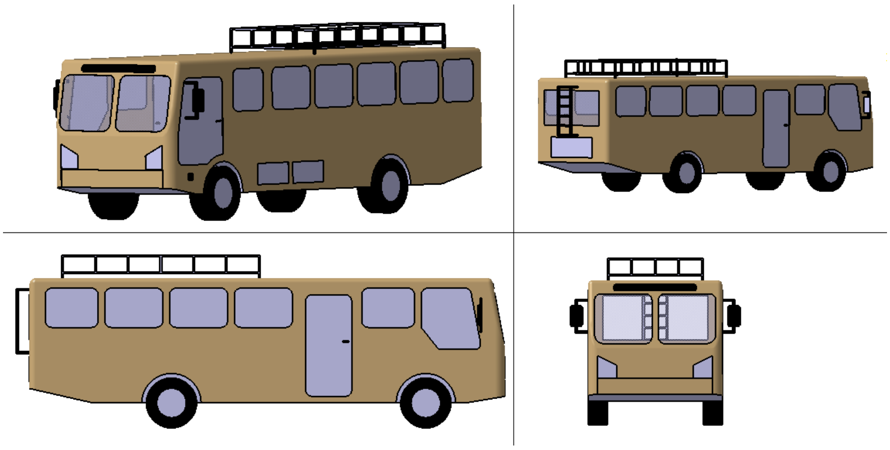

Figure 4.2: Different views of the existing bus model with roof rack

Case 3: The Existing Bus model loaded with luggage

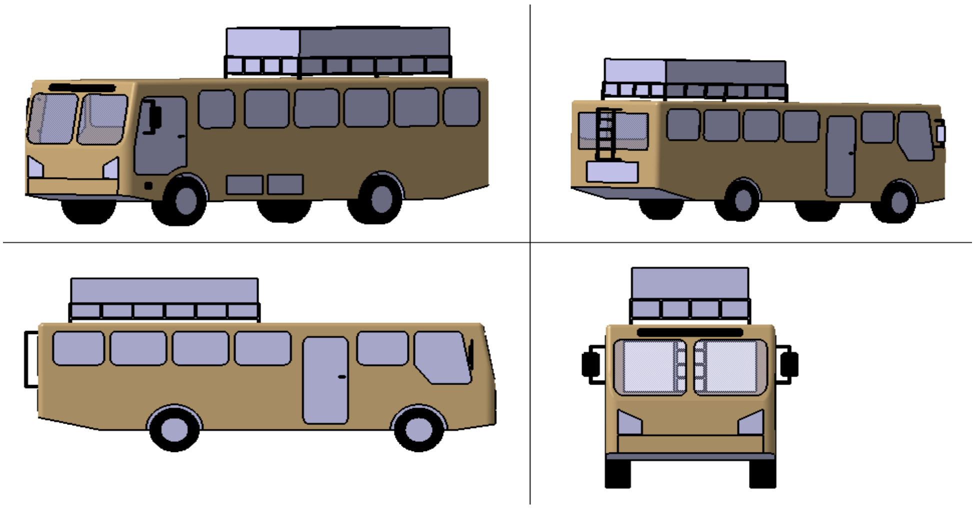

Figure 4.3: Different views of the existing bus model loaded with luggage

4.3 Design of the Luggage Compartment

The main aim of this thesis is to design rooftop luggage compartment for the existing local bus. Therefore, the luggage compartment should fulfill the following criteria. These are:

- ✓ It should have enough space to accommodate the luggage of all passengers
- ✓ It should improve the aerodynamic performance of the bus
- ✓ It should not affect the stability of the bus significantly
- ✓ It should be strong enough to withstand the applied loads

The modification is carried out on an intercity bus produced by ANTA PLC. Any modification should be according to the standard given by ministry of transport. According to the standards:

- ✓ Average weight of a passenger is assumed to be 75 kg and each passenger is allowed to have 25 kg of luggage.
- ✓ Only luggage (suitcase or other bags which is used to pack personal belongings) is allowed to be loaded on the bus. Agricultural products, Animals and Industrial products are not allowed to be loaded.
- ✓ The bus body builder is not allowed to do any modification on the frame of the vehicle which is used for mounting the bus body.

4.3.1 Dimensions of Luggage Bags

In order to know the space required to accommodate the luggage of the passengers, type and dimension of various luggage bags should be known and analyzed. According to the standard given by Ministry of transport only luggage is allowed to be loaded on the bus. The size (dimension) of the luggage compartment depends on the size of the luggage bags. Therefore it is necessary to know the type and dimension of the luggage to design the compartment. From the field survey at Lamberet bus station, frequently used luggage bags by passengers are identified. These are hard sided suitcase, soft sided suitcase, duffel bags, back bags and plastic bags (locally called kurtu festal).

Since the types of the luggage bags are identified, the next step is finding the dimension of each type by taking direct measurement. Each type of the bags mentioned above is available in different sizes. Therefore, in order to know the right dimension of the luggage compartment, the larger one of each type is considered.

Dimension of luggage bags

- ✓ **Hard sided suitcase and Soft sided suitcase**

  Length = 47 cm, Width = 26 cm, Height = 60 cm
- ✓ **Duffle bags**

  Length = 60 cm, Width = 30 cm, Height = 40 cm
- ✓ **Back bags**

  Length = 35 cm, Width = 30 cm, Height = 45 cm

Therefore, from the dimensions given above the biggest one is hard sided and soft sided suitcase. In order to have enough space, all of the passengers are assumed to bring this suitcase. Now it is easy to calculate the space required to accommodate the luggage. Therefore:

- ✓ The compartment should improve the aerodynamic performance of the bus
- ✓ The compartment must accommodate luggage of 25 passengers
- ✓ The weight of the luggage per each passenger is 25 kg
- ✓ The compartment must fit in the entire length of the bus with a maximum height of 0.7 m.
- ✓ The compartment is to be fastened to the roof of the bus
- ✓ A light weight material must be used.
- ✓ All government and industry safety standards must be met

The roof of the baseline bus has two areas that need a special interest for implementing aerodynamic measures. The first area is the top edge of the bus and the second area is the luggage loaded on the bus. Therefore, a wind deflector should be fitted on the top front part of the bus to minimize the flow separation occurring on the top edge of the bus. In addition to that the modified model is prepared with an enclosed luggage compartment. The height of the compartment is 0.7m with 0.1m clearance which is used to control the temperature inside the compartment.

4.4 CAD Modeling of the Modified Bus

To improve the aerodynamic performance of the bus a wind deflector is fitted on the front top part of the bus which is all integral part of the luggage compartment. The performance of the wind deflector depends on its inclination angle. Khosravi (2015) investigated the effects of adding append devices like deflector and cab vane corner on heavy commercial vehicle. According to the result the most effective supplementary part is the deflector, and by adding this part, the drag coefficient is decreased considerably. Finally, the researcher obtained that the best angle of deflector is between 20^0-40^0 and when the angle exceeds or lessens this angle, the drag coefficient increases because of disturbing airflow. Therefore, in this thesis in order to select the optimum angle of inclination the CFD analysis is carried out at different angles which are 20^0, 25^0, 30^0, 35^0 and 40^0 and the optimum angle is found to be 25^0.

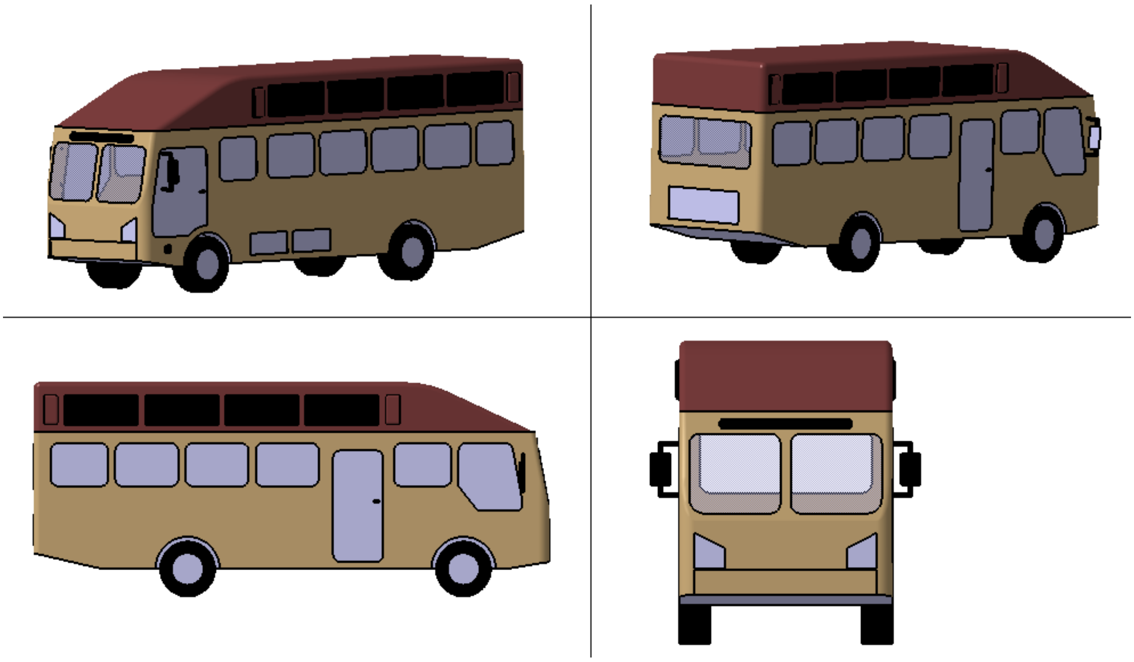

Figure 4.4: Different view of the modified bus model created using CATIA V5

Thus, the luggage compartment which is fitted over the entire length of the bus prevents the loaded luggage from obstructing the air flowing over the body. The height of the compartment is 0.7 m and the inclination angle of the deflector is 25^0. As it is seen from Figure 4.5, there are two geometric features on each side of the luggage compartment. The first feature is fresh air inlet and hot air outlet which is used to control the temperature inside the compartment. The second feature is doors of the luggage compartment.

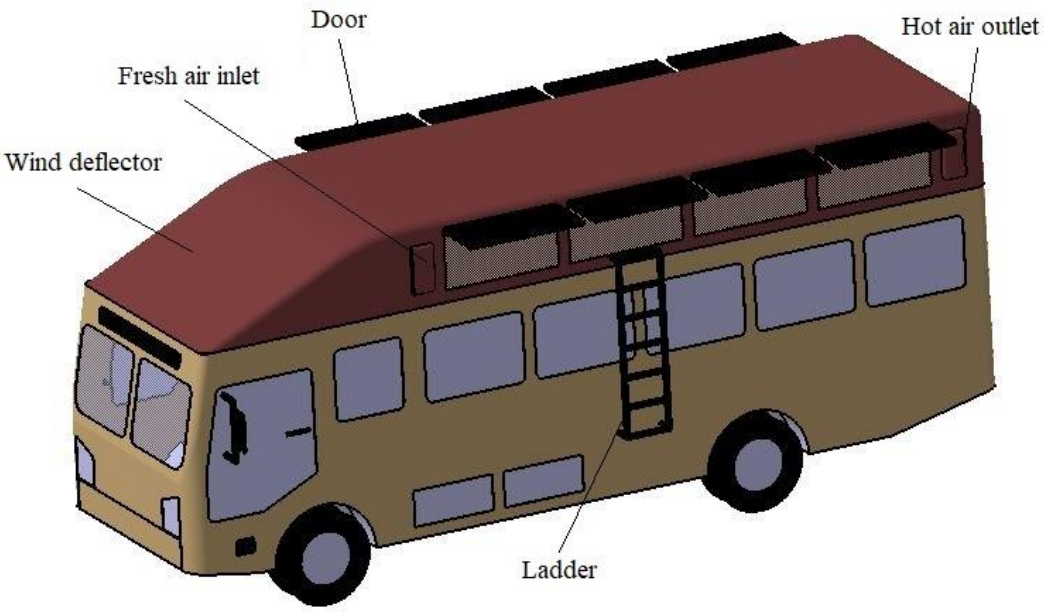

Figure 4.5: The modified bus model during luggage loading

The doors are placed on both sides of the luggage compartment. There are a total of eight doors with a length and height of 1m and 0.48m respectively. The doors are closed after loading the luggage. The ladder is used to load and unload the luggage and it can be used on both side of the compartment. After loading the luggage the ladder is kept inside the rear under body luggage compartment and the doors of the compartment will be closed. During hot seasons the temperature inside the compartment will be higher, in order to control that Fresh air inlet and hot air outlet is used. The dimension of these parts is shown in the appendix.

Figure 4.6: The Modified Bus model from the left side

4.4.1 Luggage Holding Capacity of the Compartment

In order to know the luggage holding capacity of the compartment, the volume of a single bag and the volume of the compartment should be calculated.

- ✓ ***The volume of a single luggage bag (V_L)***

Since the size of hard/soft sided suitcase is large, it is considered to calculate the volume of a single luggage bag.

$$V_L = l \times w \times h \qquad \text{Equ}(4.1)$$

Where l= length of the bag (0.47m)

w= width of the bag (0.26m)

h= height of the bag (0.6m)

$$V_L = 0.47\text{m} \times 0.26\text{m} \times 0.6\text{m}$$

$$V_L = 0.07332\ \text{m}^3$$

Therefore, the volume of a single luggage bag is 0.07332 m^3.

✓ ***The volume of the luggage compartment (V_{LC})***

The luggage compartment is fitted over the entire length of local bus. The luggage compartment has two basic parts these are the luggage carrier and the wind deflector. Since the luggage is loaded on the luggage carrier, its dimension is considered to calculate the volume of the luggage compartment. The length, height and width of the luggage carrier are 5m, 0.6m and 2.1m respectively.

$$V_{LC} = L \times W \times H \qquad Equ\ (4.2)$$

Where L= length of the luggage compartment (5 m)

W= width of the luggage compartment (2.1m)

H= height of the luggage compartment (0.6m)

$$V_{LC} = 5m \times 2.1m \times 0.6m$$

$$V_{LC} = 6.3\ m^3$$

Therefore, the volume the luggage compartment is 6.3 m^3. Then, the total number of luggage that can be accommodated by the compartment is calculated as follows:

$$N_T = \frac{V_{LC}}{V_L} \qquad Equ\ (4.3)$$

$$N_T = \frac{6.3\ m^3}{0.07332\ m^3}$$

$$N_T = 86$$

Therefore the luggage compartment can accommodate 86 hard/soft sided suit cases.

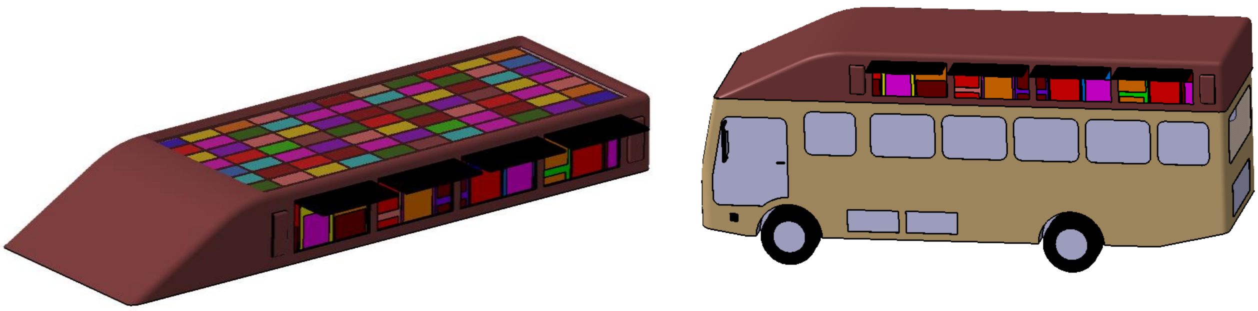

Figure 4.7: Modified bus loaded with luggage

Figure 4.7 shows the luggage loaded on the compartment, the roof of the compartment is transparent to visualize the inside part of the compartment but in actual condition it is closed.

4.4.2 The Effect of the Luggage Compartment on Stability

As it is known change in height of the bus affects its stability. To study the stability of the bus, center of gravity and weight distribution of the bus should be known. However, to know these parameters an experiment should be carried out. Unfortunately, there is no previous research which is conducted on the stability of local buses. Therefore, the centroid of the existing buses and the modified bus is considered to predict the effect of the luggage compartment on the stability of the bus. Table 4.1 shows centroid of the existing and the modified bus which is obtained from ANSYS, where X and Z represent longitudinal and vertical direction of the buses respectively. Since the buses are symmetric along their lateral axis their lateral centroid is existing at the middle.

Table 4.1: Centroid of local buses

Local Buses	X (m) (Longitudinal Direction)	Z (m) (Vertical Direction)
Existing Bus Without Roof Rack	3.6081	1.3254
Existing Bus With Roof Rack	3.6096	1.3265
Existing Bus Loaded With Luggage	3.9119	1.5475
Modified Bus	3.7261	1.6378

As it is seen from Table 4.1, the centroid of the modified bus along the vertical is higher than the existing buses. But when it is compared to the loaded existing bus, the deviation is 5.83% which is very less. Additionally, since there is no any means which limits the height of the loaded luggage on the existing bus its centroid height increases with the increasing luggage height. So there will be cases in which the centroid of the modified bus is lower than the loaded bus. Generally, the luggage compartment will not affect the stability of the bus significantly. The total mass of the luggage compartment is 184 kg. Since the roof rack is removed from the existing bus, its mass is subtracted from the mass of the compartment and its mass is 65 kg. Therefore, the net addition of mass is 119 kg, which is 3.13% compared to the tare weight of the bus. Therefore, the mass of the luggage compartment will not affect the performance of the bus significantly.

4.5 Stress Analysis of the Luggage Compartment

The luggage compartment has two basic parts these are the luggage carrier and the wind deflector. The structure of the luggage compartment and the panel which covers the structure should withstand the applied loads due to the pressure of the air and the load due to the weight of the entire luggage. In order to know the maximum pressure applied on the compartment an ideal speed of a vehicle is taken and CFD analysis is conducted at 150 km/hr from the result the pressure at that particular speed is 240 Pa. The weight of the luggage per each passenger is 25 kg and the bus has a capacity to carry 25 passengers therefore the total weight of the luggage is 6132 N. Since fuel consumption depends on weight, the weight of the luggage compartment should be light and in order to achieve this, the materials used to construct the structure of the compartment have better strength to weight ratio. The materials used to construct the structure are RHS (rectangular hollow section) steel and ABS (Acrylonitrile Butadiene Styrene). The design is carried out in CATIA V5 and to know the equivalent stress and total deformation of the structure, stress analysis is conducted using ANSYS.

4.5.1 Material Selection

The materials which are selected to construct the structure of the luggage compartment and the panel (the cover over the structure) are RHS steel and ABS sheet respectively.

I. Steel hollow sections (RHS)

Rectangular hollow sections (RHS) are a popular choice for mechanical, structural and construction applications. It is selected to construct the structure of the luggage compartment because of the following properties:

- ✓ The flat surface resulting in a structural solution that is more economical for joining and various other types of fabrication works.
- ✓ Rectangular and square structural hollow sections have economic advantages as well as great resistance to torsion and buckling
- ✓ It gives structures a better strength to weight ratio this results in lightweight
- ✓ It is also easy to fabricate, weld and manipulate to save processing time and cost.
- ✓ It gives greater flexibility in use and hollow sections create lightweight and visually attractive structures

II. ABS (Acrylonitrile Butadiene Styrene)

ABS stands for Acrylonitrile Butadiene Styrene. ABS is an impact-resistant engineering thermoplastic & amorphous polymer. It is made up of three monomers: acrylonitrile, butadiene and styrene. It has been used in a number of car interior applications such as the rigid parts of instrument panels and doors, consoles, glove boxes, HVAC parts and loudspeaker housings. It is also used in chrome-plated parts. For exterior applications such as radiator grilles, wheel covers, mirrors and rear light housings (Omnexus, 2021). ABS is selected because of its several physical properties such as:

- ✓ High rigidity
- ✓ Good impact resistance, even at low temperatures
- ✓ Good insulating properties
- ✓ Good abrasion and strain resistance
- ✓ High dimensional stability (Mechanically strong and stable over time)
- ✓ Offers a high degree of surface quality

4.5.2 Stress Analysis

The stress analysis of the compartment is carried out in ANSYS. After importing the geometry to ANSYS workbench, the solid geometry is converted to surface. Therefore, it is possible to vary the thickness of the RHS steel and the panel made of ABS sheet depending on the results. The structure is constructed from 20 mm × 20 mm RHS steel and it is selected for the reason that its mass per meter is minimum compared to other RHS steel. The other benefit of conducting the analysis in ANSYS is it calculates the total mass of the compartment. The thickness of the structure and the ABS sheet is 1.5 mm and 2 mm respectively.

I. Load applied on the compartment

The loads which are applied on the compartment are the load due to the pressure of the air and the weight of the entire luggage.

- ✓ **Weight of the entire luggage**

The mass of the luggage which is allowed per each passenger is 25 kg and the bus has a capacity to carry 25 passengers.

Therefore, the total mass on the luggage compartment is 625 kg and the applied weight is:

$$W = mg \qquad \text{Equ}(4.1)$$

$$W = 625\ \text{kg} \times 9.81 \text{m/s}^2$$

$$W = 6132\ \text{N}$$

Where W= weight, m= mass and g= gravity

- ✓ **Load due to the pressure of the air**

In order to know the maximum pressure on the deflector the CFD analysis is conducted by taking an ideal speed of 150 km/hr and as it is seen form the pressure contour given below the maximum pressure on the deflector at that particular speed is 240 Pa.

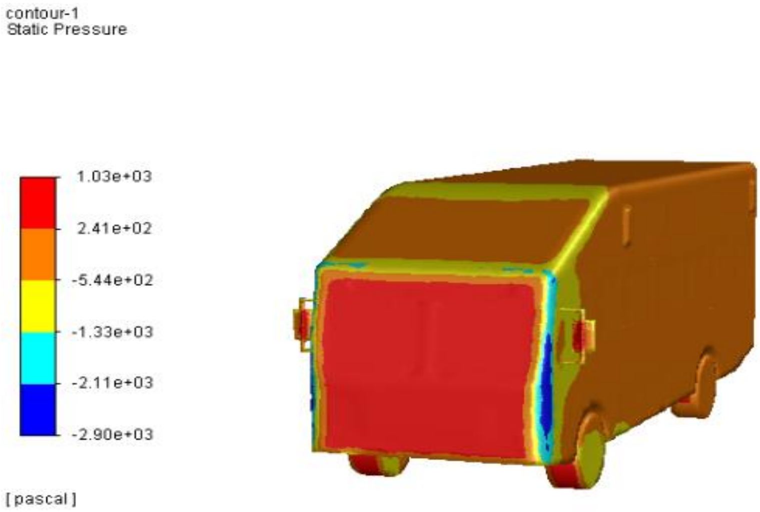

Figure 4.8: Pressure contour of the modified bus at 150 Km/hr

4.5.3 Geometry creation

The luggage compartment has two basic parts; these are the luggage carrier and the wind deflector.

I. Luggage carrier

The luggage carrier is used to accommodate the luggage of the entire passengers. Its length, width and height are 5 m, 2.1 m and 0.7 m respectively and it has a capacity to accommodate 86 hard case suitcases. The maximum allowable weight of the luggage is 625 kg. The structure is constructed from RHS steel and ABS sheet is used to cover the structure.

II. Wind deflector

A wind deflector is a device that changes the air flow around the bus. An effective wind deflector will reduce wind resistance while the bus is in motion and consequently increases stability and fuel efficiency. The structure of the wind deflector is constructed from RHS steel.

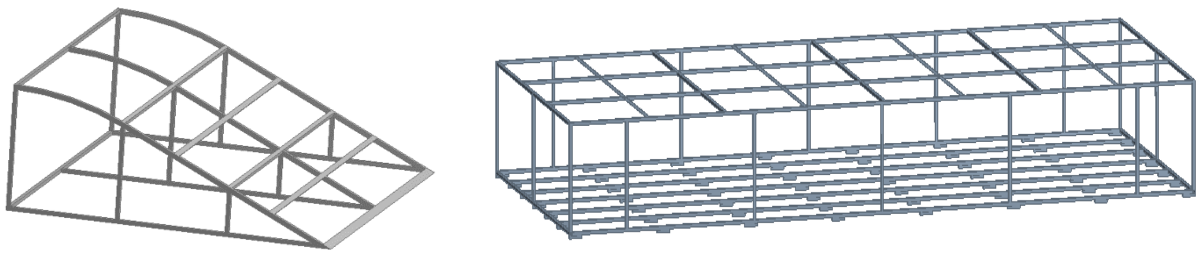

Figure 4.9: Structure of the wind deflector and Structure of the luggage carrier

Then, the two parts are assembled to do the analysis. The mass of the structure is 122 kg and the total mass of the luggage compartment after the structure is covered with ABS sheet is 184 kg.

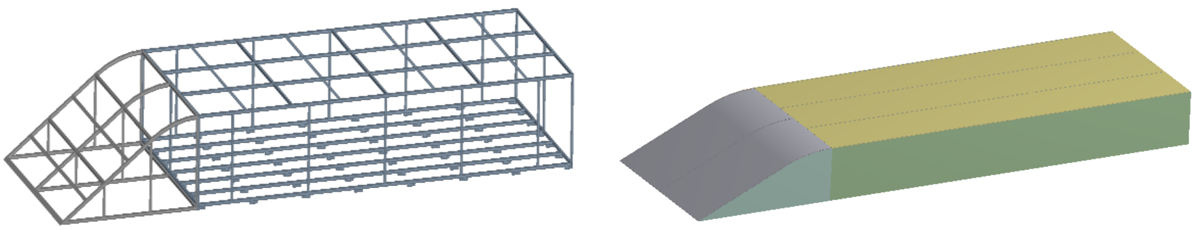

Figure 4.10: The assembled model of the luggage compartment

III. Fastening Mechanism

Welded joint is recommended to be used to join the compartment structure, Welding is one type of permanent joining process by which two or more solid parts are joined together. Since strength of welded joint is similar to that of parent parts, load carrying capacity of welded components remains unchanged before and after joining. Additionally, rivets are recommended to be used to join the ABS Sheet with the structure. A riveted joint is used for heterogeneous materials and it is used to make permanent joints between two plates.

4.5.4 Results of the Stress Analysis

I. Equivalent (Von-Mises) Stress

Von Mises stress is a value used to determine if a given material will yield or fracture. The yield point is the point on a stress-strain curve that indicates the limit of elastic behaviour and the beginning of plastic behaviour. A material is said to start yielding when the von Mises stress reaches a value known as yield strength. According to Figure 4.11, the maximum equivalent stress of the structure is 12.775 MPa which is very less compared to the yield strength of the material which is 269 MPa. Additionally, as it is seen in Figure 4.12 the maximum equivalent Stress of the structure with ABS Sheet cover is 19.092 MPa which is less than the yield strength of ABS which is 45 MPa. Therefore, the luggage compartment can withstand the load applied to it.

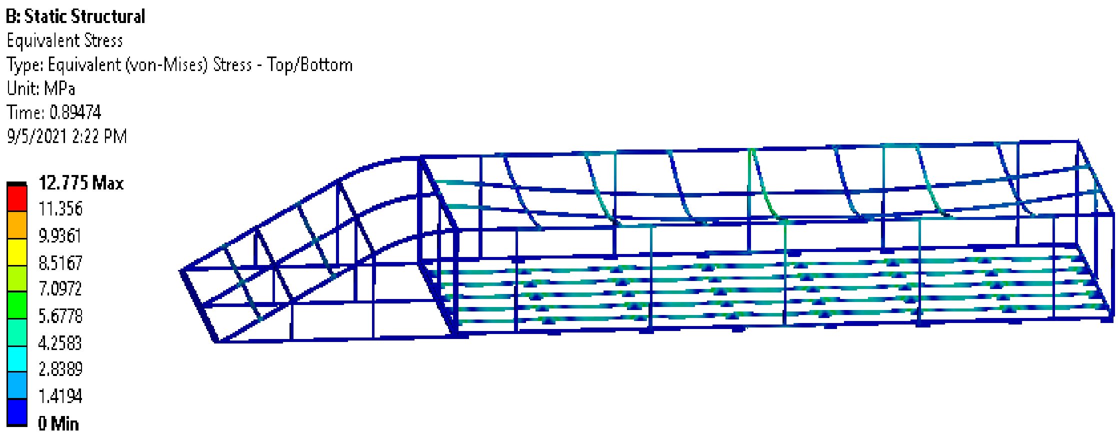

Figure 4.11: Equivalent (Von-Mises) Stress of the structure

Figure 4.12: Equivalent (Von-Mises) Stress the structure with ABS Sheet cover

II. Total deformation

Deformation refers to the change in size or shape of an object. In ANSYS Workbench there are two types of deformation these are total deformation and directional deformation. Both deformations are used to find displacement through stress. Directional deformation acts in directions like X, Y and Z. In the case of total deformation, it is the square root of the total of the square of X, Y & Z direction (Balwant, 2020).

$$\text{Total Deformation} = \sqrt{x^2 + Y^2 + Z^2} \qquad \text{Equ}(4.2)$$

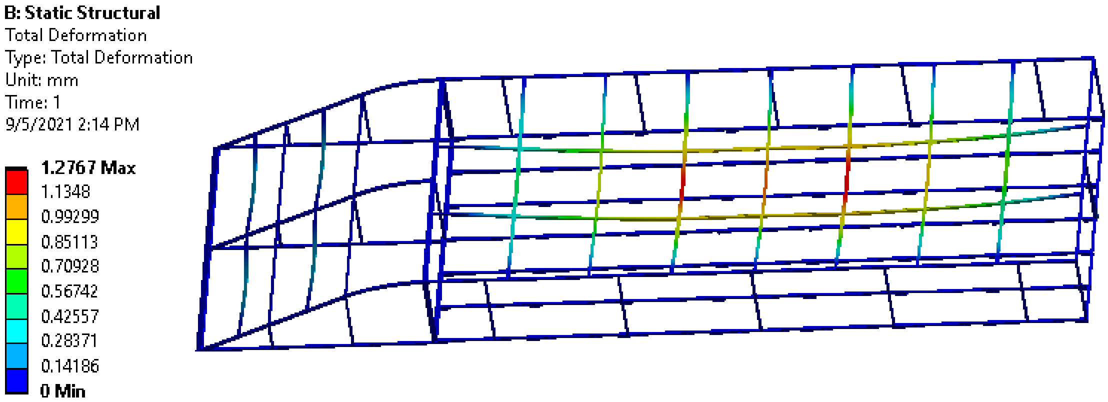

Figure 4.13: Total deformation of the structure

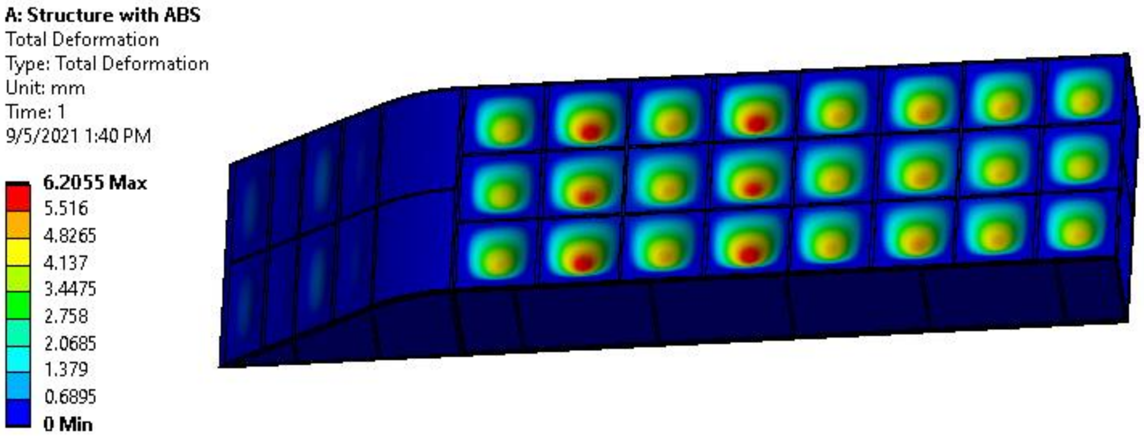

Figure 4.14: Total deformation of the structure with ABS sheet cover

As it is seen from Figure 4.13-4.14, the maximum deformation of the structure and the structure with a cover is 1.2767 mm and 6.2055 mm. Since the cover is made of ABS plastic the deformation is higher than the steel structure but it is to minimum. Therefore the luggage compartment is safe regarding deformation.

III. Maximum shear stress

The maximum shear stress is the maximum concentrated shear force in a small area. The neutral axis of a cross section is the axis at which the value of the normal stress and strain is equal to zero. According to Figure 4.15, the maximum shear stress of the structure is 7.3754 MPa which is very less compared to the yield strength of the material which is 269 MPa. Additionally, as it is seen in Figure 4.16 the maximum shear stress the structure with ABS Sheet cover is 11.022 MPa which is less than the yield strength of ABS which is 45 MPa. Therefore, the maximum shear stress of the luggage compartment is too minimum.

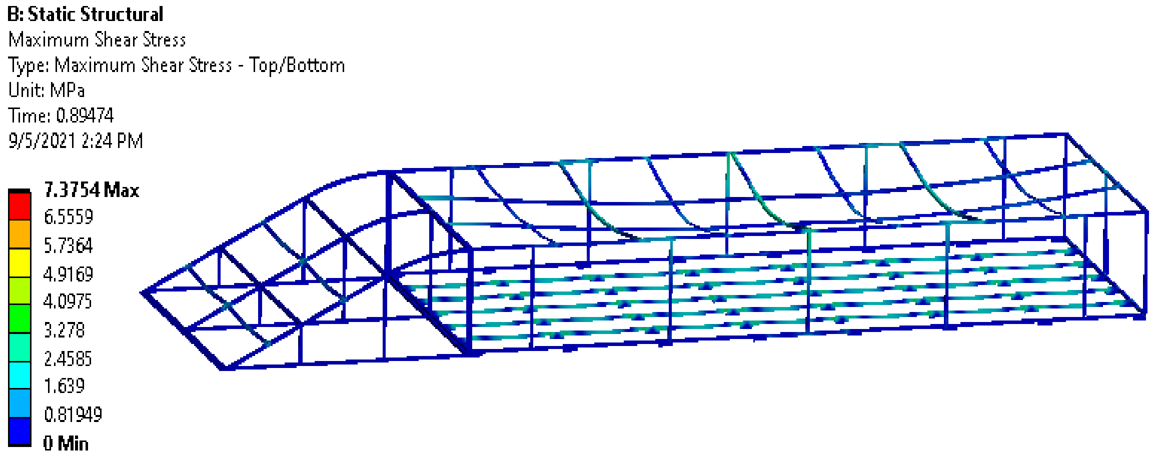

Figure 4.15: Maximum shear stress of the structure

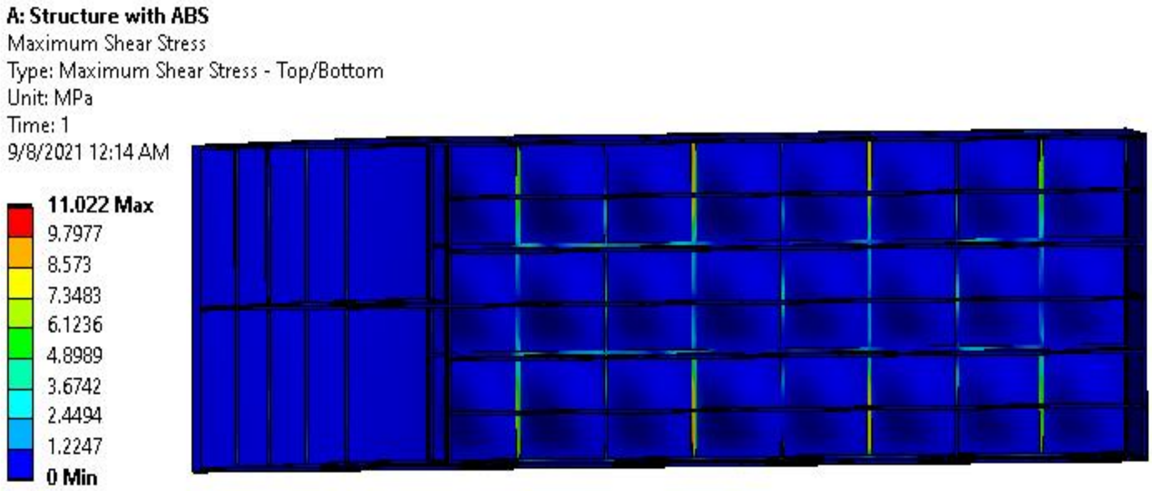

Figure 4.16: Maximum shear stress the structure with ABS sheet cover

4.6 CFD Analysis of the Buses

4.6.1 Geometry Creation

The geometry of the buses is created using CATIA V5 and imported to ANSYS workbench in IGS format. The dimensions used for geometry creation are taken form the data that is obtained from the field survey at ANTA PLC. Figure 4.17-4.20 shows the geometry after imported to ANSYS workbench in IGS format for each case. Since, the fluid flow around the bus is the domain of interest a fluid enclosure is created around the bus. The dimension of the enclosure is obtained from various researches which are conducted on related titles.

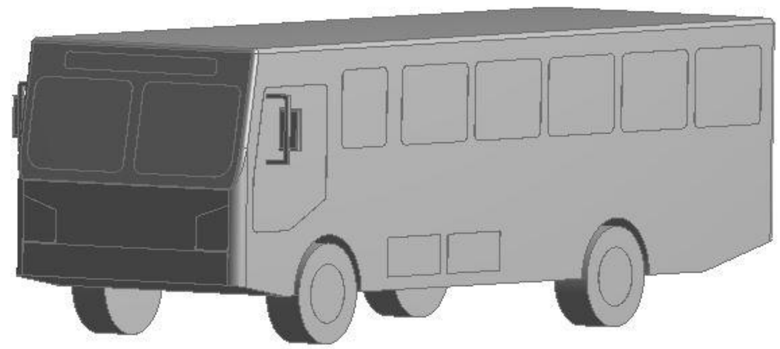

Figure 4.17: The Geometry of the bus without roof rack after imported to ANSYS

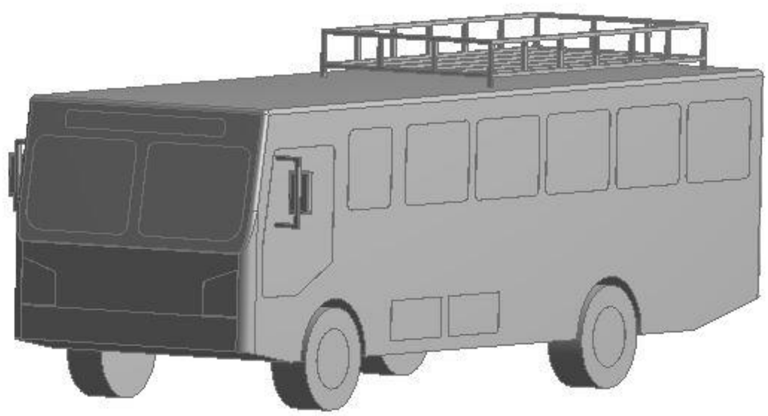

Figure 4.18: The Geometry of the bus with roof rack after imported to ANSYS

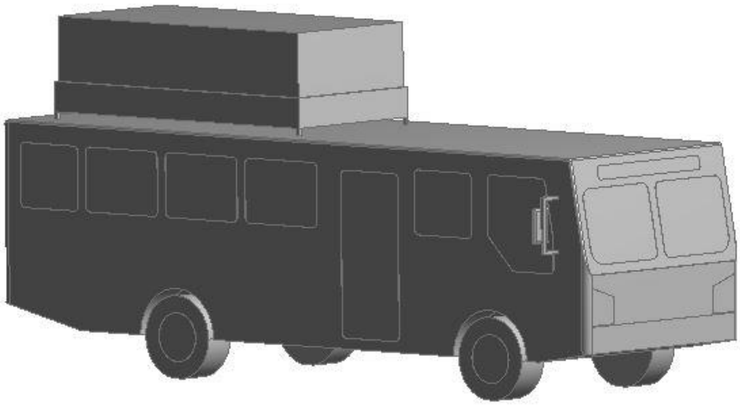

Figure 4.19: The Geometry of the bus loaded with luggage after imported to ANSYS

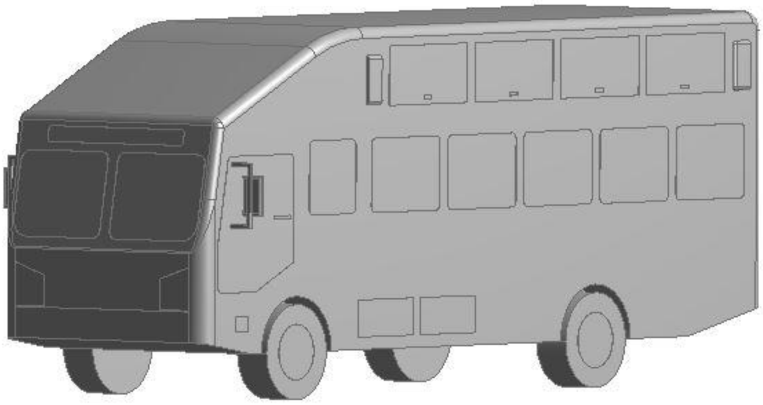

Figure 4.20: The Geometry of the modified bus after imported to ANSYS

As it is mentioned above the fluid flows around the bus is the domain of interest, hence a fluid enclosure is created around the bus. The dimension of the main enclosure is three bus lengths in front of the bus, two bus lengths to the side of the bus and five lengths behind. In order to control the mesh near the bus, three inner boxes are created. The smallest inner box extends about half a bus length in front, to the sides and to the top and about a bus length in the wake (Lanfrit, 2005). The bus model inside an enclosure is shown in Figure 4.21.

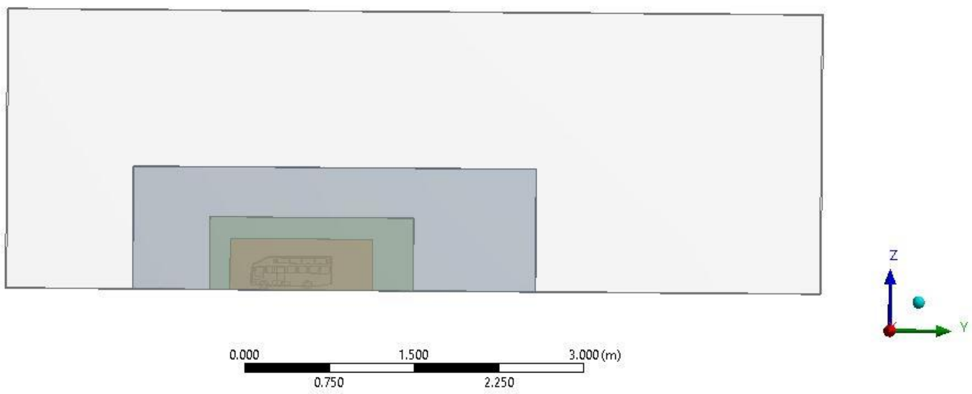

Figure 4.21: Geometry of the modified bus inside an enclosure and inner boxes

Since, similar enclosure and inner boxes are used in all of the cases only the enclosures of the modified bus is shown in the Figure 4.21.

4.6.2 Mesh Generation

Drag and lift predictions are strongly affected by the locations of flow separation and reattachment. Therefore, it is important that the surface mesh resolves all relevant details of the geometry and satisfies the requirements of the physical models used in the simulation (Lanfrit, 2005). In order to capture the flow physics near the bus, a fine mesh of unstructured triangles was put on the boundary of the bus. As we go away from the bus model the flow will be more or less uniform, hence element sizes have been increased so as to reduce the cell count and solver time.

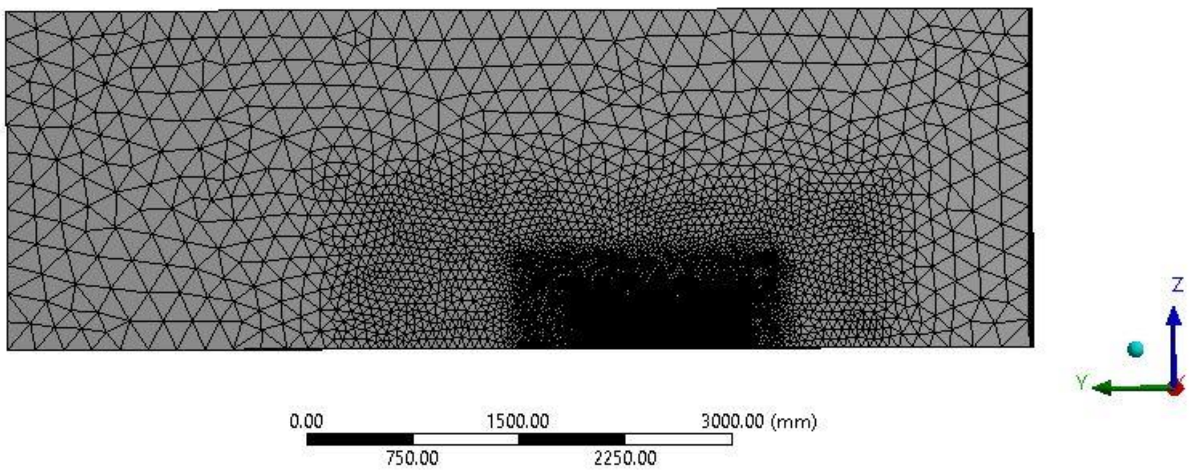

Figure 4.22: The mesh generated for the bus

As it is shown in Figure 4.23 the mesh near the bus is very fine so as to get an accurate result. The outer volume was meshed with coarse elements. In all of the cases nearly 2.2 million Unstructured tetrahedral and prism elements were used to mesh the entire fluid domain.

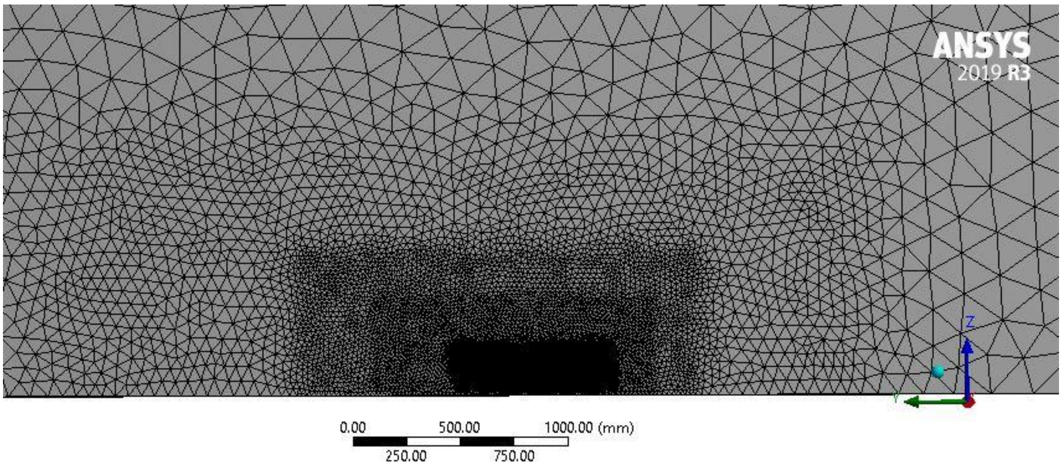

Figure 4.23: Fine mesh generated near the bus

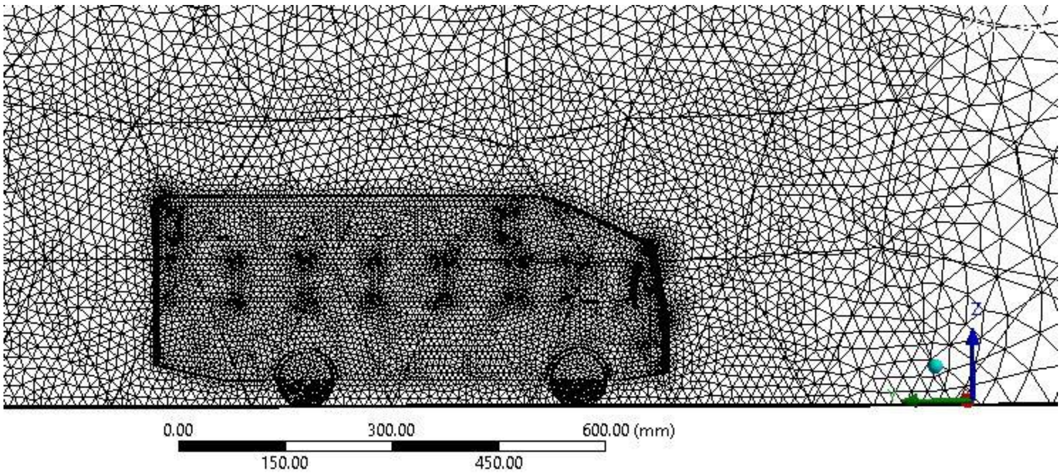

Figure 4.24: The mesh generated on the bus

The other thing that must be considered here is quality of the mesh. As it is mentioned in Fluent User's Guide the quality of the mesh plays a significant role in the accuracy and stability of the numerical computation. According to Fluent User's Guide Minimum orthogonal quality is an important indicator of mesh quality. Values for orthogonal quality can vary between 0 and 1 with lower values indicating poorer quality cells.

In general, the minimum orthogonal quality should not be below 0.01 with the average value significantly larger. The figures given below shows quality of the mesh for each case:

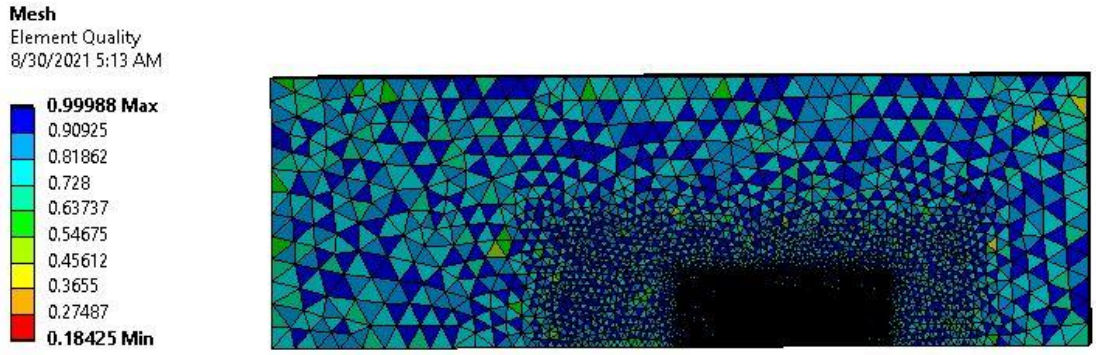

Figure 4.25: The quality of the mesh for the baseline bus without roof rack

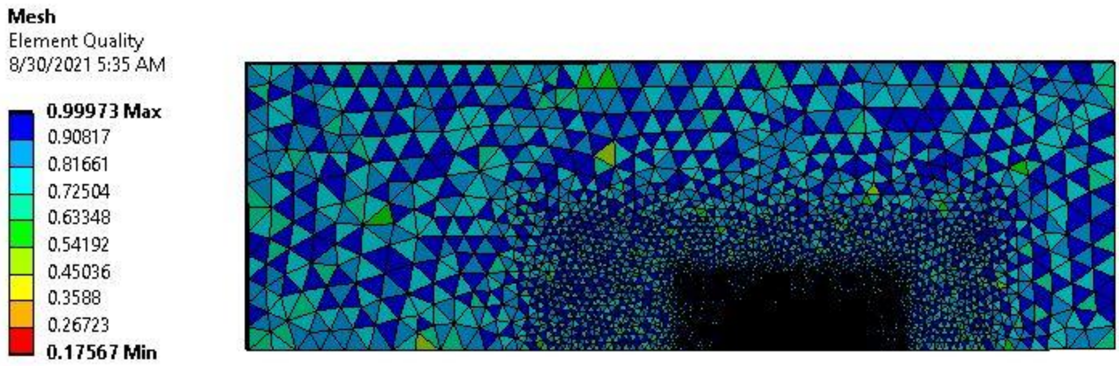

Figure 4.26: The quality of the mesh for the baseline bus with roof rack

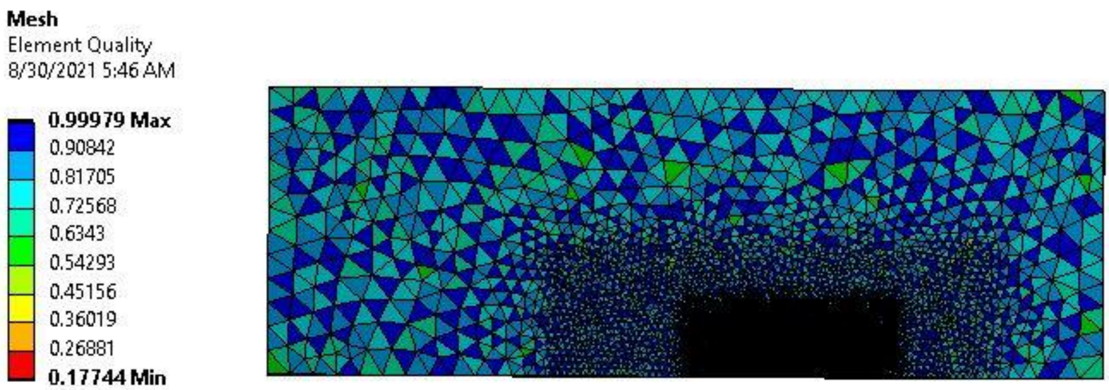

Figure 4.27: The quality of the mesh for the baseline bus loaded with luggage

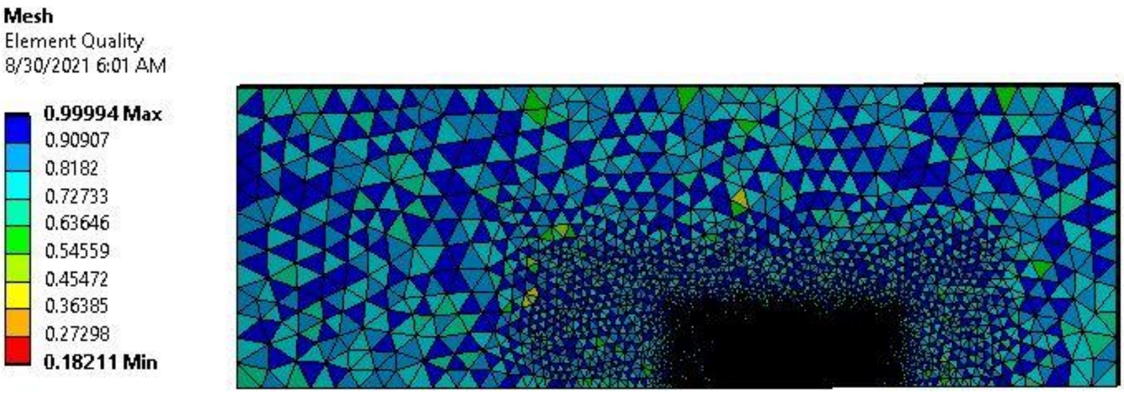

Figure 4.28: The quality of the mesh for the modified bus

As it is shown in Figure 4.25-4.28, the minimum quality of the mesh is 0.18425, 0.17567, 0.17744 and 0.18211 respectively which is greater than 0.01. Therefore, the quality of the mesh is as per the standard given in Fluent manual.

Finally, named sections were created to differentiate among the faces, which are also used to establish the boundary condition. The plane of the enclosure in front of the vehicle was named as velocity inlet while the plane behind was the pressure outlet and the bottom face is named as road. The sides and top of the enclosure was named as symmetry-side and symmetry-top respectively because, since the symmetry top and symmetry side surfaces of the enclosures are far away from the vehicle, it has no influence on aerodynamic performance of the vehicle at all. Therefore, it gives them the same boundary conditions as symmetric surface (which is slip wall with zero shear forces).

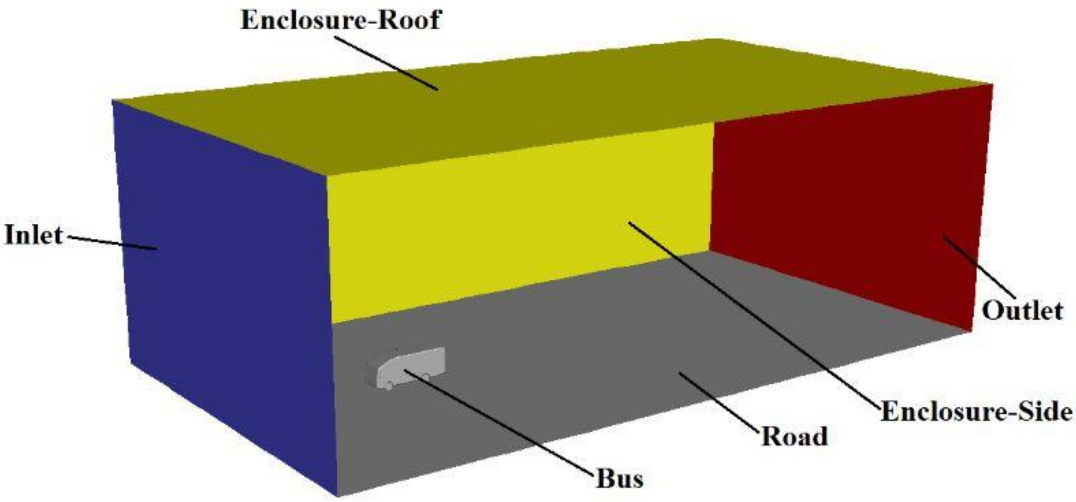

Figure 4.29: Named selections

4.6.3 Grid Independence Test

The choice of mesh size is always a critical thing in most of numerical analysis; hence it is one of the most influencing factors which determine the computational time and accuracy (Ali, 2017). Therefore, it is important to choose an optimum mesh size. A typical way of choosing mesh size is predicting the sensitivity on results (Wagner, 2018). In this case, the effect of mesh size on drag coefficient and lift coefficient is studied and the mesh size is selected appropriately. Grid independent test is carried out from 0.89 million to 2.08 million elements. The results of grid independence test are summarized in the tables given below.

Table 4.2: Grid independence test for the baseline bus without roof rack

Mesh	**Nodes**	**Elements**	**Drag coefficient (C_D)**	**Lift Coefficient (C_L)**
1	114206	638511	0.6404	- 0.2086
2	190445	1081587	0.6378	- 0.1929
3	260938	1489469	0.6286	- 0.1894
4	382356	2185039	0.6237	- 0.1875

Table 4.3: Grid independence test for the baseline bus with roof rack

Mesh	**Nodes**	**Elements**	**Drag coefficient (C_D)**	**Lift Coefficient (C_L)**
1	116786	651995	0.6195	- 0.1863
2	195784	1111590	0.6211	- 0.1869
3	265999	1516936	0.6238	- 0.1989
4	387585	2213861	0.6242	- 0.2052

Table 4.4: Grid independence test for the baseline bus with luggage

Mesh	Nodes	Elements	Drag coefficient (C_D)	Lift Coefficient (C_L)
1	115966	646112	0.6710	- 0.1714
2	194733	1101784	0.6360	- 0.1654
3	257524	1468742	0.6289	- 0.1609
4	334086	1920998	0.6256	- 0.1570

Table 4.5: Grid independence test for the modified bus

Mesh	Nodes	Elements	Drag coefficient (C_D)	Lift Coefficient (C_L)
1	114282	636953	0.4292	- 0.1221
2	186757	1059757	0.4282	- 0.1389
3	271613	1557239	0.4176	- 0.1409
4	351073	2017001	0.4142	- 0.1435

As it is seen from Table 4.2-4.5, the drag coefficient deviation between the values obtained in mesh 3 and mesh 4 is 0.64%, 0.79%, 1.57% and 0.729% respectively. Additionally, the lift coefficient deviation is 3.1%, 1.07%, 1.29% and 2.14% respectively. Therefore, since the variation is very less mesh 4 is applied for all the cases.

4.6.4 Fluent Solver

The CFD prediction for turbulent flow is highly dependent upon the quality of the turbulence modeling. According to ANSYS Fluent manual, where highly accurate resolution of boundary layers is critical such as applications involving flow separation or finely resolved heat transfer profiles, SST k-w (K-Omega) is preferred. It was also established that for a wide range of studied cases, the SST k-ω turbulence model makes it possible to achieve CFD results close to the experimental data (Jakub et al., 2019). Therefore, SST k-w (K-Omega) turbulence modeling is used to perform the analysis.

The simulation is considered at three different speeds of 80, 100, 120 kmph and Zero gauge pressure is applied at the outlet with operating pressure as atmospheric pressure. The courant number was set to 50 and the relaxation factors were taken as 0.25. For inlet condition the turbulence intensity was set to 1% and turbulent viscosity ratio as 10. For outlet, they were set to 5% and 10 respectively. All the boundary conditions used in the analysis are listed in Table 4.6.

Table 4.6: Boundary Conditions

Surface/Part	**Type**	**Condition**
Enclosure-Inlet	Velocity Inlet	Constant velocity: 22.22 m/s, 27.78 m/s, 33.33 m/s Turbulent intensity: 1% Viscosity ratio: 10
Enclosure-Outlet	Pressure Outlet	Gauge pressure=0 Pa Turbulent intensity: 5% Viscosity ratio: 10
Enclosure-Sides	Symmetry	-
Enclosure-Roof	Symmetry	-
Enclosure-Floor (Road)	Wall (Moving)	Constant velocity: 22.22 m/s, 27.78 m/s, 33.33 m/s
Bus	Walls (Stationary)	No-slip

CHAPTER FIVE
EXPERIMENTAL SETUP AND PROCEDURE

5.1 Introduction

This subtopic mainly focused on experimental validation of the numerical analysis of the modified bus using wind tunnel testing. The validation is done by comparing results obtained through numerical analysis with results obtained from experiment. A scale down 3D model of the modified bus is used for the experimentation. The experiment is carried out in Adama Science and Technology University using HM 170 open wind tunnel. The HM 170 demonstration wind tunnel was developed for experimentation and demonstration purposes in the fields of aerodynamics and fluid mechanics. It is a subsonic, open wind tunnel with a square measurement-section profile (Gerätebau, 2012). The model being studied remains at rest while the flow medium is set in motion, and thus the desired flow around the model is generated.

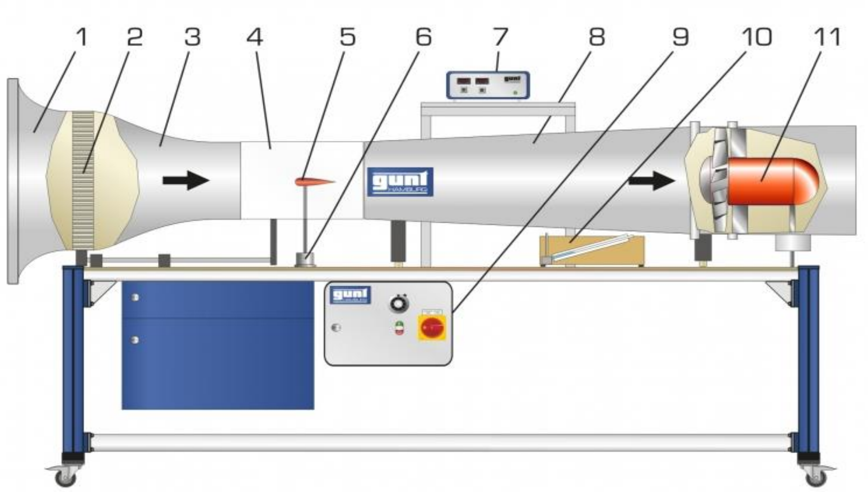

1: Funnel (inlet)

2: Flow straightener

3: Jet

4: Measurement section

5: model

6: Electronic two-component force transducer

7: Measurement amplifier with force display

8: diffuser

9: Switch box with fan speed control

10: Inclined-tube manometer for air speed

11: axial fan

Figure 5.1: Schematic drawing of HM 170 Educational wind tunnel (Gerätebau, 2012)

Figure 5.1 shows Schematic drawing of HM 170 Educational wind tunnel, the jet and a flow straightener ensure a uniform velocity distribution with little turbulence in the closed measuring section. The flow cross-section of the measuring section is square. The built in axial fan with outlet guide vane system and a variable speed drive is characterized by an energy efficient operation at high efficiency. Air velocities of up to 28m/s can be reached in this open wind tunnel. The trainer is equipped with an electronic two-component force sensor. Lift and drag are detected and displayed digitally. The air velocity in the measuring section is displayed on the inclined tube manometer (Gerätebau, 2012).

5.2 Specification of the Wind Tunnel

Rated performance is only possible if there is an unhindered inflow and outflow of air. The minimum distances from walls or other objects are to be ensured on installation, which is 1m from the intake and 2m from the blower outlet (Gerätebau, 2012).

Table 5.1: Specification of HM 170 Wind Tunnel (Gerätebau, 2012)

Dimensions	**L×W×H:** 2850mm×750mm×1700mm **Weight:** 250 kg **Power supply:** 230 VAC, 50 Hz
Measurement Section	**Cross-Section:** 292mm×292mm **Length:** 450mm
Measurement Range	**Lift:** 10 N **Drag:** 3 N **Resolution:** 0.01 N **Air Velocity:** 0 – 28 m/s
Fan	**Max. air flow:** 2.5 m^3/s **Motor Power:** 2.25 kW

5.3 Model Preparation (3D Model)

In wind tunnel experiment, the blockage effect is a very important factor which affects the test results significantly. Blockage ratio is the ratio of the projected area of the test model to the test section cross sectional area of the wind tunnel. According to a result obtained by Choi (1998), the aerodynamic behavior of square models with up to 10% blockage ratio are almost the same and square models with up to 10% blockage ratio can be tested as a group which behaves similarly.

$$B.R = \frac{A_m}{A_{TS}} \qquad \text{Equ(5.1)}$$

Where B.R = Blockage Ratio

A_m = Frontal area of model

A_{TS} = Cross-sectional area of the test section

Therefore, since the cross-sectional area of the test section is known, it is necessary to calculate the area of the model which has a blockage ratio less than 10%. According to the specification, the cross section of the measurement section is 292mm×292mm. Therefore, cross-sectional area of the test section is:

$$A_{TS} = 0.292m \times 0.292m = 0.0853\ m^2$$

Then, in order to have a blockage ratio of 10%, the frontal area of the model is:

$$\mathrm{A_m} = \mathrm{A_{TS}} \times \frac{10}{100}$$

$$\mathrm{A_m} = 0.0853 \times \frac{10}{100} = 0.00853\ \mathrm{m}^2$$

Therefore, to get a blockage ratio less than 10%, the front area of the model should be less than 0.00853 m^2. The model which is used for the 3D printing is modeled in CATIA V5 with a scale of 1:30 and its frontal area is 0.0067m^2. Thus the blockage ration is 7.85% which is less than 10%.

The 3D model of the Modified Bus was printed in Next 3D Studio in Addis Ababa with a scale of 1:30 (comparing to the actual model). The printer is shown in Figure 5.2.

Figure 5.2: Prusa i3 MK3S 3D Printer

The 3D model is saved in STL format. Then, an input code which tells the printer to print layer by layer is generated and saved to an SD card. The printer used plastic material, which is supplied to the printer in a form of filament and then melted in a hot-end at high temperature. The printer head distributes the material layer by layer, basing on the input code.

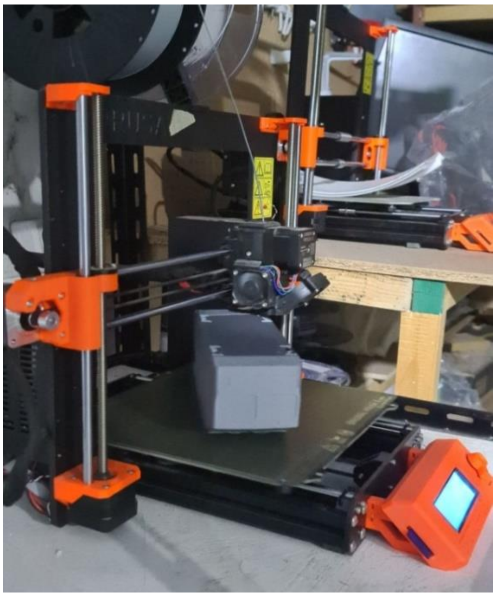

Figure 5.3: During printing the modified bus model

Figure 5.4: 3D printed model of the Modified Bus

5.4 Testing Procedure

The experiment was conducted on HM 170 Educational wind tunnel (Figure 5.5) which is subsonic, open wind tunnel with a square measurement section profile.

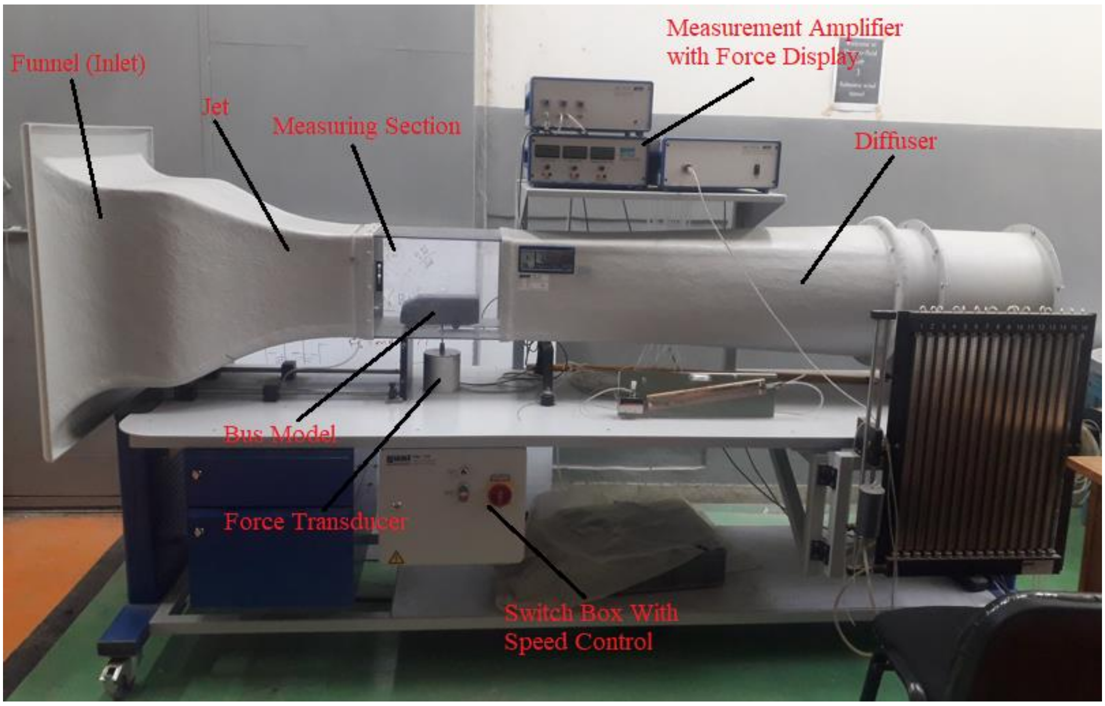

Figure 5.5: HM 170 Educational wind tunnel (Adama Science and Technology University)

This wind tunnel is used to determine drag force and lift force of the modified bus model. The First task was measuring the temperature and relative humidity of the room which is used to calculate the density of air. The temperature and relative humidity of the room is 25.4 ^{0}C and 60 % respectively. Therefore, the density of the air is 1.17 kg/m^3. In order to mount the model on the Electronic force transducer the model is drilled at its center with a diameter of 4 mm.

The next task was securing the modified bus model in the wind tunnel (Figure 5.6), Securing the model was done by using a model holder. Then, the model holder is attached to the Electronic two-component force transducer which measures the drag and lift forces acting on the model.

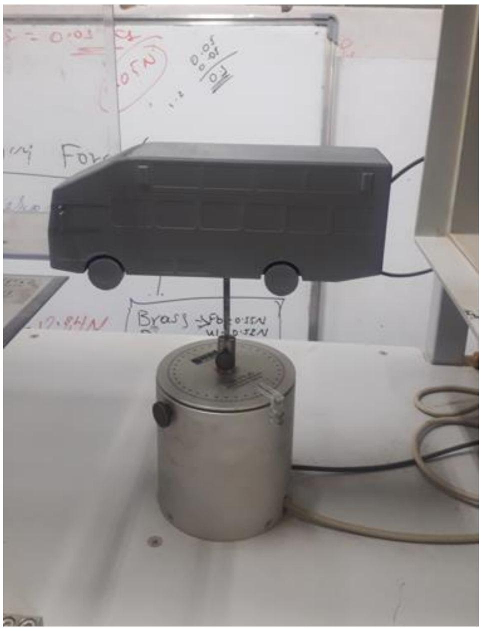

Figure 5.6: Securing the modified bus model in the wind tunnel

The next step was zeroing the measurement amplifier which display drag and lift force of the bus (Figure 5.7). In order to zero the measurement amplifier, two radial dials were adjusted until the values of the lift and drag displays were as close as possible to zero. The dials are very sensitive and it was quite hard to have the readout on the displays show exactly zero.

Figure 5.7: Zeroing the measuring equipment

Before starting the wind tunnel's motor, the enclosure lid was closed to avoid injury to the operator or damage to the enclosure. Once the motor had been started the wind tunnel's speed was adjusted. The model was tested at different speeds with the values of 2.8 to 22.4 m/s at zero-degree angle of attack and the values of the normal and axial forces were obtained. Lift and drag are detected and displayed digitally on the measurement amplifier. The test was conducted twice to establish more accurate results.

Figure 5.8: Model of the Modified Bus mounted in the wind-tunnel

CHAPTER SIX

RESULTS AND DISCUSSION

6.1 Results and Discussions of CFD Analysis

A 3D steady-state, incompressible solution was performed using ANSYS FLUENT. SST k-w (K-Omega) turbulence modeling is used to perform the analysis. The computational results of different models are presented and discussed. All the results for different cases were obtained with similar meshing resolution, similar turbulence modeling and also similar boundary conditions. For the first 100 iterations, a first-order upwind discretization was used to accelerate the convergence then 1000 iterations of second-order upwind scheme has been applied and iterations have continued until it reached to the convergence criteria. The convergence criteria were having all residuals below 10^{-5}.

6.1.1 Results of the Baseline Bus without Roof Rack

I. Residual History

The numerical computation is conducted with first-order discretization for the first 100 iterations then second-order scheme is applied for the remaining iterations to ensure numerical stability and accuracy. The simulation is carried out for 1100 iterations so as to get a negligible drag and lift coefficient. Since the graph of the residual history at 80, 100, 120 Km/hr is nearly the same, only the residual history at 80 Km/hr is shown in Figure 6.1. The remaining graphs are included in the appendix.

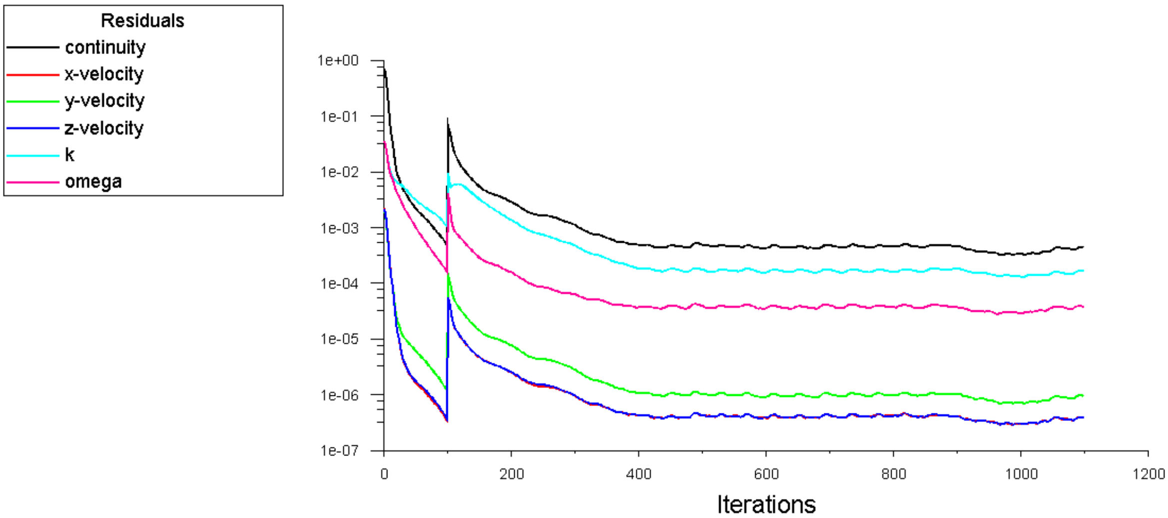

Figure 6.1: Residual history of the baseline bus without roof rack at 80 Km/hr

II. Drag Coefficient

As it is shown in Figure 6.2 – 6.4 the drag coefficient converges after 200th iteration. Due to the top edge of the bus, flow separation occurred on the roof of the bus. The drag coefficient of the baseline bus without roof rack at 80 km/hr, 100 km/hr and 120 km/hr is 0.6237, 0.6197 and 0.6165 respectively. Therefore, since the values are nearly the same the drag coefficient can be taken as 0.62.

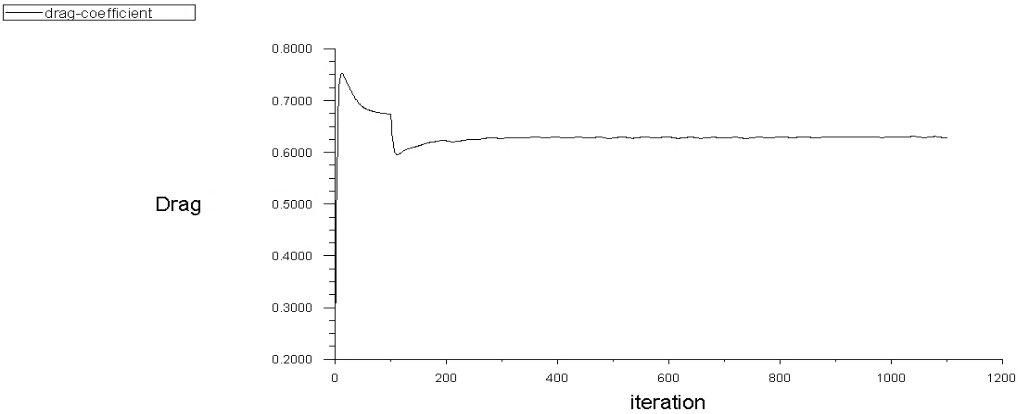

Figure 6.2: Drag coefficient of the baseline bus without roof rack at 80 km/hr

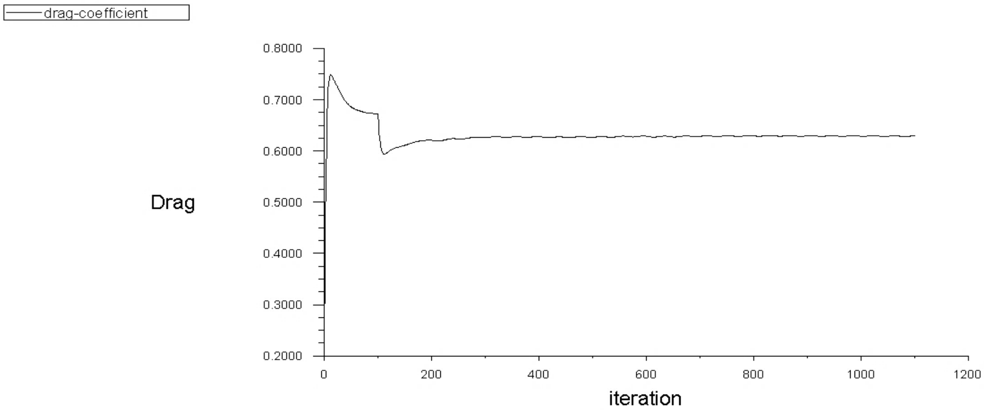

Figure 6.3: Drag coefficient of the baseline bus without roof rack at 100 km/hr

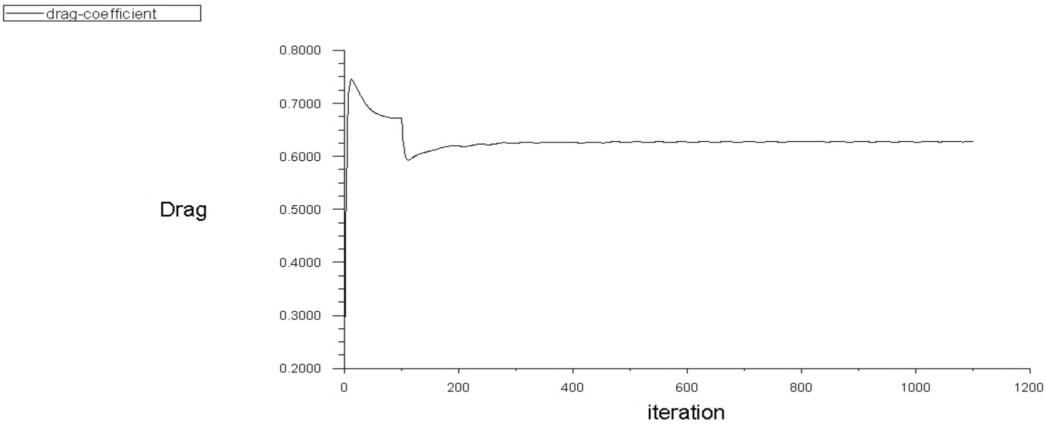

Figure 6.4: Drag coefficient of the baseline bus without roof rack at 120 km/hr

III. Lift Coefficient

As it is shown in Figure 6.5 – 6.7 the lift coefficient of the baseline bus without roof rack at 80 km/hr, 100 km/hr and 120 km/hr is - 0.1875, - 0.1868 and - 0.1804 respectively. Since the values are almost similar, the lift coefficient can be taken as - 0.18. Negative lift is desirable as it tends to increase the contact pressure acting between the wheels and ground. Therefor the baseline bus has better performance regarding lift force.

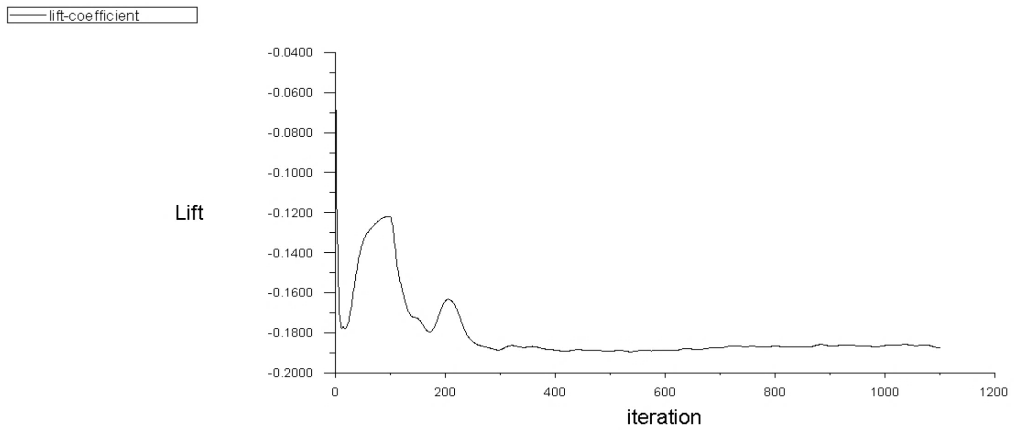

Figure 6.5: Lift coefficient of the baseline bus without roof rack at 80 km/hr

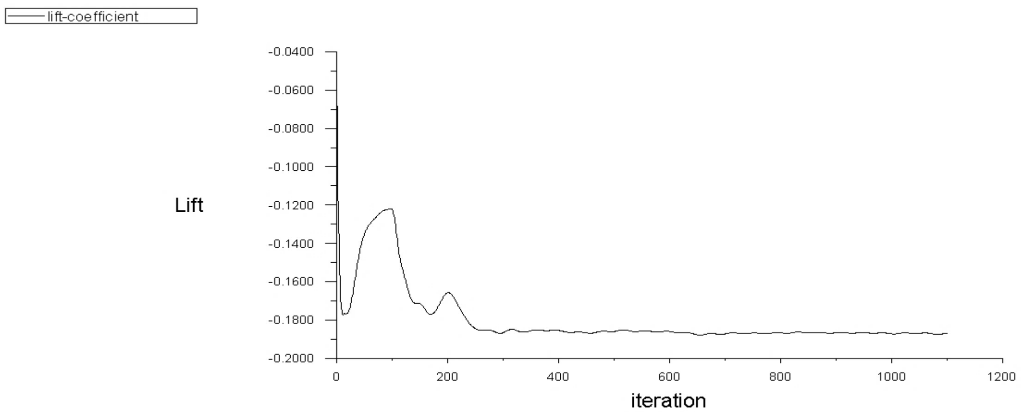

Figure 6.6: Lift coefficient of the baseline bus without roof rack at 100 km/hr

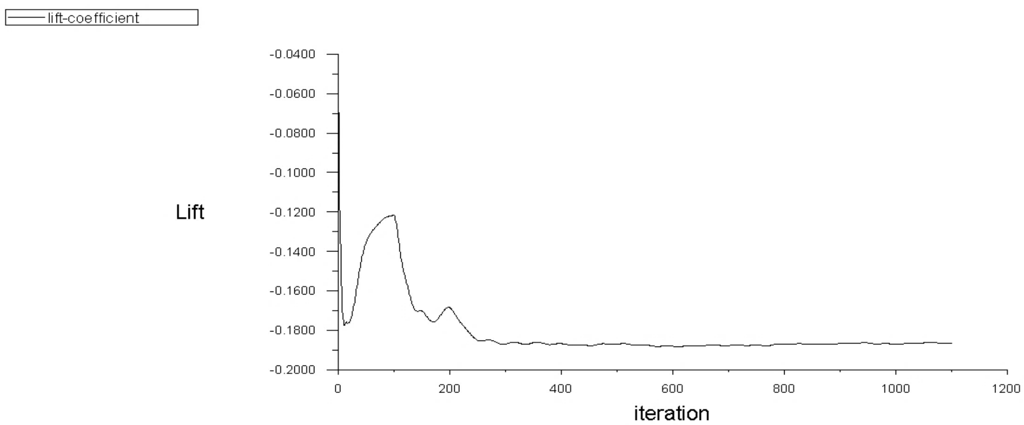

Figure 6.7: Lift coefficient of the baseline bus without roof rack at 120 km/hr

IV. Pressure Contour

As it is seen in Figure 6.8 – 6.10 the pressure at the front face of the bus is very high. The high pressure in the front part of the bus indicates that the velocity is low at that point. The pressure distribution over the bus body is not symmetric and the pressure on the rear is lower than the front, as a result there is rearward directed drag force. The colors on the pressure contour indicate the intensity of the pressure. The red color indicates the maximum pressure and the blue color shows the minimum pressure. The value for each color map is also given on the left of the contour.

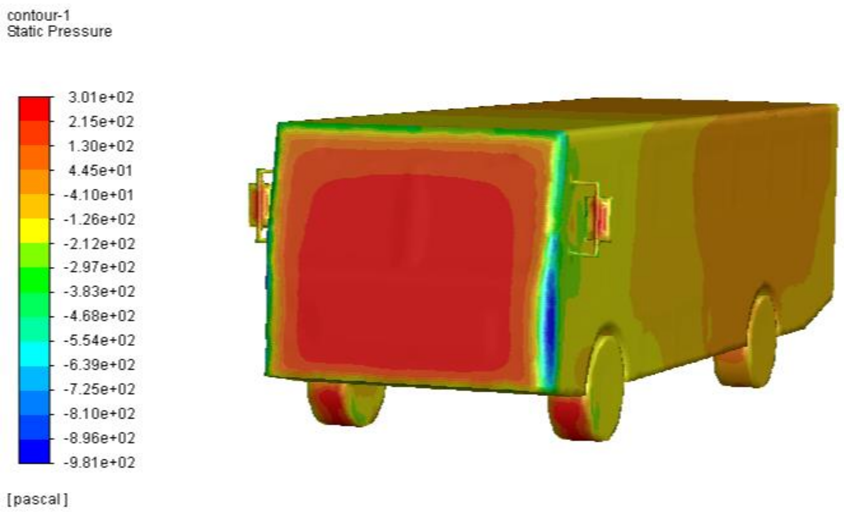

Figure 6.8: Pressure contour of the baseline bus without roof rack at 80 km/hr

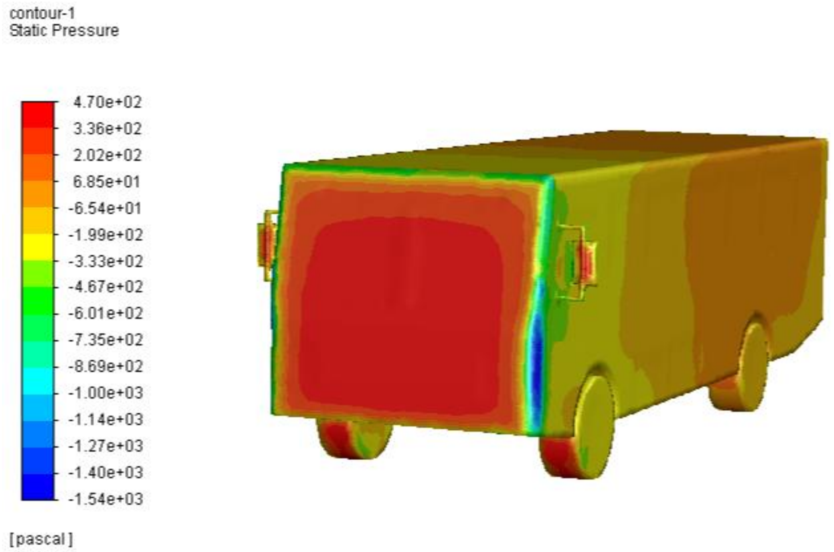

Figure 6.9: Pressure contour of the baseline bus without roof rack at 100 km/hr

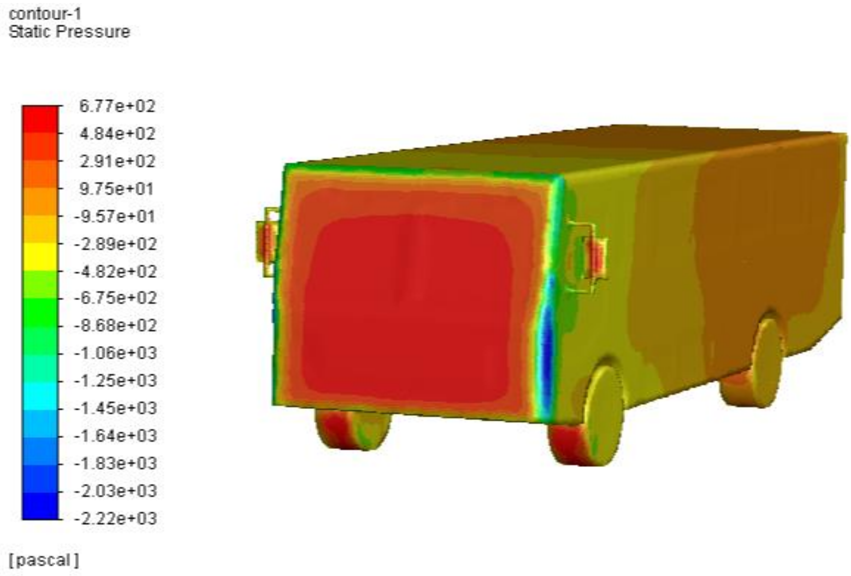

Figure 6.10: Pressure contour of the baseline bus without roof rack at 120 km/hr

V. Velocity Contour

As it is given in Figure 6.11 – 6.13 at the stagnation point the air velocity and pressure reaches its lowest and highest values respectively. Due to the flow separation occurred on the top edge of the bus, turbulence kinetic energy is high over the roof of the bus. When viscous air flows over and past the bus, vortices are created at the rear causing the flow to deviate from the smooth streamline flow. Under these conditions the air flow pressure in front of the bus is higher than atmospheric pressure while the pressure behind is lower than that of the atmosphere, consequently the bus will be sucked in the direction of air movement.

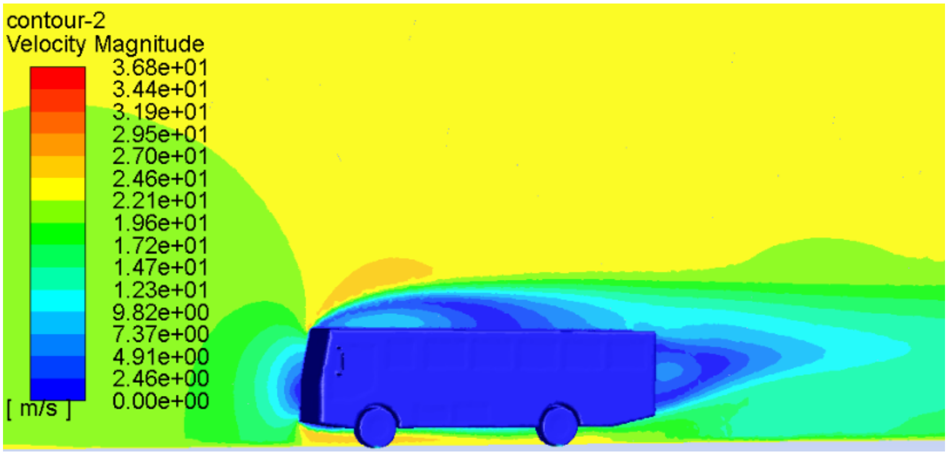

Figure 6.11: Velocity Contour of the baseline bus without roof rack at 80 km/hr

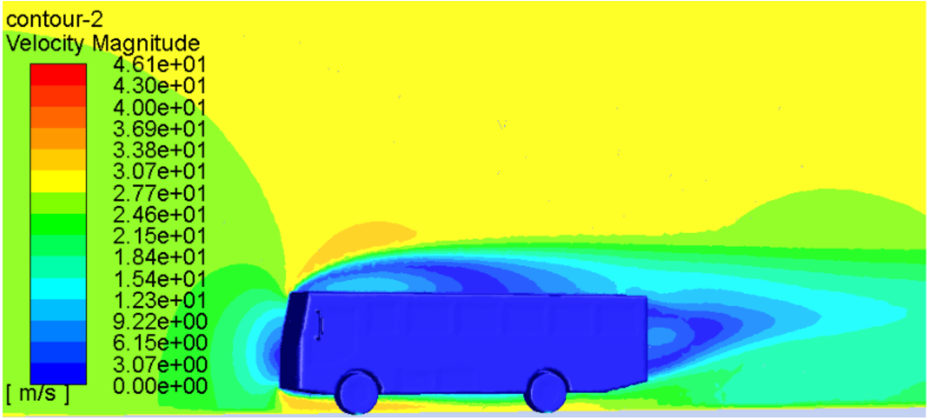

Figure 6.12: Velocity Contour of the baseline bus without roof rack at 100 km/hr

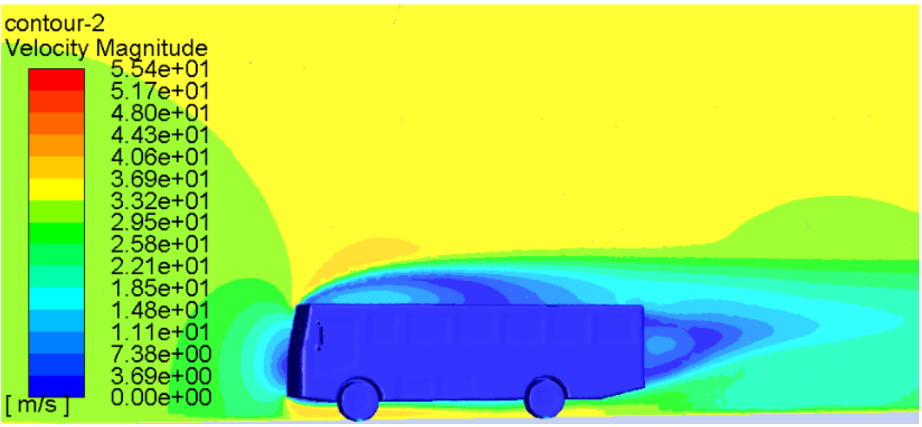

Figure 6.13: Velocity Contour of the baseline bus without roof rack at 120 km/hr

Table 6.1 summarizes the results of the baseline bus without roof rack. According to the result, the drag force increase with respect to the speed of the bus whereas the lift force decreases as the speed of the bus increases in which it tends to increase the contact pressure acting between the wheels and ground.

Table 6.1: Summary of drag and lift coefficients of the baseline model without roof rack

Frontal area (m^2)	**Speed (km/hr)**	**Drag**		**Lift**	
		Drag Coefficient	**Drag Force (N)**	**Lift Coefficient**	**Lift Force (N)**
4.43	80	0.6237	835.55	- 0.1875	- 251.19
	100	0.6197	1297.65	- 0.1868	- 391.15
	120	0.6165	1858.29	- 0.1804	- 543.77

6.1.2 Results of the Baseline Bus with Roof Rack

I. Residual history

The numerical computation is conducted with first-order discretization for the first 100 iterations then second-order scheme is applied for the remaining iterations. The simulation is carried out for 1100 iterations.

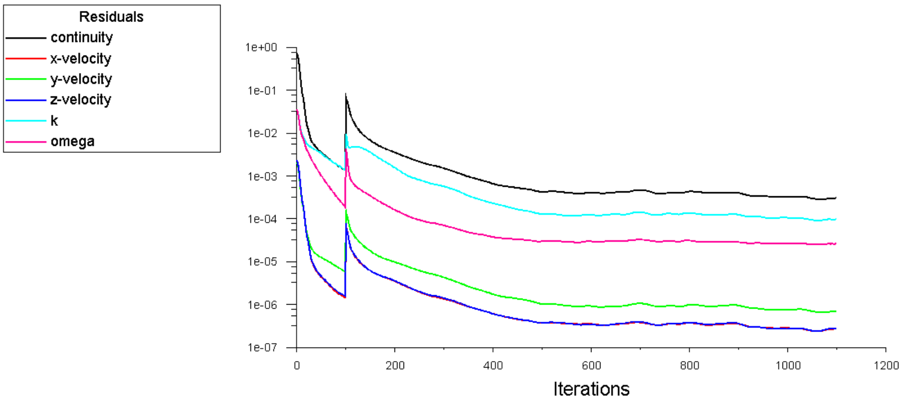

Figure 6.14: Residual history of the baseline bus with roof rack at 80 km/hr

II. Drag Coefficient

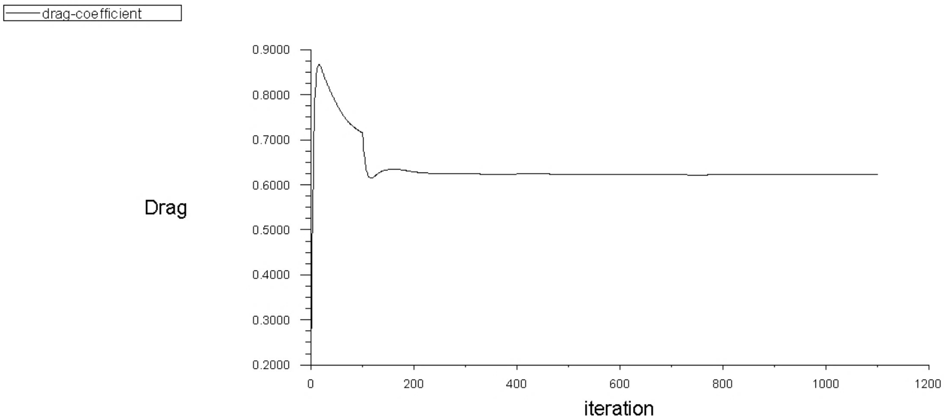

Figure 6.15: Drag coefficient of the baseline bus with roof rack at 80 km/hr

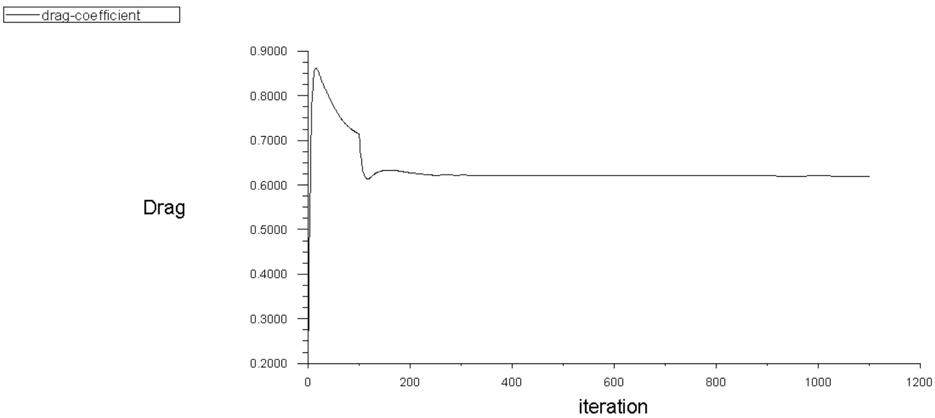

Figure 6.16: Drag coefficient of the baseline bus with roof rack at 100 km/hr

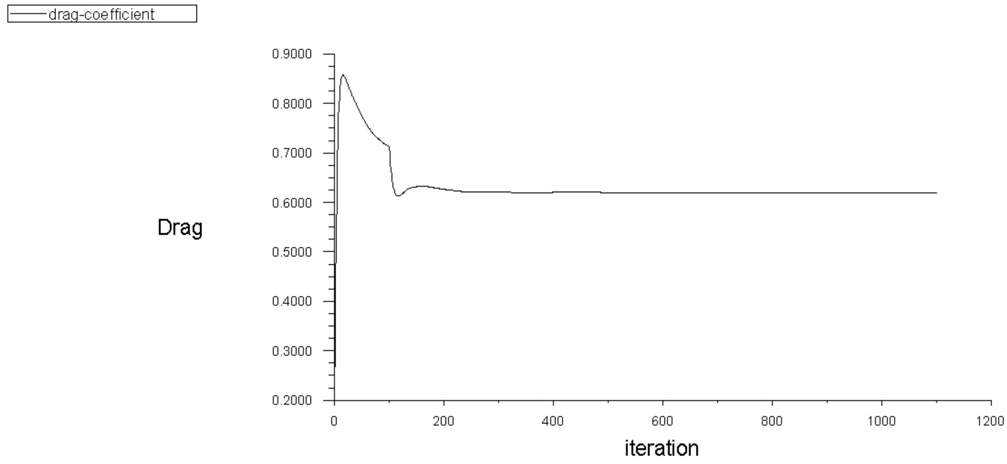

Figure 6.17: Drag coefficient of the baseline bus with roof rack at 120 km/hr

As it is shown in Figure 6.15 – 6.17 the drag coefficient of the baseline bus with roof rack at 80 km/hr, 100 km/hr and 120 km/hr is 0.6242, 0.6208 and 0.6195 respectively. Therefore, since the values are nearly the same the drag coefficient can be taken as 0.62. When comparing the values with the clean roof baseline bus their drag coefficient is almost similar. This is due to the flow separation occurred on the top edge of the bus.

III. Lift Coefficient

As it is shown in Figure 6.18 – 6.20 the lift coefficient of the baseline bus with roof rack at 80 km/hr, 100 km/hr and 120 km/hr is - 0.2052, - 0.1979 and - 0.1859 respectively. The average value of the lift coefficient of the bus with roof rack is - 0.19. Since the lift coefficient is negative, it enhances the tire's road holding.

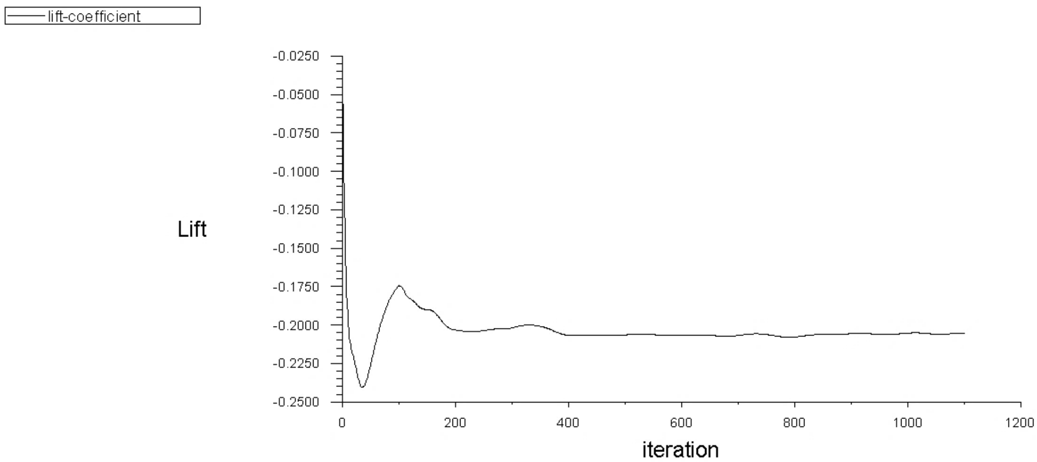

Figure 6.18: Lift coefficient of the baseline bus with roof rack at 80 km/hr

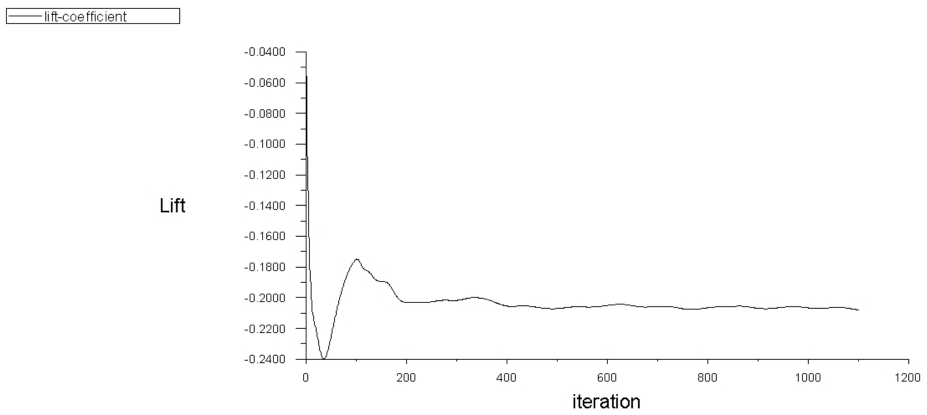

Figure 6.19: Lift coefficient of the baseline bus with roof rack at 100 km/hr

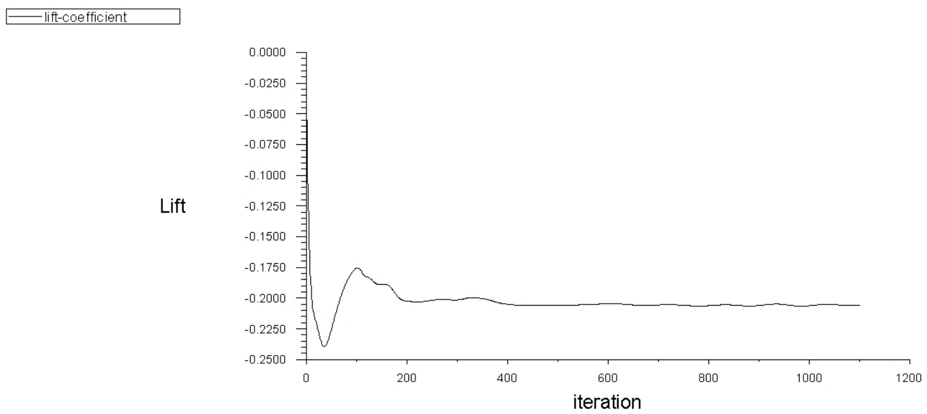

Figure 6.20: Lift coefficient of the baseline bus with roof rack at 120 km/hr

IV. Pressure Contour

As it is seen from Figure 6.21 – 6.23 the pressure in the front part of the bus is very high and it similar with the bus without roof rack. The red color represents the maximum pressure and the blue color represents the minimum pressure. There is a rearward directed drag force, because of the pressure variation between front and rear part of the bus.

Figure 6.21: Pressure contour of the baseline bus with roof rack at 80 km/hr

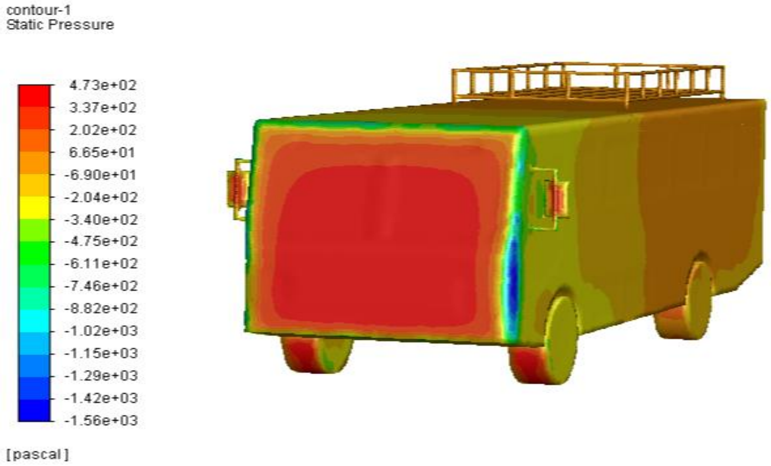

Figure 6.22: Pressure contour of the baseline bus with roof rack at 100 km/hr

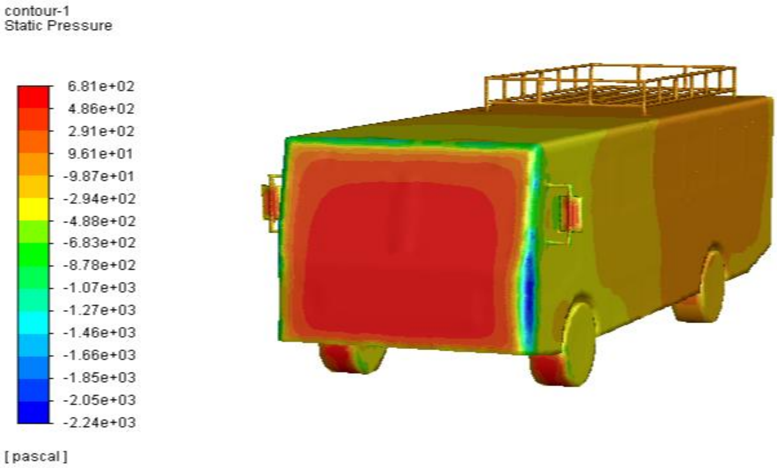

Figure 6.23: Pressure contour of the baseline bus with roof rack at 120 km/hr

As it is shown in the pressure contour the maximum value of the pressure at 80 km/hr, 100 km/hr and 120 km/hr is 303 Pa, 473 Pa and 681 Pa respectively.

V. Velocity Contour

The velocity at the central portion of front face is very less. This value is varied from 0 – 9.85 m/s. The velocity at the rear of the bus (wake region) varied from 0 – 14.8 m/s.

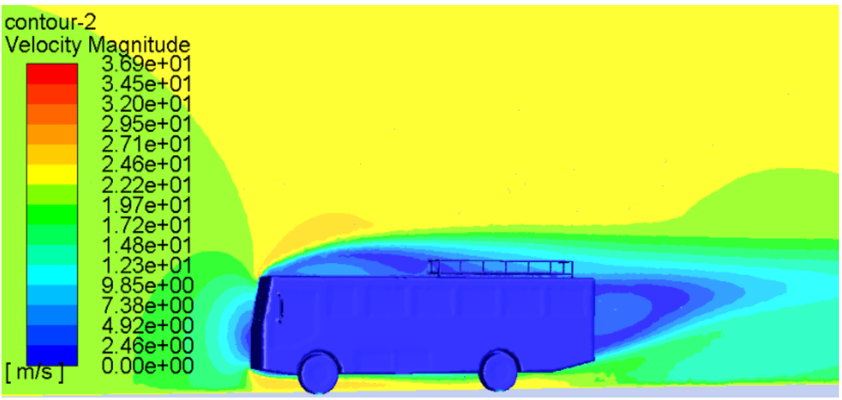

Figure 6.24: Velocity Contour of the baseline bus with roof rack at 80 km/hr

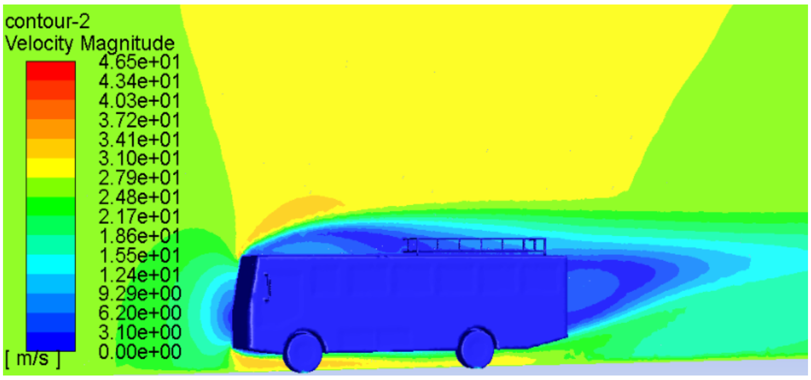

Figure 6.25: Velocity Contour of the baseline bus with roof rack at 100 km/hr

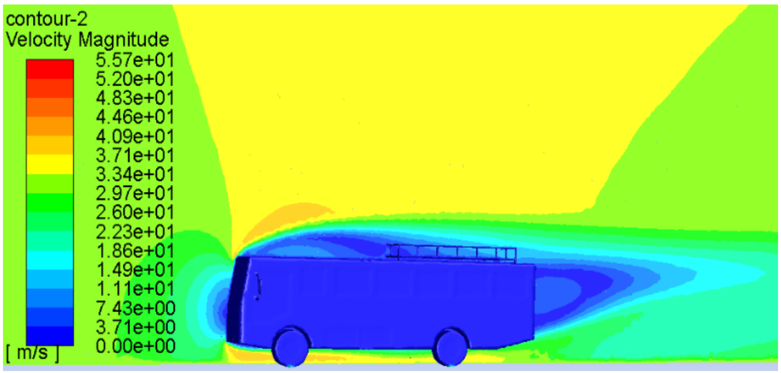

Figure 6.26: Velocity Contour of the baseline bus with roof rack at 120 km/hr

As it is shown in Figure 6.24 – 6.26 the velocity is low in the front and rear part of the bus. Due to the flow separation at the rear of the bus, a suction pressure is created on the wake region of the bus therefore there will be rearward directed drag force.

Table 6.2: Summary of drag and lift coefficients of the baseline model with roof rack

Frontal area (m^2)	**Speed (km/hr)**	**Drag**		**Lift**	
		Drag Coefficient	**Drag Force (N)**	**Lift Coefficient**	**Lift Force (N)**
4.59	80	0.6242	866.42	- 0.2052	- 284.83
	100	0.6208	1346.89	- 0.1979	- 429.37
	120	0.6195	1934.78	- 0.1859	- 580.59

As it is given in Table 6.2 the drag coefficient of the baseline bus with roof rack at 80 km/hr, 100 km/hr and 120 km/hr is 0.6242, 0.6208 and 0.6195 respectively. Whereas the lift coefficient -0.2052, -0.1979 and -0.1859 respectively. Therefore, the average value of drag coefficient and lift coefficient is 0.62 and – 0.19. Due to the flow separation occurred on the top edge of the bus with roof rack, there is a very high turbulence on the roof of the bus.

6.1.3 Results of the Baseline Bus with Luggage

I. Residual History

The simulation is carried out for 1100 iterations.

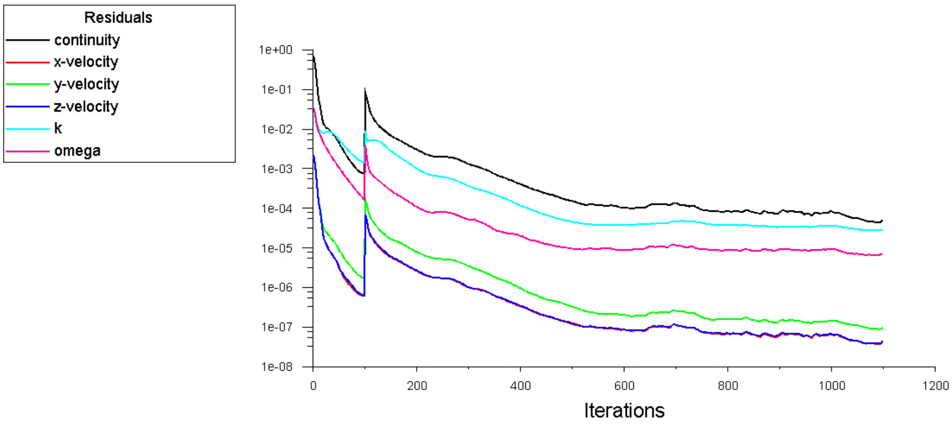

Figure 6.27: Residual history of the baseline bus with luggage at 80 km/hr

II. Drag Coefficient

As it is shown in Figure 6.28 – 6.30 the average value of the drag coefficient of the bus with luggage is 0.62.

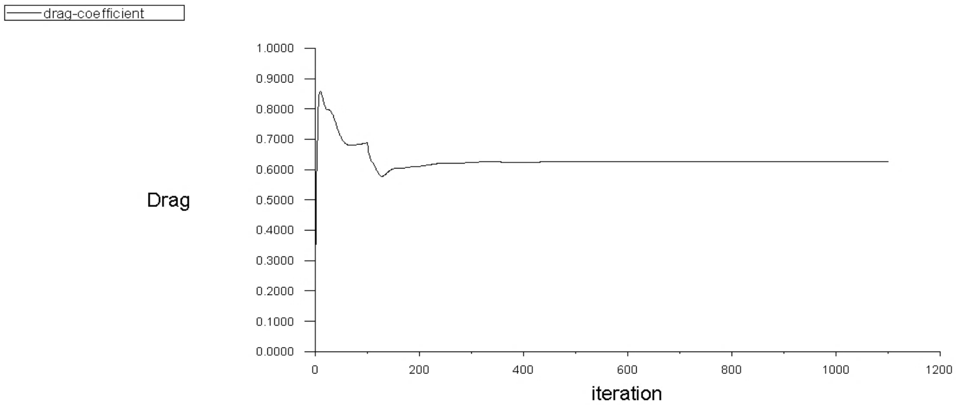

Figure 6.28: Drag coefficient of the baseline bus with luggage at 80 km/hr

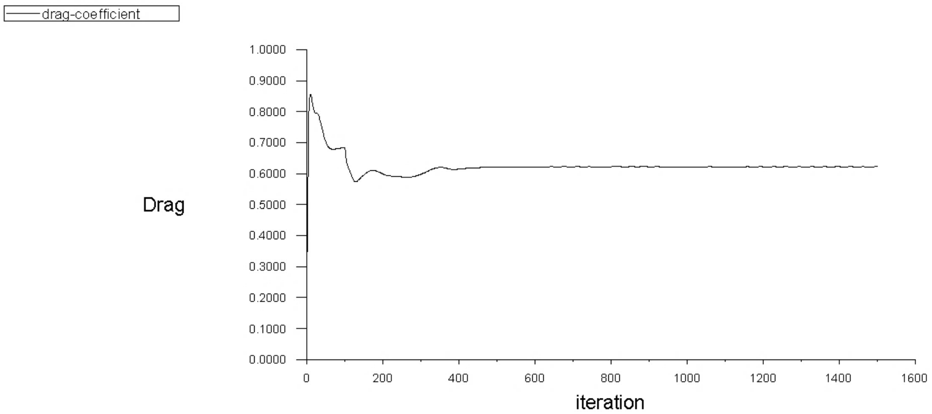

Figure 6.29: Drag coefficient of the baseline bus with luggage at 100 km/hr

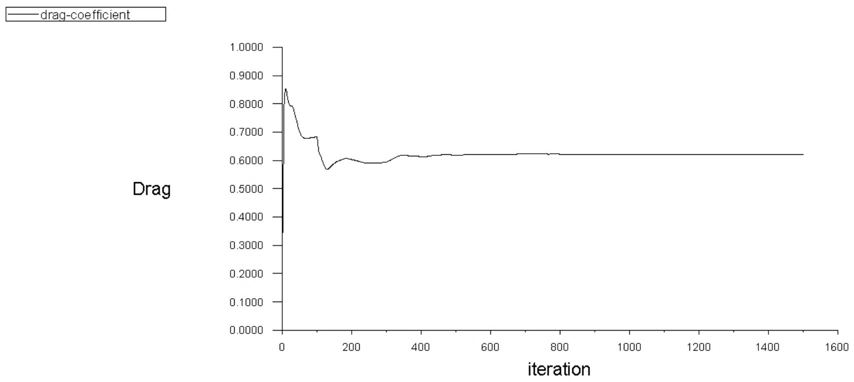

Figure 6.30: Drag coefficient of the baseline bus with luggage at 120 km/hr

The drag coefficient of the baseline bus with luggage at 80 km/hr, 100 km/hr and 120 km/hr is 0.6256, 0.6222 and 0.6218 respectively. Therefore, since the values are nearly the same the drag coefficient can be taken as 0.62. The drag coefficient of all the baseline buses is almost the same.

III. Lift Coefficient

As it is shown in Figure 6.31 – 6.33 the lift coefficient of the baseline bus with luggage at 80 km/hr, 100 km/hr and 120 km/hr is - 0.1570, - 0.1551 and - 0.1532 respectively. On average it can be taken as -0.15.

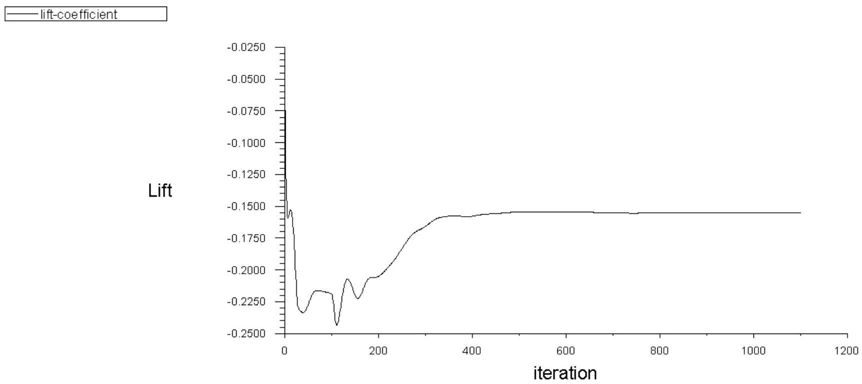

Figure 6.31: Lift coefficient of the baseline bus with luggage at 80 km/hr

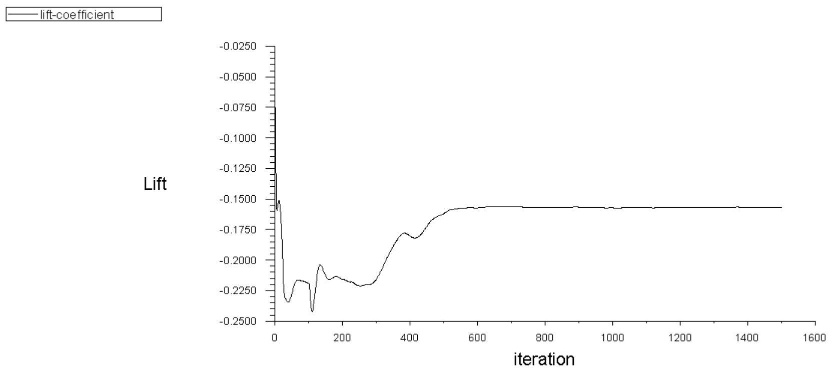

Figure 6.32: Lift coefficient of the baseline bus with luggage at 100 km/hr

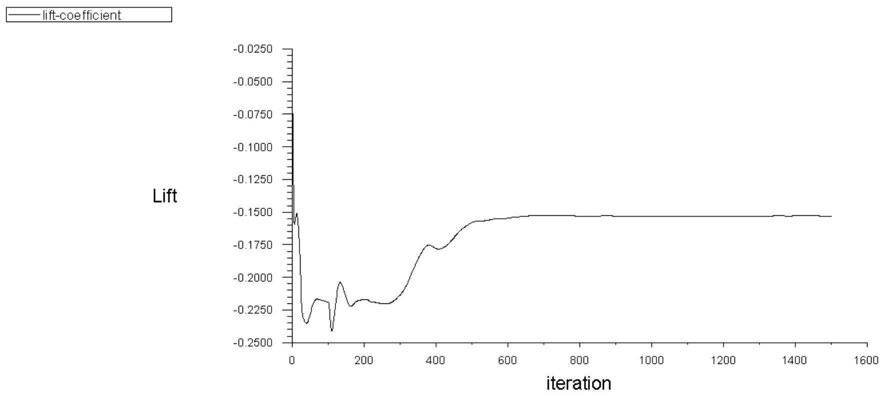

Figure 6.33: Lift coefficient of the baseline bus with luggage at 120 km/hr

IV. Pressure Contour

As it is seen in Figure 6.34 – 6.36 the pressure at the front face of the bus is very high. The colors on the pressure contour indicate the intensity of the pressure. The red color indicates the maximum pressure and the blue color shows the minimum pressure. The value for each color map is also given on the left of the contour.

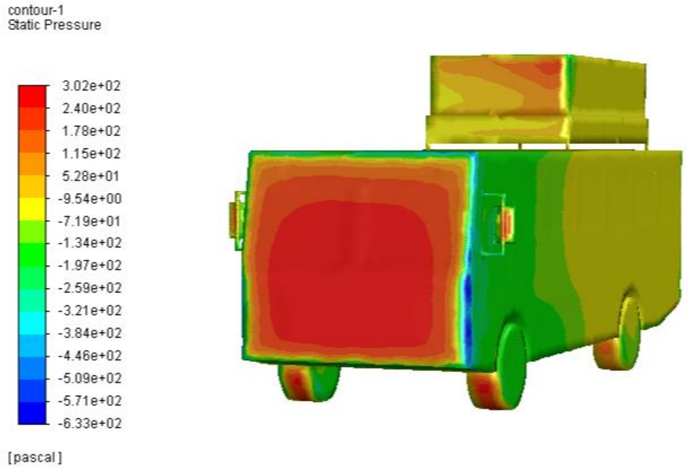

Figure 6.34: Pressure contour of the baseline bus with luggage at 80 km/hr

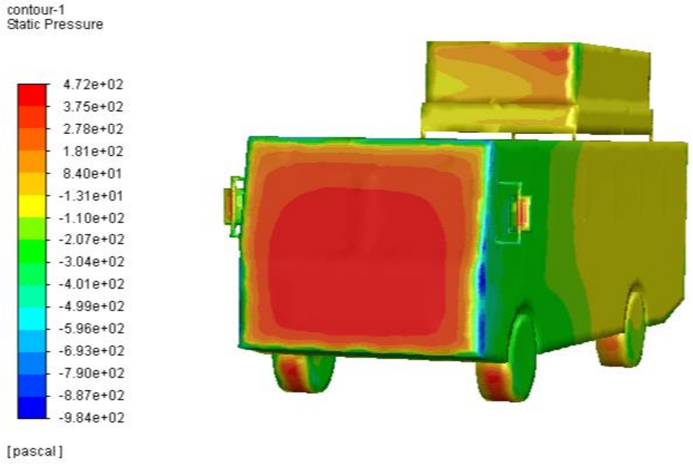

Figure 6.35: Pressure contour of the baseline bus with luggage at 100 km/hr

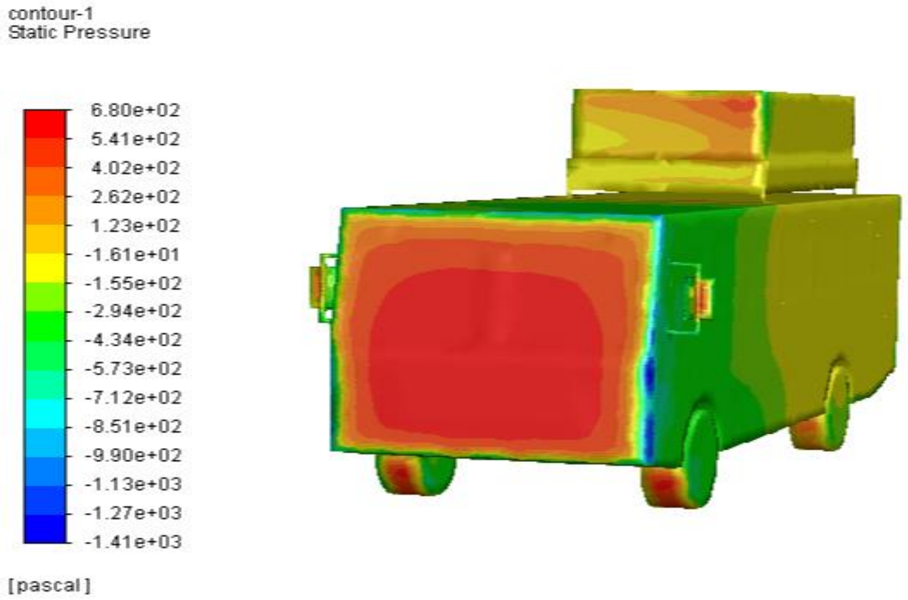

Figure 6.36: Pressure contour of the baseline bus with luggage at 120 km/hr

As it is shown in the pressure contour the maximum value of the pressure at 80 km/hr, 100 km/hr and 120 km/hr is 302 Pa, 472 Pa and 680 Pa respectively.

V. Velocity Contour

The velocity at the central portion of front face is very less. This value is varied from 0 – 8.26 m/s. The velocity at the rear of the bus (wake region) varied from 0 – 12.4 m/s.

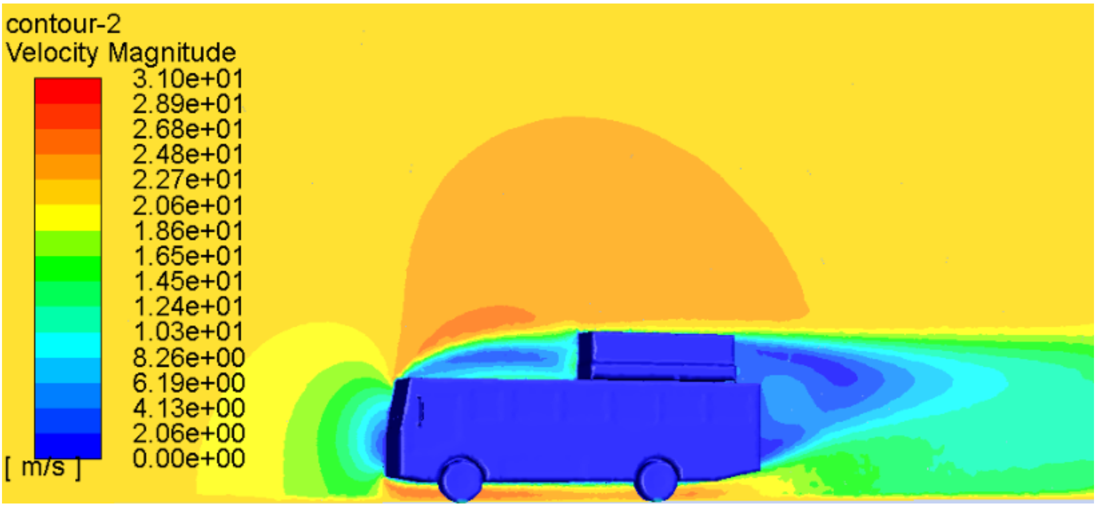

Figure 6.37: Velocity Contour of the baseline bus with luggage at 80 km/hr

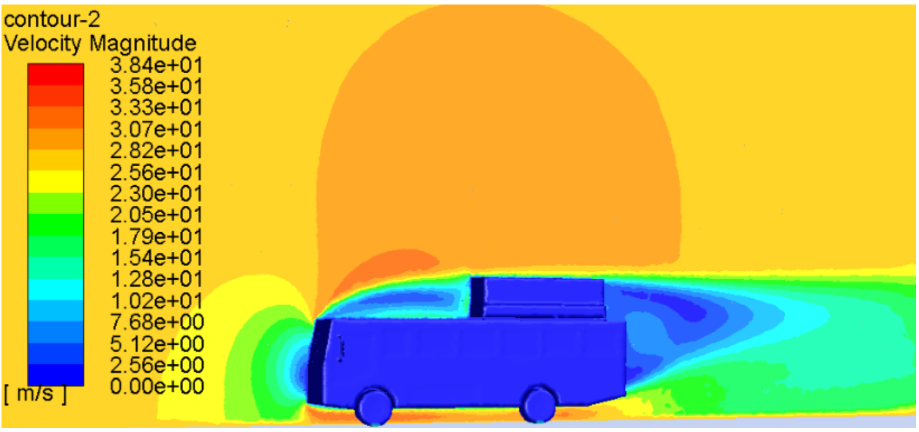

Figure 6.38: Velocity Contour of the baseline bus with luggage at 100 km/hr

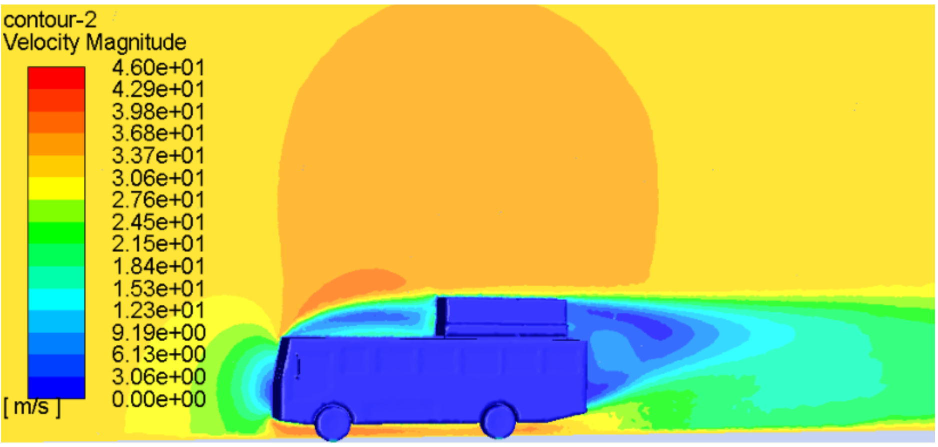

Figure 6.39: Velocity Contour of the baseline bus with luggage at 120 km/hr

The suction pressure created on the wake region due to rapid flow acceleration is much higher in the bus with luggage therefore there will be rearward directed drag force. In case of the bus loaded with luggage it is observed that the wake formation is much higher compared to the bus without roof rack and with rack. Therefore it increases the drag force and affects the performance.

Table 6.3: Summary of drag and lift coefficients of the baseline model with luggage

Frontal area (m^2)	**Speed (km/hr)**	**Drag**		**Lift**	
		Drag Coefficient	**Drag Force (N)**	**Lift Coefficient**	**Lift Force (N)**
5.75	80	0.6256	1087.87	- 0.155	- 272.99
	100	0.6222	1691.09	- 0.157	- 421.55
	120	0.6218	2432.74	- 0.153	- 599.38

6.1.4 Results of the Modified Bus

I. Aerodynamic analysis of the modified bus at different inclination angle

A wind deflector encourages the air to flow smoothly over the roof of the bus in which it avoids the flow separation occurred on the top edge of the bus and the turbulence kinetic energy on the roof of the bus reduced. Therefore, to improve the aerodynamic performance of the modified bus a wind deflector is fitted on the front top part of the bus which is one part of the luggage compartment. However, the performance of the wind deflector depends on its inclination angle. Thus, to select the optimum inclination angle of the wind deflector five different angles were selected. In all models the procedure followed to create the geometry and to generate the mesh were similar. The CFD analysis is carried out at a speed of 120 km/hr for each case. Finally, the wind deflector with better aerodynamic performance will be selected. The drag and lift coefficient at each angle is given in the table given below.

Table 6.4: Effect of deflector angle on drag coefficient and lift coefficient

Deflector Inclination Angle (^{0})	**Drag Coefficient**	**Lift Coefficient**
20	0.414	-0.134
25	0.411	-0.137
30	0.417	-0.136
35	0.427	-0.138
40	0.437	-0.143

According to Table 6.4, the drag coefficient is less at an inclination angle of 25^0 this implies that the streamline shape of the bus body enables it to move easily through the surrounding viscous air with minimum resistance and when the angle exceeds or lessens this angle, the drag coefficient increases.

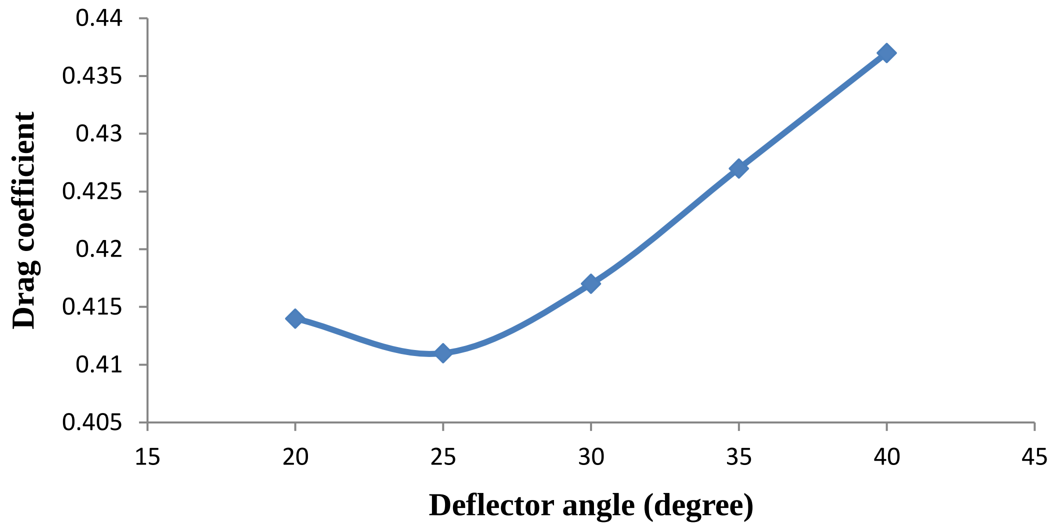

Figure 6.40: Effect of inclination angle of the wind deflector on drag coefficient

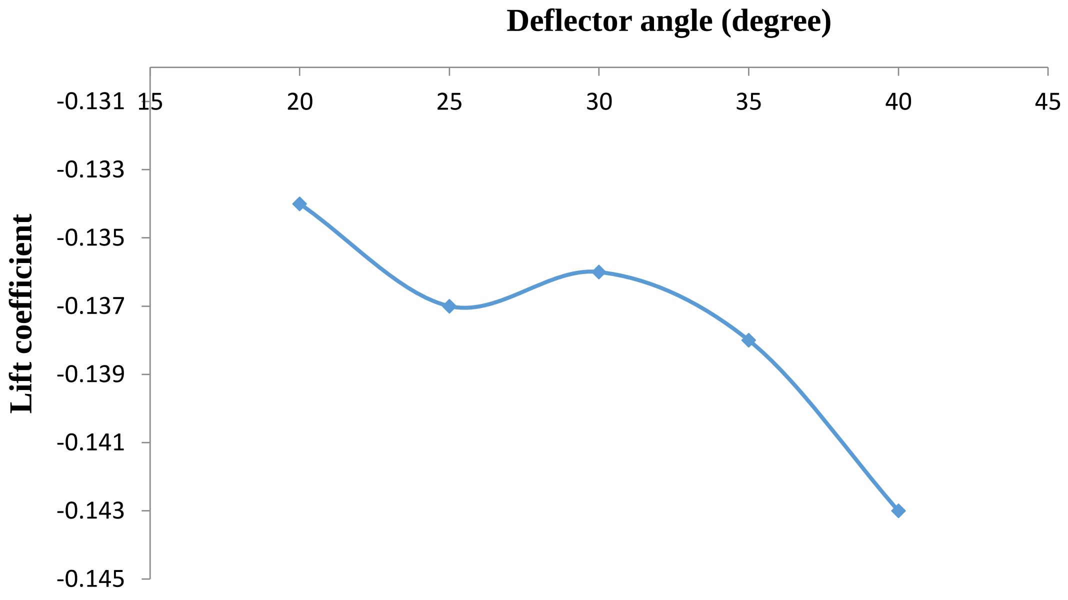

Figure 6.41: Effect of inclination angle of the wind deflector on lift coefficient

According to Figure 6.40 – 6.41, better lift coefficient is obtained at an angle of 40^0 but at this angle the drag coefficient is high as compared to others. The lift coefficient is negative in all inclination angles and the deviation between them is very less. The negative lift coefficient implies that it tends to increase the contact pressure acting between the wheels and the ground. Therefore, it is possible to select the inclination angle of the deflector based on drag coefficient and inclination angle of 25^0 is selected.

II. Residual History

The numerical computation is conducted with first-order discretization for the first 100 iterations then second-order scheme is applied for the remaining iterations. The simulation is carried out for 1100 iterations.

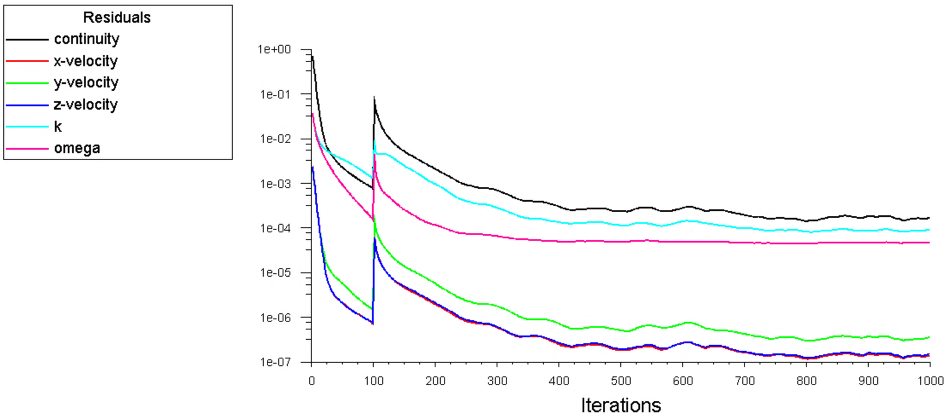

Figure 6.42: Residual history of the modified bus at 80 km/hr

III. Drag Coefficient

As Figure 6.43 – 6.45 shows, the average drag coefficient of the modified bus is 0.41.

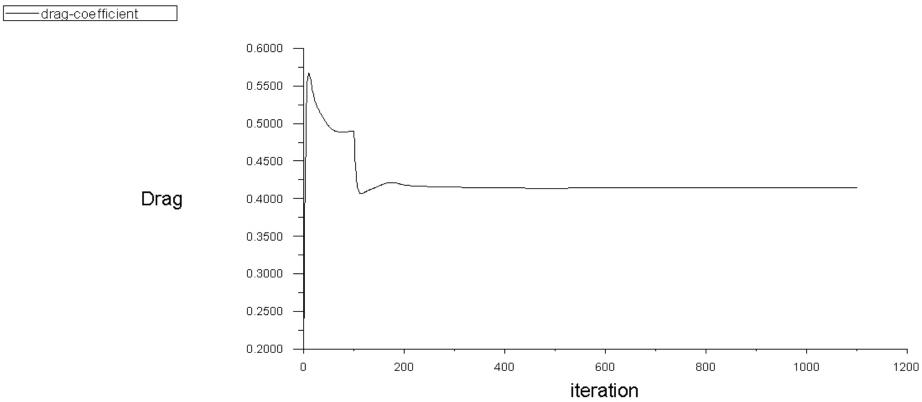

Figure 6.43: Drag coefficient of the modified bus at 80 km/hr

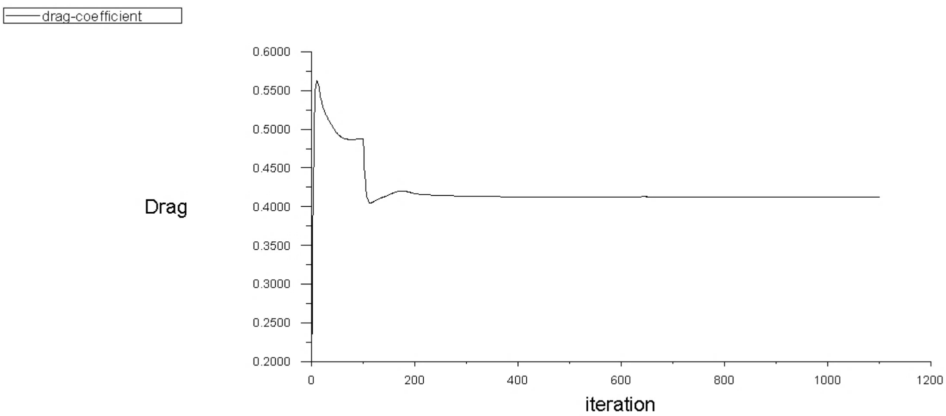

Figure 6.44: Drag coefficient of the modified bus at 100 km/hr

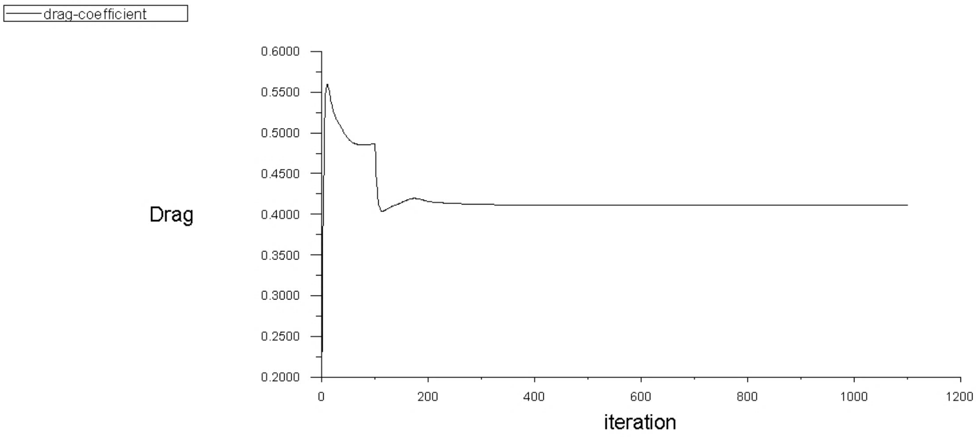

Figure 6.45: Drag coefficient of the modified bus at 120 km/hr

According to Figure 6.43 – 6.45, the drag coefficient of the modified bus at 80 km/hr, 100 km/hr and 120 km/hr is 0.4142, 0.4126 and 0.4113 respectively. Therefore, since the values are nearly the same the drag coefficient can be taken as 0.41. This shows that the modification made to the existing bus improved the drag coefficient of the bus. As a result, the drag force of the modified bus is minimum compared to the existing bus. In general, the aerodynamic performance of the modified bus is better than the existing bus.

IV. Lift Coefficient

As it is shown in Figure 6.46 – 6.48, the lift coefficient of the modified bus at 80 km/hr, 100 km/hr and 120 km/hr is - 0.1435, - 0.1426 and - 0.1376 respectively. The average lift coefficient of the modified bus is - 0.14.

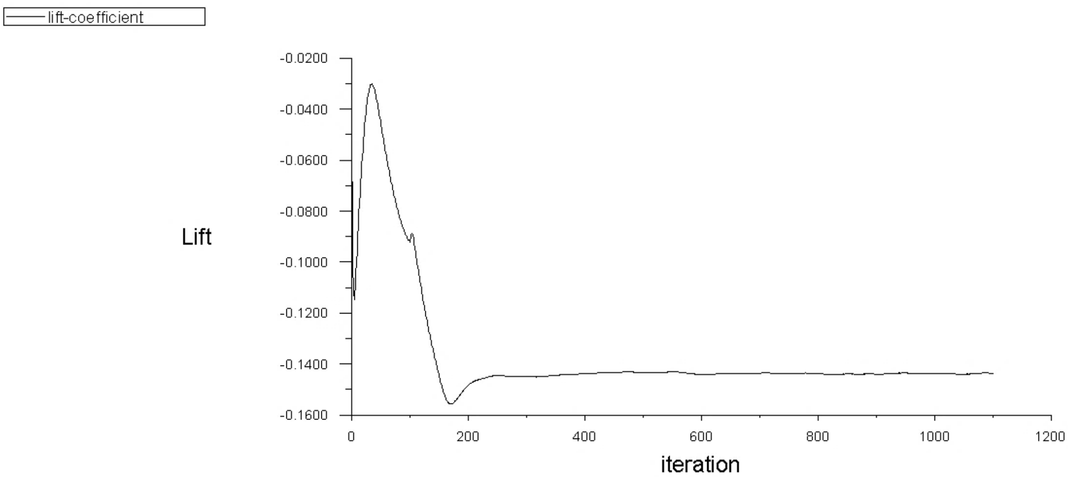

Figure 6.46: Lift coefficient of the modified bus at 80 km/hr

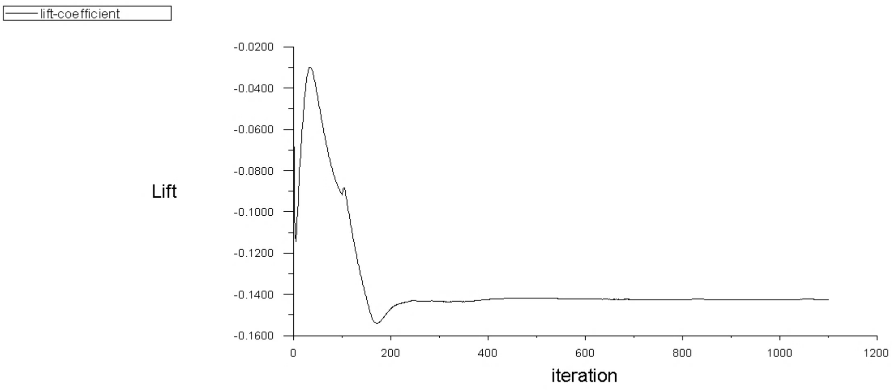

Figure 6.47: Lift coefficient of the modified bus at 100 km/hr

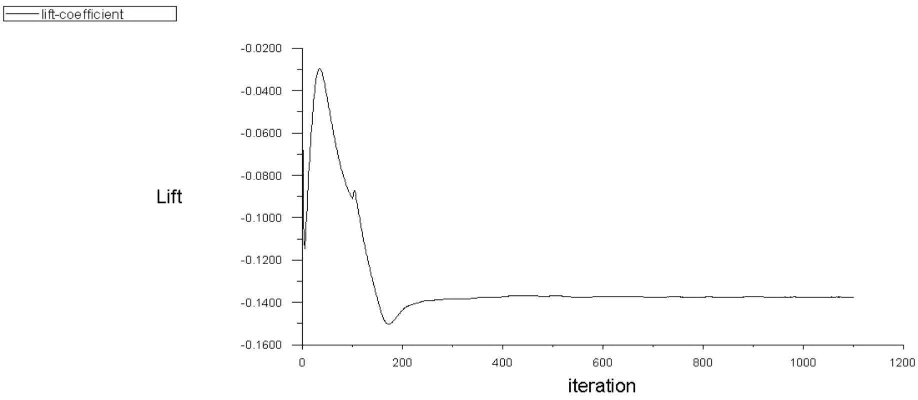

Figure 6.48: Lift coefficient of the modified bus at 120 km/hr

V. Pressure Contour

In all of the selected speeds the pressure at the front face of the bus is very high. As it is seen in Figure 6.49 – 6.51 the pressure in the frontal part of the bus is very high. Since no modification is made on the front of the bus, the pressure distribution of the modified bus is similar with the existing bus. However, the overall performance of the modified bus is improved.

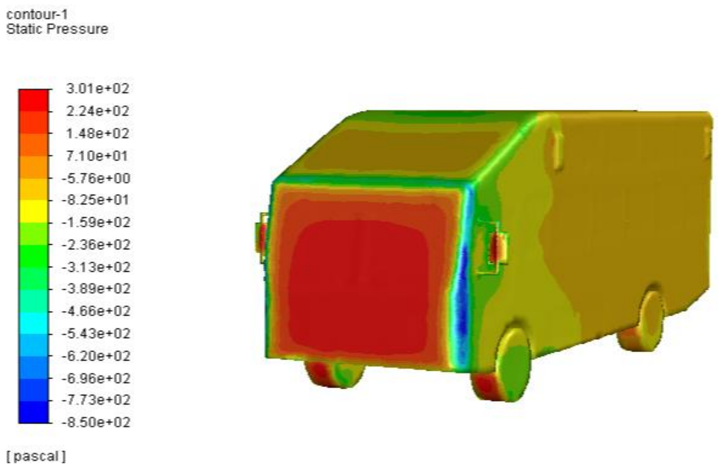

Figure 6.49: Pressure contour of the modified bus at 80 km/hr

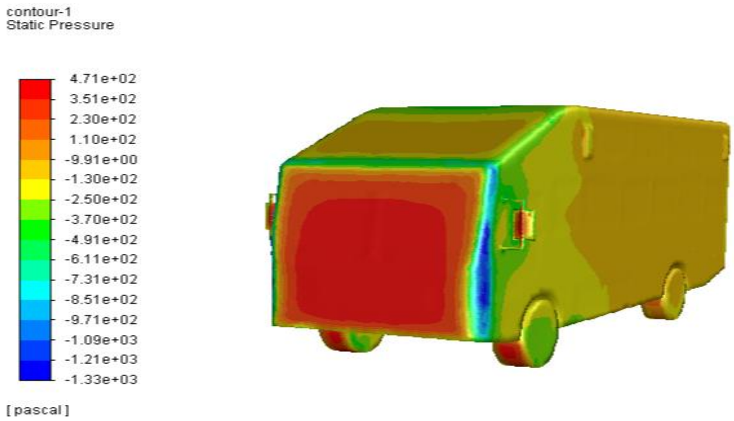

Figure 6.50: Pressure contour of the modified bus at 100 km/hr

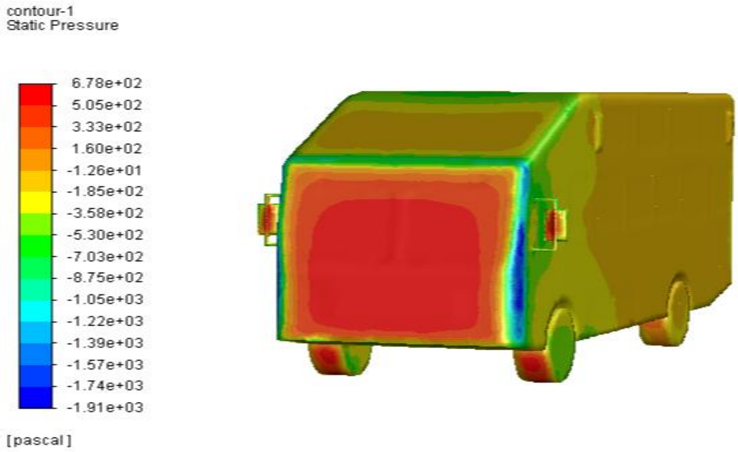

Figure 6.51: Pressure contour of the modified bus at 120 km/hr

As it is shown in the pressure contour the maximum value of the pressure at 80 km/hr, 100 km/hr and 120 km/hr is 301 Pa, 471 Pa and 678 Pa respectively.

VI. Velocity Contour

The velocity at central portion of front face is very less. The wind deflector which is fitted on the top front part of the bus minimizes flow separation occurring on the top edge of the bus.

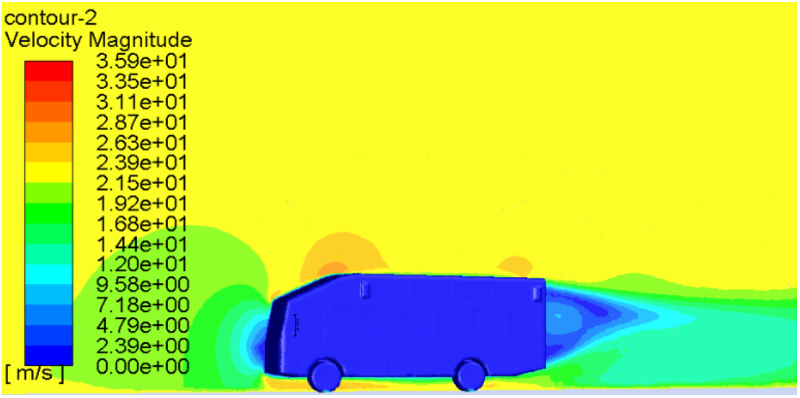

Figure 6.52: velocity contour of the modified bus at 80 km/hr

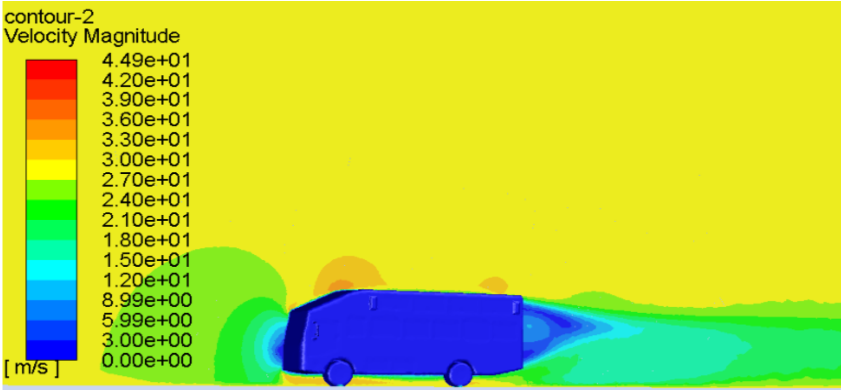

Figure 6.53: velocity contour of the modified bus at 100 km/hr

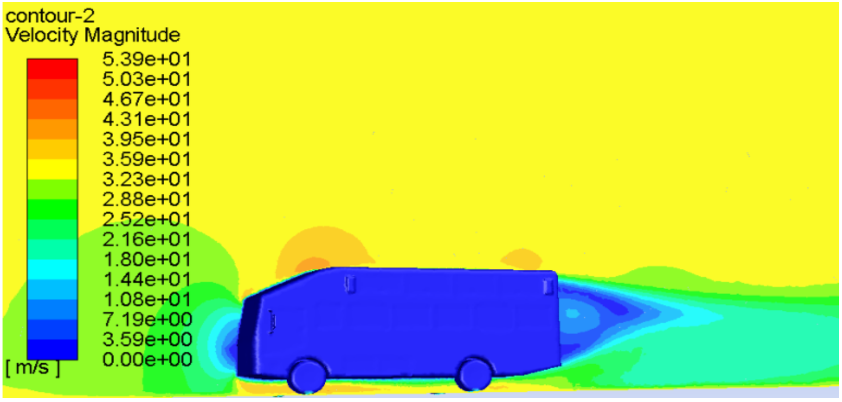

Figure 6.54: velocity contour of the modified bus at 120 km/hr

The roof of the baseline bus had two areas that are of special interest for implementing aerodynamic measures. The first area was the top edge of the bus and the second area was the luggage loaded on the bus. Therefore in order to address this problem a wind deflector is fitted on the top front part of the bus. As it is seen from the velocity contours the installed wind deflector minimizes flow separation occurring on the top edge of the bus. The suction pressure created on the wake region is minimum compared to the baseline buses.

Table 6.5: Summary of drag and lift coefficients of the modified bus

Frontal area (m^2)	Speed (km/hr)	Drag		Lift	
		Drag Coefficient	Drag Force (N)	Lift Coefficient	Lift Force (N)
5.93	80	0.4142	743.44	- 0.1435	- 257.70
	100	0.4126	1157.53	- 0.1426	- 399.96
	120	0.4113	1660.87	- 0.1376	- 555.65

6.2 Comparison between Models

6.2.1 Comparison between Baseline Buses

I. Comparison of baseline bus with and without roof rack

Comparison in terms of Frontal Area

$$\%\ \text{Frontal area increase} = \frac{4.59 - 4.43}{4.43} \times 100 = 3.62\ \%$$

Therefore, the frontal area of the baseline bus with roof rack is increased by 3.62 % as compared to the bus with no roof rack.

Comparison in terms Drag Force

Percentage of drag Force increase at 80,100,120 km/hr.

$$\%\ Drag\ force\ \ increase\ = \frac{866.42 - 835.55}{835.55} \times 100 = 3.69\ \% \ldots\ldots\ldots\ldots..(80\ km/hr)$$

$$\%\ Drag\ force\ \ increase\ = \frac{1346.89 - 1297.65}{1297.65} \times 100 = 3.79\ \% \ldots\ldots..(100\ km/hr)$$

$$\%\ Drag\ force\ \ increase\ = \frac{1934.78 - 1858.29}{1858.29} \times 100 = 4.11\ \% \ldots\ldots..(120\ km/hr)$$

Therefore, the drag force of the baseline bus with roof rack is increased by 3.69 %, 3.79 % and 4.11 % at 80 km/hr, 100 km/hr and 120 km/hr respectively as compared to the bus with no roof rack.

II. Comparison of baseline bus without roof rack and with luggage

Comparison in terms of Frontal Area

$$\%\ \text{Frontal area increase} = \frac{5.75 - 4.43}{4.43} \times 100 = 23.79\ \%$$

Therefore, the frontal area of the baseline bus with luggage is increased by 23.79 % as compared to the bus with no roof rack.

Comparison in terms of Drag Force

Percentage of drag Force increase at 80,100,120 km/hr.

$$\% \text{ Drag force increase } = \frac{1087.82 - 835.55}{835.55} \times 100 = 30.19\ \% \ldots\ldots..(80\ km/hr)$$

$$\% \text{ Drag force increase } = \frac{1691.09 - 1297.65}{1297.65} \times 100 = 30.32\ \% \ldots.(100\ km/hr)$$

$$\% \text{ Drag force increase } = \frac{2432.74 - 1858.29}{1858.29} \times 100 = 30.91\ \% \ldots.(120\ km/hr)$$

Therefore, the drag force of the baseline bus with luggage is increased by 30.19 %, 30.32 % and 30.91 % at 80 km/hr, 100 km/hr and 120 km/hr respectively as compared to the bus with no roof rack.

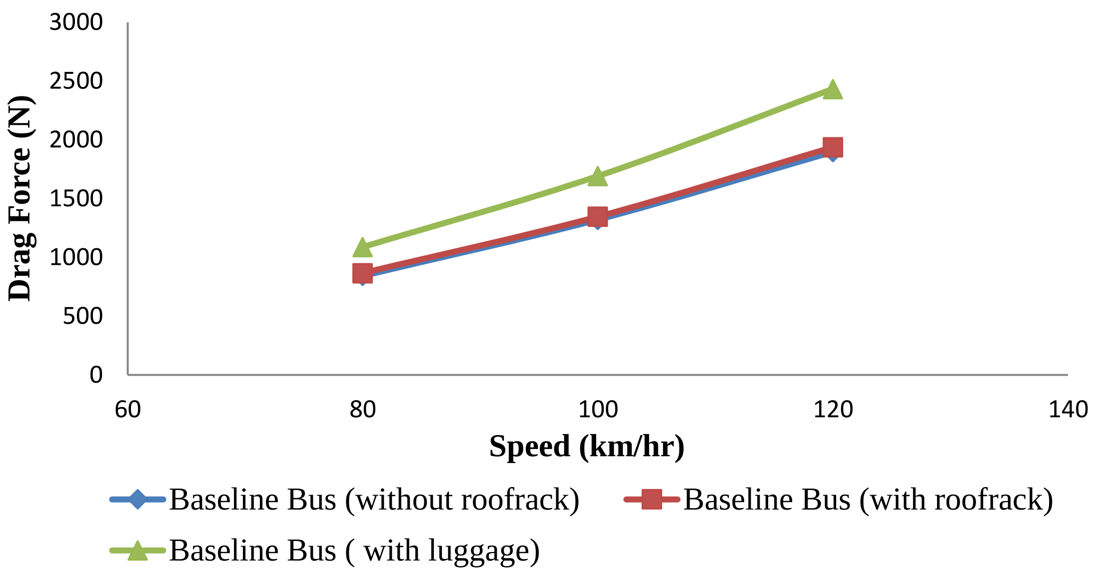

Figure 6.55: Drag force Comparison of the baseline bus

Finally, it is known that if the bus is loaded with a luggage of 70 cm high the drag force will increased by 30.19 %, 30.32 % and 30.91 % at 80 km/hr, 100 km/hr and 120 km/hr respectively. Since there is no rule which limit the maximum height of the luggage, the drag force will increase as the height on the loaded luggage increases. Therefore, there has to be a mechanism which will improve this problem by reducing the frontal projected area and drag coefficient.

6.2.2 Comparison between the Existing Bus and Modified Bus

Table 6. 6: Drag and lift of the existing bus and the modified bus

Case	Frontal Area (m^2)	Speed (km/hr)	Drag		Lift	
			Drag Coefficient	Drag Force (N)	Lift Coefficient	Lift Force (N)
Baseline Bus Without Roof Rack	4.43	80	0.6237	835.55	- 0.1875	- 251.19
		100	0.6197	1297.65	- 0.1868	- 391.15
		120	0.6165	1858.29	- 0.1804	- 543.77
Baseline Bus With Roof Rack	4.59	80	0.6242	866.42	- 0.2052	- 284.83
		100	0.6208	1346.89	- 0.1979	- 429.37
		120	0.6195	1934.78	- 0.1859	- 580.59
Baseline Bus With Luggage	5.75	80	0.6256	1087.82	- 0.1570	- 272.99
		100	0.6222	1691.09	- 0.1551	- 421.55
		120	0.6218	2432.74	- 0.1532	- 599.38
Modified Bus	5.93	80	0.4142	743.44	- 0.1435	- 257.70
		100	0.4126	1157.53	- 0.1426	- 399.96
		120	0.4113	1660.89	- 0.1376	- 555.65

As it is given in Table 6.6, the drag coefficient of the existing buses is almost similar; this is due to the front top edge of the bus and the wake formation at the rear of the bus. However, since their projected area is different their drag force is different. Additionally, the frontal area of the modified bus is higher than the existing bus due to the addition of the luggage compartment but it is relatively close to the existing bus loaded with luggage, whereas the drag coefficient of the modified bus is lower than the existing buses. Since aerodynamic drag of depends on drag coefficient and projected frontal area, the drag force of the modified bus is low compared to the existing bus. A negative lift is desirable as it tends to increase the contact pressure acting between the wheels and the ground. The negative sign indicates the direction of the force. Therefore, according to Table 6.6, the lift force of the existing bus and the modified bus enhances the tire's road holding. The down force of the bus increases with respect to the speed of the bus which is desirable.

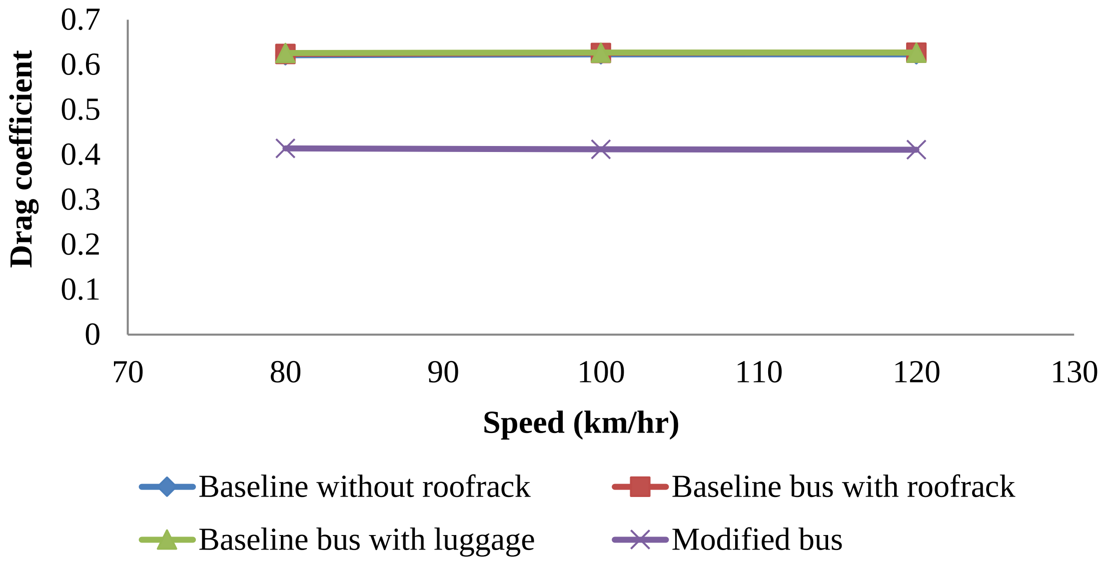

Figure 6.56: Drag coefficient comparison of all models at different speed

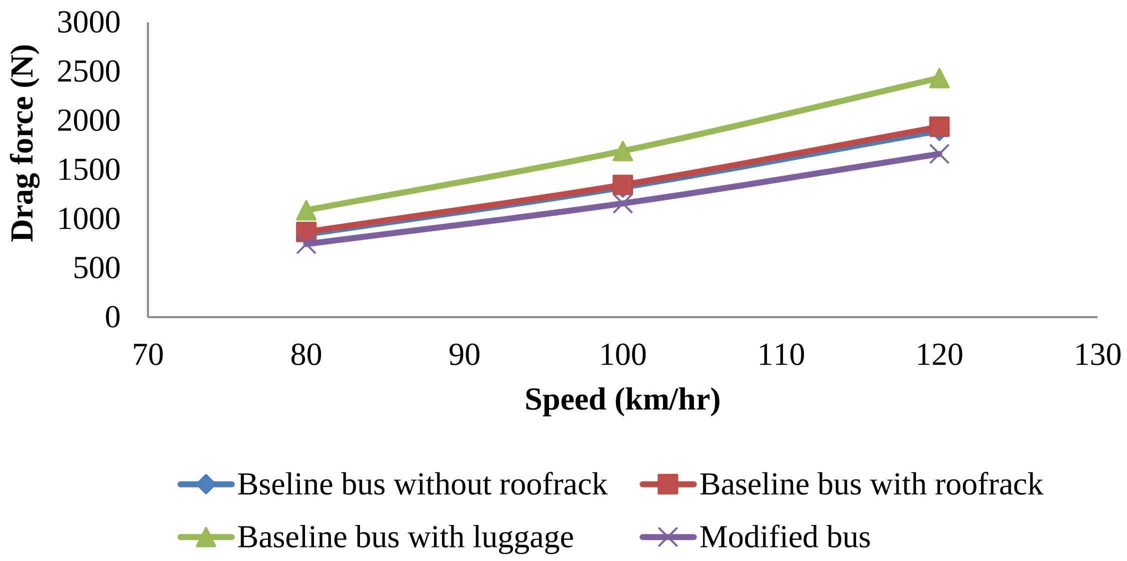

Figure 6.57: Drag force comparison of all models at different speed

The lines that show the drag coefficient of the existing bus overlaps this imply that their drag coefficient is almost similar and it is higher than the modified bus. . However, since different cases were considered to study the aerodynamic performance of the existing bus there frontal area is different this results the drag force of the baseline bus with luggage to be higher. The drag coefficient of the modified bus is low compared to the existing one and it enables the bus to move easily through the surrounding viscous air with the minimum of resistance.

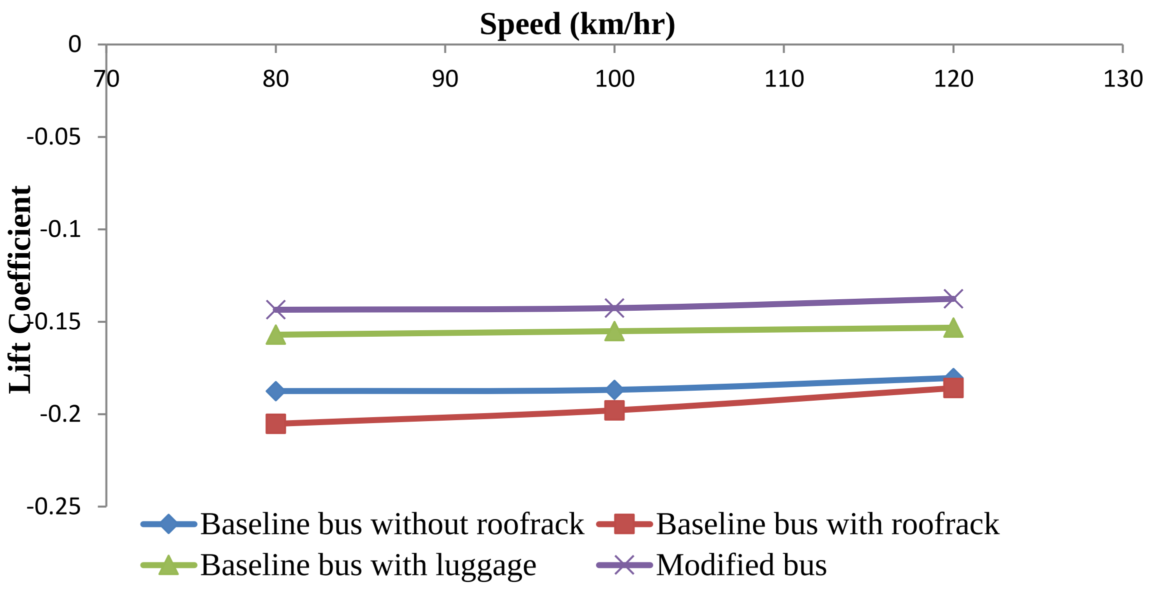

Figure 6.58: Lift coefficient comparison of all models at different speed

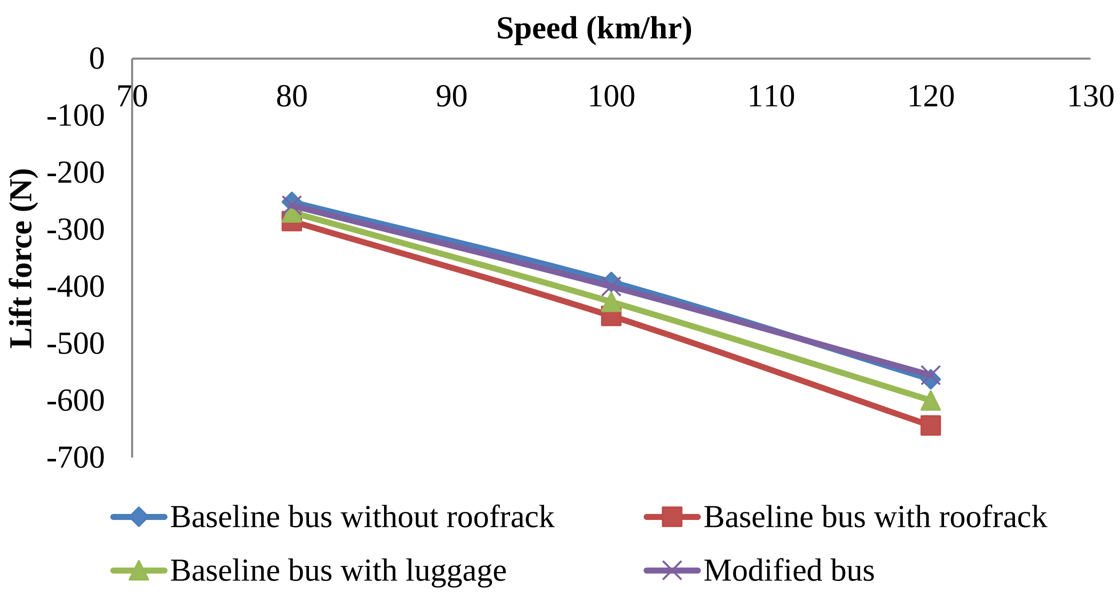

Figure 6.59: Lift force comparison of all models at different speed

The negative sign indicates the direction of the force which is down force. Therefore, as the magnitude of the down force increases the performance of the bus in terms of lift will become better. As it is seen from Figure 6.59 the lift coefficient of the existing bus and the modified bus is all negative and the down force increases with respect to the speed of the bus. Thus, it enhances the tire to road grip.

6.3 Percentage of Drag Reduction

The percentage of drag reduction and fuel consumption of the modified model is compared with each of the baseline model separately.

Table 6.7: Comparison of modified bus with baseline bus without roof rack

Model	Speed (km/hr)	Drag Coefficient (C_d)	Drag Force (N)	Percentage of C_d Reduction (%)	Percentage of Drag Force Reduction (%)
Baseline Bus Without Roof Rack	80	0.6237	835.55	-	-
	100	0.6197	1297.65	-	-
	120	0.6165	1858.29	-	-
Modified Bus	80	0.4142	743.44	33.33	11.78
	100	0.4126	1157.53	33.86	12.37
	120	0.4113	1660.87	34.02	12.47

Table 6.8: Comparison of modified bus with baseline bus with roof rack

Model	Speed (km/hr)	Drag Coefficient (C_d)	Drag Force (N)	Percentage of C_d Reduction (%)	Percentage of Drag Force Reduction (%)
Baseline Bus With Roof Rack	80	0.6242	866.42	-	-
	100	0.6208	1346.89	-	-
	120	0.6195	1934.78	-	-
Modified Bus	80	0.4142	743.44	33.65	14.22
	100	0.4126	1157.53	34.18	14.01
	120	0.4113	1660.87	34.44	14.25

Table 6.9: Comparison of modified bus with baseline bus with luggage

Model	Speed (km/hr)	Drag Coefficient (C_d)	Drag Force (N)	Percentage of C_d Reduction (%)	Percentage of Drag Force Reduction (%)
Baseline Bus With Luggage	80	0.6256	1087.82	-	-
	100	0.6222	1691.09	-	-
	120	0.6218	2432.74	-	-
Modified Bus	80	0.4142	743.44	33.86	31.66
	100	0.4126	1157.53	34.29	31.55
	120	0.4113	1660.87	34.44	31.74

When comparing the modified bus with the clean roof baseline bus, the drag coefficient and the drag force is improved by 34% and 12% respectively on average. Additionally, when comparing the modified bus with the baseline bus with roof rack it is reduced by 34.5% and 14%. In both cases, the reduction of the drag force is minimum compared to the drag coefficient. This is due to the fact that, the frontal area of the modified bus is larger than the clean roof baseline bus and the baseline bus with roof rack. However, even if the frontal area is large, the modified bus had a better aerodynamic performance.

According to Table 6.9, when comparing the modified bus with the baseline bus loaded with luggage the drag coefficient and the drag force is reduced by 34% and 32% respectively on average. The height of the loaded luggage and the compartment is similar but their width is different. Thus, the frontal area of the modified bus is slightly higher and this makes the drag force to be slightly lower than the drag force. In general, the modified bus improved the aerodynamic performance of the existing bus.

6.4 Fuel Consumption and Power Saving

6.4.1 Power Saved

Power saved on the streamlined bus model with respect to the original bus model is calculated using the equation given below (Kim, 2011).

$$\mathrm{P_{sav}} = (\mathrm{F_{D-Bas}} - \mathrm{F_{D-Mod}}) \times V_{bus} \qquad \mathrm{Equ}(6.1)$$

Where P_{sav} = Power saved (W)

$F_{D\text{-}Bas}$ = Drag force of the baseline bus (N)

$F_{D\text{-}Mod}$ = Drag force of the Modified bus (N)

V_{bus} = Speed of the bus (m/s

6.4.2 Fuel Saved

Fuel saved by the reduction of the drag force is calculated using the equation given below **(**Kim, 2011**).**

$$\dot{\mathrm{m}}_{\mathrm{fuel}} = \frac{\mathrm{P_{sav}}}{\mathrm{Q_{LHV}} \times \rho_{\mathrm{fuel}} \times \eta_{\mathrm{engine}}} \qquad \mathrm{Equ}(6.2)$$

Where $\dot{m}_{fuel}$ = Mass flow rate (m^3/s)

P_{sav} = Power saved (W)

Q_{LHV} = Lower heating value (lower heating value of diesel fuel is 42.5 MJ/kg)

ρ_{fuel} = Density of fuel at ambient temperature (860 kg/m^3)

η_{engine} = Thermal efficiency of the engine (thermal efficiency of the engine is 35%)

According equation 6.2, the unit of fuel consumption is m^3/s but in this paper it is given in L/hr. Therefore, the conversion is carried out using the relation given below.

$$1\ m^3/s = 3.6 \times 10^6\ L/hr$$

6.4.3 Result Summary of Power Saved and Fuel Consumption

Table 6.10: Power saved and fuel consumption of the modified bus with respect to the clean roof baseline bus

Model	Speed (m/s)	Drag Force (N)	Drag Force Reduction (N)	Power Saved (W)	Fuel Saved (L/hr)
Baseline Bus Without Roof Rack	22.22	835.55	-	-	-
	27.78	1297.65	-	-	-
	33.33	1858.29	-	-	-
Modified Bus	22.22	743.44	99.32	2206.89	0.62
	27.78	1157.53	163.43	4540.08	1.28
	33.33	1660.87	236.62	7886.54	2.23

Table 6.11: Power saved and fuel consumption of the modified bus with respect to the baseline bus with roof rack

Model	Speed (m/s)	Drag Force (N)	Drag Force Reduction (N)	Power Saved (W)	Fuel Saved (L/hr)
Baseline Bus With Roof Rack	22.22	866.42	-	-	-
	27.78	1346.89	-	-	-
	33.33	1934.78	-	-	-
Modified Bus	22.22	743.44	123.31	2739.95	0.77
	27.78	1157.53	188.64	5240.42	1.48
	33.33	1660.87	276.15	9204.08	2.6

Table 6.12: Power saved and fuel consumption of the modified bus with respect to the baseline bus with luggage

Model	Speed (m/s)	Drag Force (N)	Drag Force Reduction (N)	Power Saved (W)	Fuel Saved (L/hr)
Baseline bus with luggage	22.22	1087.82	-	-	-
	27.78	1691.09	-	-	-
	33.33	2432.74	-	-	-
Modified bus	22.22	743.44	344.52	7655.23	2.15
	27.78	1157.53	533.66	14825.07	4.17
	33.33	1660.87	772.31	25741.09	7.24

As it is mentioned in Table 6.10 – 6.12, the modified bus improved the power requirement and fuel consumption of the existing bus. According to Table 6.10, when comparing the modified bus with the clean roof baseline bus the power requirement at 80 km/hr, 100 km/hr and 120 km/hr is reduced by 2206.89W, 4540.08W and 7886.54W respectively. In addition to that, the fuel consumption is 0.62 L/hr, 1.28 L/hr and 2.23 L/hr respectively.

As it is seen from Table 6.11, the reduction of power requirement and fuel consumption of the modified bus with respect to the baseline bus with roof rack at 80 km/hr, 100 km/hr and 120 km/hr is 2739.95W, 5240.42W, 9204.08W and 0.77L/hr, 1.48 L/hr, 2.6 L/hr respectively.

Finally, when comparing the modified bus with the loaded baseline bus the power requirement at 80 km/hr, 100 km/hr and 120 km/hr is reduced by 7655.23W, 14825.07W and 25741W respectively. In addition to that, the fuel consumption is 2.15 L/hr, 4.17 L/hr and 7.24 L/hr respectively.

6.5 Experimental Results

In addition to the CFD analysis, the aerodynamic performance of the modified bus was examined on HM 170 Educational wind tunnel by using a small scale 3D printed model. The test was done at a wind speed of 5.6 m/s, 11.2 m/s, 16.8 m/s and 22.4 m/s. The drag force is detected and displayed digitally on the measurement amplifier. Table 6.13 shows the displayed drag force with respect to the wind speed.

Table 6.13: Drag force of the model at 0^0 yaw angle

Frontal Area of the Model (m^2)	**Wind Speed (m/s)**	**Drag Force (N)**
0.0067	5.6	0.06
	11.2	0.23
	16.8	0.51
	22.4	0.89

The drag coefficient can be determined from the drag force at the given speed by using equation 6.3. The room temperature and relative humidity while conducting the experiment were 25.4^0c and 60% respectively. The air density at this condition is 1.17 kg/m^3.

$$C_d = \frac{2F_{D-Mod}}{\rho A V^2} \qquad \text{Equ}(6.3)$$

Where A: Projected Area (m^2)

C_d: Drag Coefficient

F_{D-Mod}: Drag Force of the Modified Bus (N)

ρ: Density (Kg/m^3) and V: Speed (m/s)

Table 6.14: Drag coefficient of the numerical and experiment result

Speed (m/s)	Drag Coefficient (C_d)		Deviation (%)
	Numerical Result	Experimental Result	
5.6	0.449	0.487	8.64
11.2	0.434	0.468	7.83
16.8	0.429	0.461	7.45
22.4	0.425	0.452	6.35

As it is given in Table 6.14, the drag coefficient of the experimental result deviates from the numerical result by 8.64%, 7.83%, 7.45 and 6.35% at a speed of 5.6m/s, 11.2m/s, 16.8m/s and 22.4m/s respectively. This is due to irregularity of speed, vibration of model at higher speed while conducting the experiment. Additionally, the operating conditions like temperature and density is different in both cases. However, according to many researches the percentage of the deviation is normal.

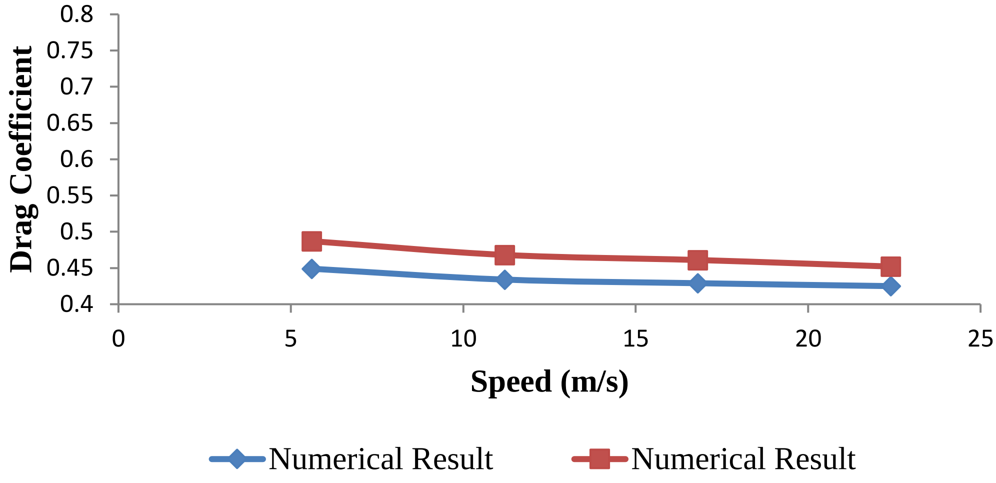

Figure 6.59: Comparison of Numerical and Experimental Result

The experimental result conforms that the modified bus improves the aerodynamic performance of the existing bus.

CHAPTER SEVEN

CONCLUSIONS AND RECOMMENDATIONS

7.1 Conclusions

From the CFD analysis, it was found that a large circulation region was formed in the top and at the back of the existing bus. Due to this a high pressure difference is created between the front and the rear of the existing bus, causing high drag. To improve the aerodynamic performance of the bus a wind deflector is fitted on the front top part of the bus which is one part of the luggage compartment. As a result, the modified bus minimizes the flow separation occurred on the top of the baseline bus and reduced the amount of swirling air at the back of the bus, hence reduced the amount of drag coefficient compared to baseline model. Additionally, the loaded luggage increased the drag by increasing the frontal area of the bus. Since there is no any mechanism to control the amount of luggage loaded on the bus, the drag force increases with respect to it. Therefore, the modified bus is prepared with an enclosed luggage compartment. The compartment is fitted over the entire length of the bus with a height of 0.7 m.

The main findings are:

- ✓ The modified bus improved the drag coefficient by 34%, 34.5% and 34%, when compared to the clean roof baseline bus, the baseline bus without roof rack and the loaded baseline bus respectively.
- ✓ The modified bus improved the drag force by 12%, 14% and 32%, when compared to the clean roof baseline bus, the baseline bus without roof rack and the loaded baseline bus respectively.
- ✓ When comparing the modified bus with the clean roof baseline bus the power requirement at 80 km/hr, 100 km/hr and 120 km/hr is reduced by 2206.89W, 4540.08W and 7886.54W respectively. In addition to that, the fuel consumption is 0.62 L/hr, 1.28 L/hr and 2.23 L/hr respectively.
- ✓ The reduction of power requirement and fuel consumption of the modified bus with respect to the baseline bus with roof rack at 80 km/hr, 100 km/hr and 120 km/hr is 2739.95W, 5240.42W, 9204.08W and 0.77 L/hr, 1.48 L/hr, 2.6 L/hr respectively.

- ✓ When comparing the modified bus with the loaded baseline bus the power requirement at 80 km/hr, 100 km/hr and 120 km/hr is reduced by 7655.23W, 14825.07W and 25741W respectively. In addition to that, the fuel consumption is 2.15 L/hr, 4.17 L/hr and 7.24 L/hr respectively.
- ✓ The experimental result showed that, the drag coefficient of the modified bus is 0.487, 0.468, 0.461 and 0.452 at a speed of 5.6m/s, 11.2m/s, 16.8m/s and 22.4m/s respectively. The drag coefficient of the experimental result deviates from the numerical result by 8.64%, 7.83%, 7.45 and 6.35% at a speed of 5.6m/s, 11.2m/s, 16.8m/s and 22.4m/s respectively. However, according to many researches the percentage of the deviation is normal.
- ✓ This work proves that possibility of refining the exterior of the existing bus for simultaneous improvement in aerodynamics and aesthetics (attractive design) from the point view of product design.

7.2 Recommendations

- ✓ Local bus body building companies have to check the aerodynamics performance of their bus body shape and have to give more emphasis on the aerodynamics of bus as there is a significant saving of fuel by reducing drag as demonstrated in this study.
- ✓ It is seen from the result that, the aerodynamic performance of the existing bus improved due to the addition of the luggage compartment. Therefore, bus body builders should use this luggage compartment instead of using roof racks.

7.3 Recommendations for Future Work

The following recommendations can be taken in to consideration as future work.

- ✓ Stability ensures safety and improves inherent characteristics that decrease the performance of the bus. Therefore, it is recommended to analyze the stability of the bus and take the right measures if it has to be improved.
- ✓ Other than aerodynamics, the weight of the existing bus affects its performance. Therefore it is recommended to analyze the material used to construct the bus and use novel materials which will provide a better performance.

Research Fund Acknowledgment

This research project is funded by Adama Science and Technology University under the grant number ASTU/SM-R/315/21, Adama, Ethiopia.

REFERENCES

Addis Ababa institute of technology (2012), "Final Report on Pilot Global Fuel Economy Initiative Study in Ethiopia", Federal Transport Authority

Australian Mill (2013), **"**Design Capacity Tables for Structural Steel Hollow Sections**",** August 2013, Queensland 4109 Australia, www.austubemills.com

A. Muthuvel, M. Murthi, N. Sachin, M. Koshy, S. Sakthi and E. Selvakumar (2013), "Aerodynamic Exterior Body Design of Bus", International Journal of Scientific & Engineering Research, Volume 4, Issue 7, ISSN 2229-5518

A. Chainani and N. Perera (2008), "CFD Investigation of Airflow on A Model Radio Control Race Car", WCE 2008, 2-4July, London

A. Kourta and P. Gilliéron (2009), "Impact of the Automotive Aerodynamic Control on the Economic Issues", Journal of Applied Fluid Mechanics, Vol.2 (2), pp69-75

A. Bhave and H. Taherian (2014), "Aerodynamics of Intercity Bus and Its Impact on Co_2 Reductions", 10.13140/2.1.1252.7046

B. Kaur, P. Kaur and A. Kuamr (2020), "Analysis of Deformation of RC Beam with addition of fly ash: a Finite element based modeling", International Research Journal of Engineering and Technology, Volume: 07, Issue: 05

B. Harinaldi, E. Warjito and S. Rustan (2012), "Modification of flow structure over a van model by suction flow control to reduce aerodynamics drag", Vol. 16(1), pp15-21

C. Kim (2011), "A Streamlined Design of a High Speed Coach for Fuel Savings and Reduction of Carbon Dioxide", International Journal of Automotive Engineering, Technical Paper 20114633

C. Choi and D. Kwon (1998), "Wind Tunnel Blockage Effects on Aerodynamic Behavior of Bluff Body", Vol. 1, No. 4, pp: 351-364

D. Yadav, S. Chauhan, S. karki, S. Nayak, N. kumar and S. Sudhakar Babu (2017), "CFD Analysis for Drag Force Reduction in Inter-City Buses", International Research Journal of Engineering and Technology, Volume: 04, Issue: 05

F. Szodrai (2020), "Quantitative Analysis of Drag Reduction Methods for Blunt Shaped Automobiles", Applied Sciences, 10(12), p.4313

F. Alam, H. Chowdhury, H. Moria and S. Watkins (2010), "Effects of Vehicle Add-Ons on Aerodynamic Performance", Proceedings of the 13th Asian Congress of Fluid Mechanics, Dhaka, Bangladesh

G.U.N.T. Gerätebau (2012), "HM 170 Educational Wind Tunnel", D-22881 Barsbüttel Germany, Publication no.: 917.000 00A 170 12

G. Sovran and M. Bohn (1981), "Formulae for the Tractive-Energy Requirements of Vehicles Driving the EPA Schedules", SAE Paper 810184, Warrendale, PA: Soc. Automotive Eng.

G. Sovran (1983), "Tractive-Energy-Based Formulae for the Impact of Aerodynamics on Fuel Economy", SAE Technical Paper 830304.Warrendale, PA: Soc. Automotive. Eng.

H. Chowdhury, F. Alam, I. Khan, V. Djamovski and S. Watkins (2012), "Impact Of Vehicle Add-Ons on Energy Consumption and Greenhouse Gas Emissions", Procedia Eng. 49, 294–302

J. Roy, T. Kumar, R. Ashish, S. Jeeva and V. Vinoth (2018), "Aerodynamic Design Improvement for an Intercity Bus", International Research Journal of Automotive Technology; 1(4); 85-90

J. Thomas, S. Huff and B. West (2014), "Fuel Economy and Emissions Effects of Low Tire Pressure, Open Windows, Roof Top And Hitch-Mounted Cargo and Trailer", SAE International journal, pp: 862–872

J. Patten, B. McAuliffe, W. Mayda and B. Tanguay (2012), "Review of Aerodynamic Drag Reduction Devices for Heavy Trucks and Buses", Technical Report National, Research Council of Canada Centre for Surface Transportation Technology

K. Weinman, M. Fragner, R. Deiterding, D. Heine, U. Fey, F. Braenstroem, B. Schultz and C.Wagner (2018), "Assessment Of The Mesh Refinement Influence On The Computed Flow-Fields About A Model Train In Comparison With Wind Tunnel Measurements", Journal of Wind Engineering and Industrial Aerodynamics, vol.179, 2018, 102-117

M. Lanfrit (2005), “Best practice guidelines for handling Automotive External Aerodynamics with FLUENT”, Fluent Deutschland

M. Lenner (1998), “Influence of Roof-Rack, Trailer etc. on Automobile Fuel Consumption and Exhaust Emissions, Measured On-The-Road”, SAE Technical paper, doi.org/10.4271/980682

M. Juhala (2014), “Improving Vehicle Rolling Resistance and Aerodynamics”, Alternative Fuels and Advanced Vehicle Technology for Improved Environmental Performance, Wood head publishing, pp.462–475

M. Ali, S. Khan, N. Mohan and P. Mandape (2014), “Aerodynamics”, IOSR Journal of Mechanical and Civil Engineering, e-ISSN: 2278-1684, p-ISSN: 2320-334X

M. Mukut and A. Mohammad (2019), “Review on Aerodynamic Drag Reduction of Vehicles”, International Journal of Engineering Materials and Manufacture, 4.10.26776/ijemm.04.01.2019.01

N. Sudin , A. Abdullah , A. Shamsuddin, R. Ramli and M. Tahir (2014), “Review of Research on Vehicles Aerodynamic Drag Reduction Methods”, International Journal of Mechanical & Mechatronics Engineering , Vol:14, No:02

Omnexus (2021), “A Detailed Guide on Acrylonitrile Butadiene Styrene”, 9 June 2021, https://omnexus.specialchem.com/selection-guide/acrylonitrile-butadiene-styrene-abs-plastic

P. Krishnani (2009), “CFD Study of Drag Reduction of a Generic Sport Utility Vehicle”, Master’s Thesis, Mechanical Engineering Department, California State University

R. Zakem (2008), “Aerodynamics of aftermarket rear spoiler”, Bachelor Thesis, University of Malaysia Pahang

L. Mott (2004), “Machine Elements in Mechanical Design”, University of Dayton, 4th ed., ISBN 0-13-061885-3

R. Wood (2004), “Impact of Advanced Aerodynamic Technology on Transportation Energy Consumption”, SAE Technical Paper, 2004-01-1306

S. Thorat, G. Amba and P. Rao (2011), “Computational Analysis of Intercity Bus with Improved Aesthetics and Aerodynamic Performance on Indian Roads”, International Journal of Advanced Engineering Technology, ISSN 0976-3945

T. Heinemann, M. Springer, H. Lienhart, S. Kniesburges and S. Becker (2012), “Active flow control on a 1: 4 car model”, In 16th International Symposium on Applications of Laser Techniques to Fluid Mechanics Lisbon, Portugal, 09-12 July.

T. Unni (2017), "Numerical Investigation on Aerodynamic Effects of Vanes and Flaps on Automotive Under body Diffusers", SAE Technical Paper 2017-01-2163, 2017, https://doi.org/10.4271/2017-01-2163

The Reynolds and Reynolds Company (2014), “Add On Auto: Auto Accessories Sales”, Mid-Year Trend Report. October, 2014.

W. Mayer and G. Wickern (2011), “The New Audi A6/A7 Family - Aerodynamic Development of Different Body Types on One Platform”, SAE International Journal of Passenger Cars-Mechanical Systems, Vol. 4(1), pp 197-206

W. Hucho and G. Sovran (1993), “Aerodynamics of Road Vehicles”, Annual Review of Fluid Mechanics, 25(1), 485-537, DOI: 10.1146/annurev.fl.25.010193.002413

W. Hucho (1998), “Aerodynamics of Road Vehicles”, Fluid Mechanics to Vehicle Engineering, February 4th ed. Society of Automotive Engineers

X. Hu and T. Wong (2011), “A numerical study on rear-spoiler of passenger vehicle”, World Academy of Science, Engineering and technology, Vol. 57, pp636-641

Y. Chen and A. Meier (2016), "Fuel Consumption Impacts of Auto Roof Racks", Energy Policy, 92: 325–333, doi:10.1016/j.enpol.2016.02.031

Y. Damissie and N. Ramesh (2017), “Aerodynamic Drag Reduction on Locally Built Bus Body using Computational Fluid Dynamics (CFD): A Case Study at Bishoftu Automotive Industry”, International Journal of Engineering Research & Technology, ISSN: 2278-0181, Vol. 6 Issue 11

Zaib Ali, Paul G Tucker and Shahrokh Shahpar (2017), “Optimal Mesh Topology Generation for CFD”, Computer Methods in Applied Mechanics and Engineering, vol. 317, 2017, 431-457

APPENDIX

Appendix A: ANSYS Results

Figure A-1: Modified bus with open compartment door

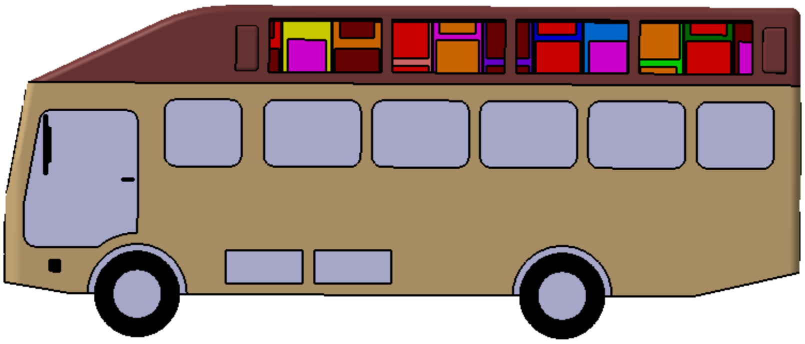

Figure A-2: Modified bus loaded with luggage

Figure A-3: Modified bus from right side

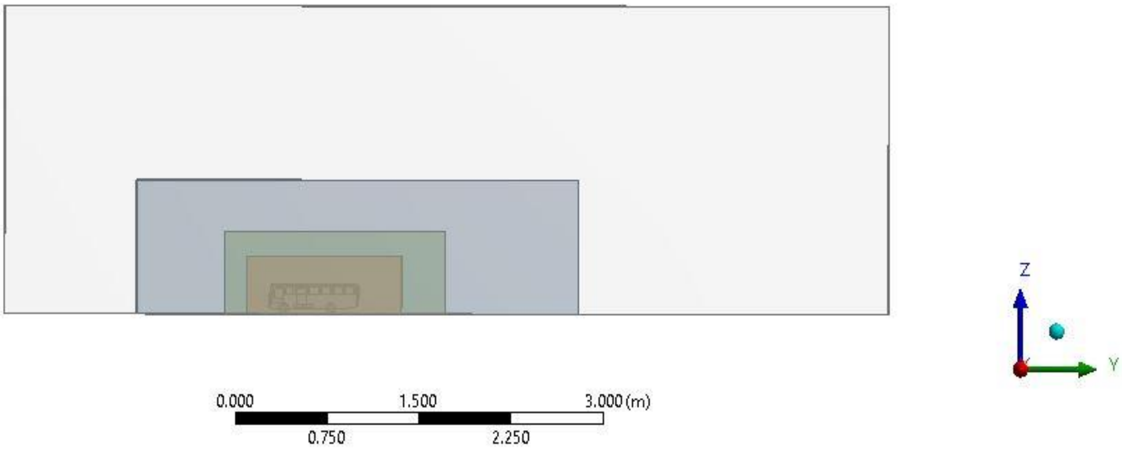

Figure A-4: Geometry of the bus without roof rack inside an enclosure and inner box

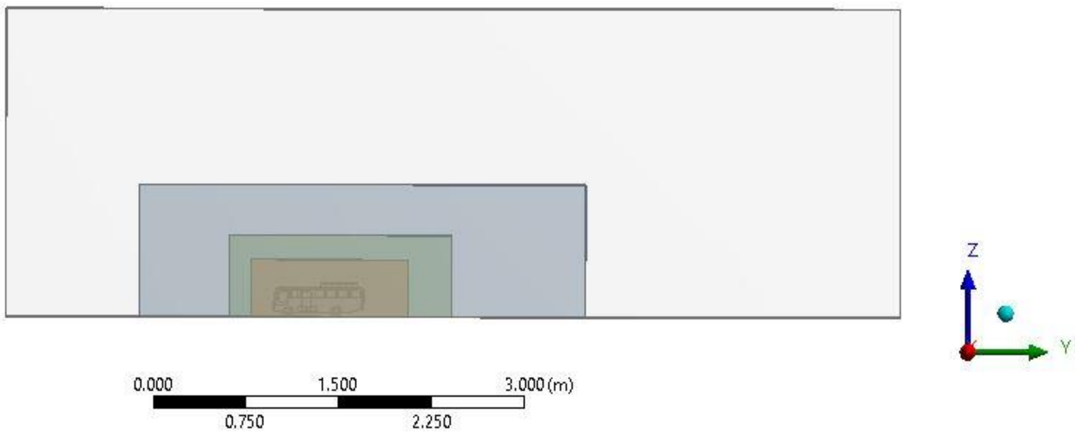

Figure A-5: Geometry of the bus with roof rack inside an enclosure and inner box

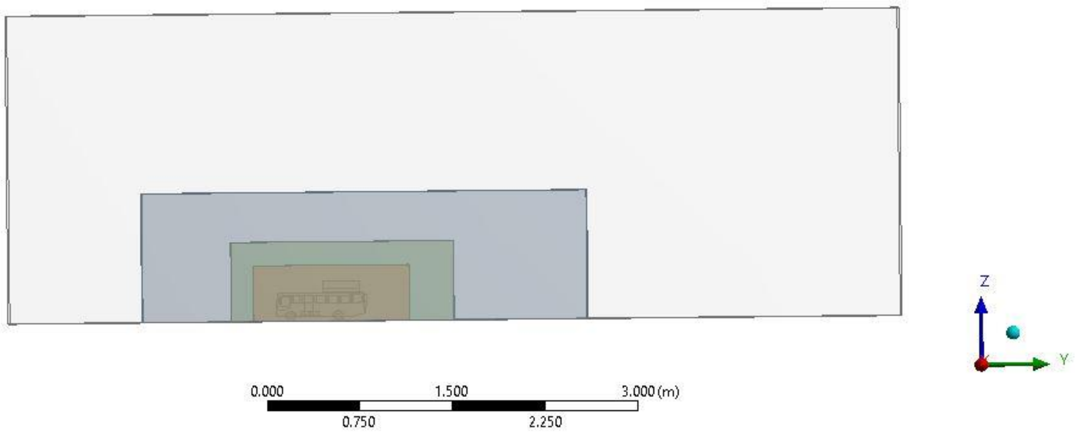

Figure A-6: Geometry of the bus with luggage inside an enclosure and inner box

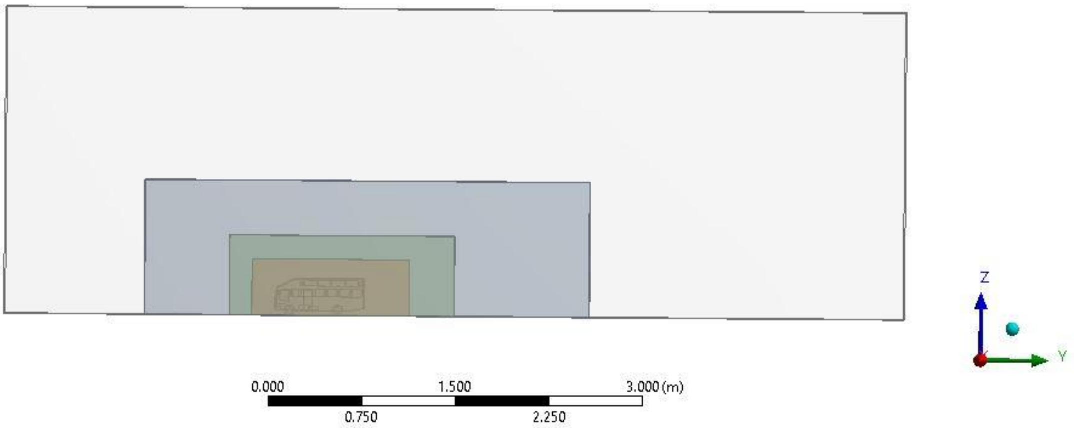

Figure A-7: Geometry of the modified bus inside an enclosure and inner box

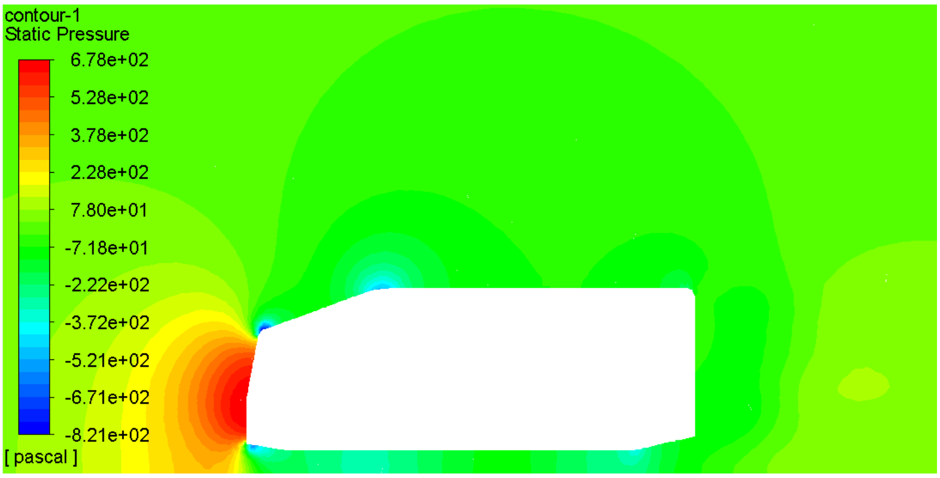

Figure A-8: Pressure Contour of the modified bus at deflector angle of 20^0

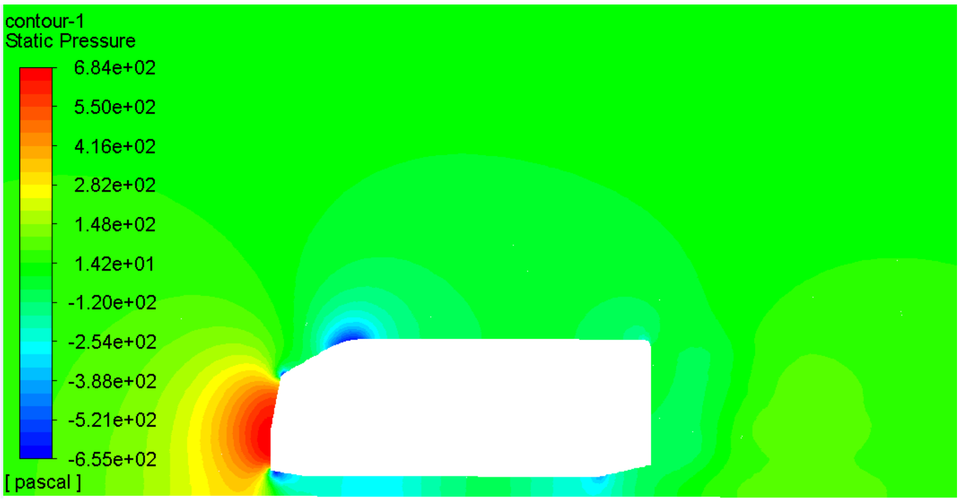

Figure A-9: Pressure Contour of the modified bus at deflector angle of 30^0

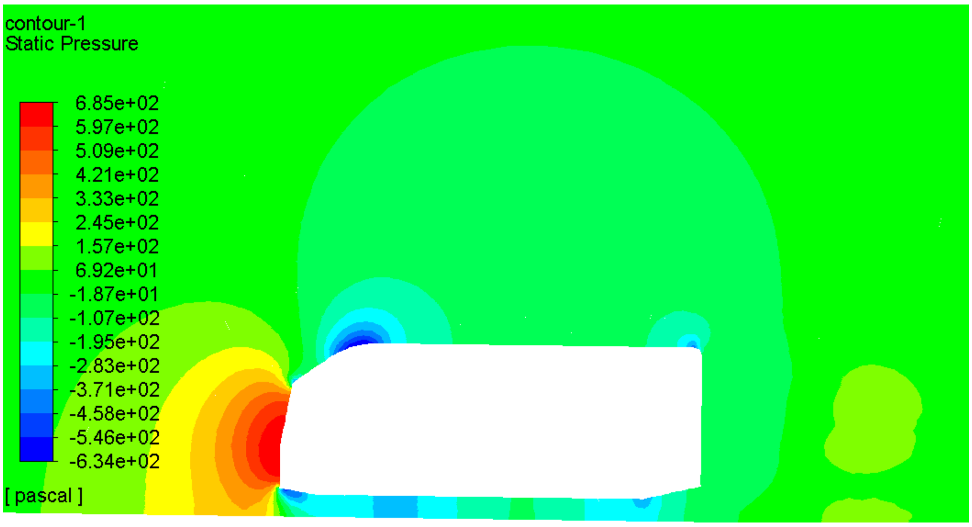

Figure A-10: Pressure Contour of the modified bus at deflector angle of 35^0

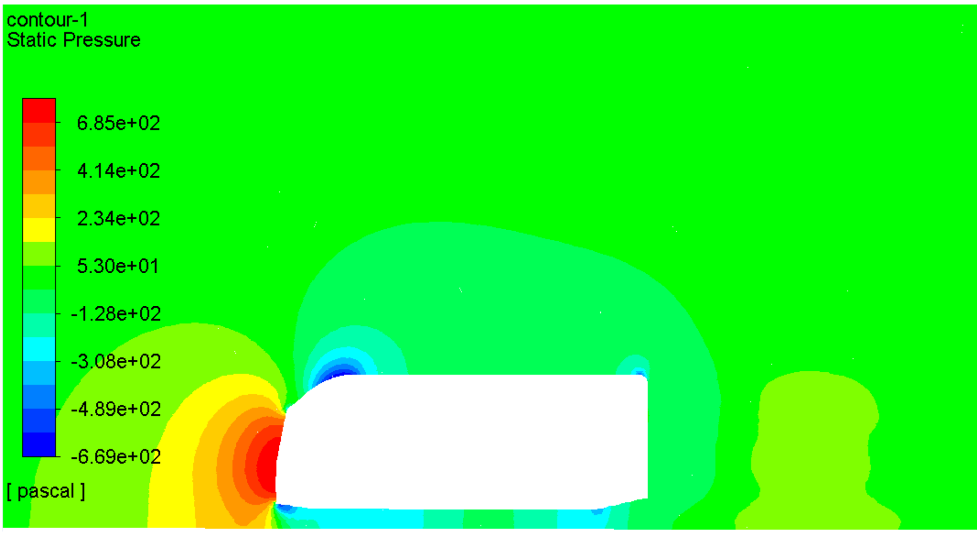

Figure A-11: Pressure Contour of the modified bus at deflector angle of 40^0

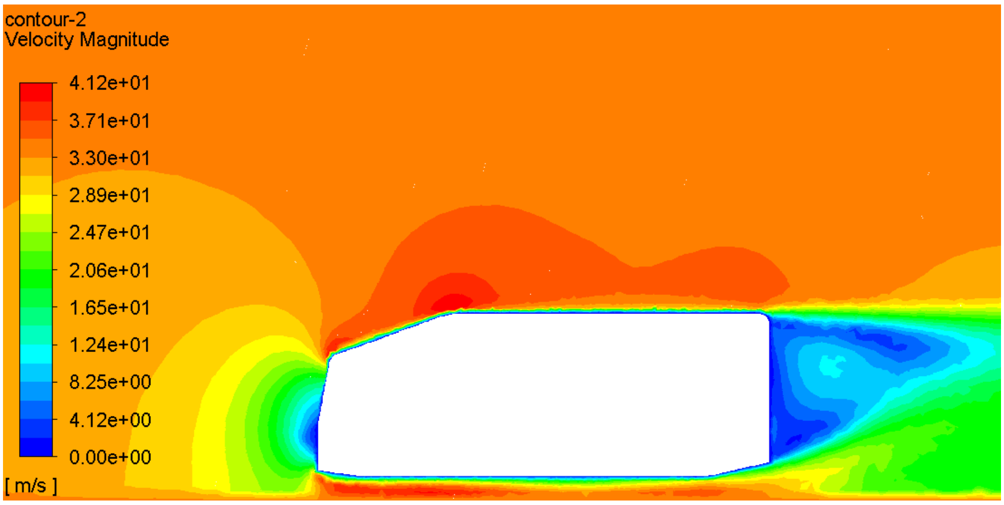

Figure A-12: Velocity Contour of the modified bus at deflector angle of 20^0

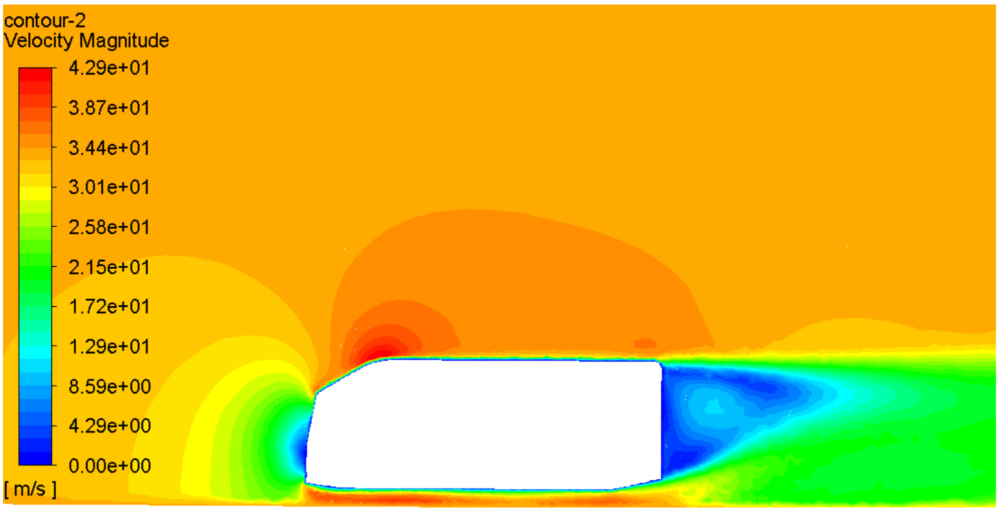

Figure A-13: Velocity Contour of the modified bus at deflector angle of 30^0

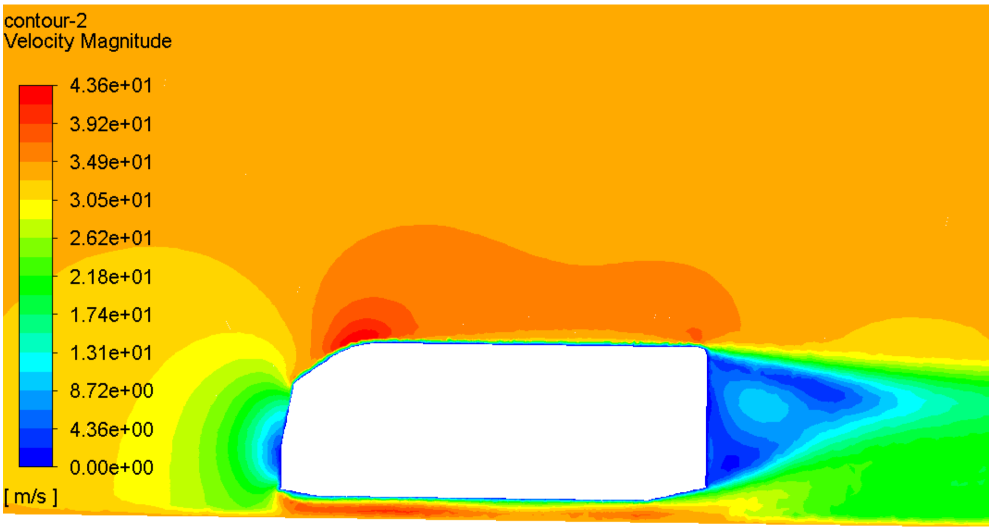

Figure A-14: Velocity Contour of the modified bus at deflector angle of 35^0

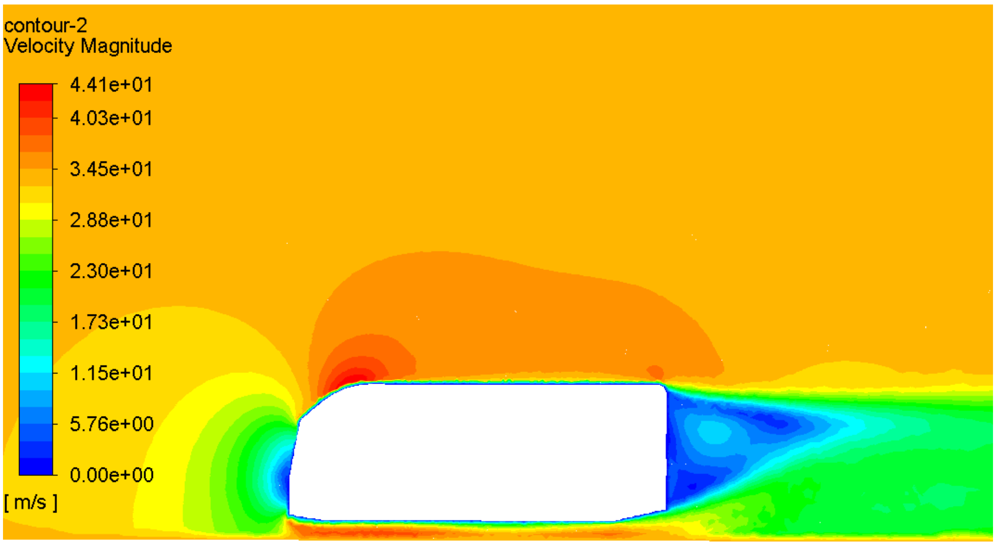

Figure A-15: Velocity Contour of the modified bus at deflector angle of 40^0

Appendix B: Property of Materials

Table B-1: Properties of structural steels (Mott, 2004)

Material designation (ASTM number)	Grade, product, or thickness	Tensile strength (ksi)	Tensile strength (MPa)	Yield strength (ksi)	Yield strength (MPa)	Ductility (percent elongation in 2 inches)
A36	$t \le 8$ in	58	400	36	250	21
A242	$t \le 3/4$ in	70	480	50	345	21
A242	$t \le 1\frac{1}{2}$ in	67	460	46	315	21
A242	$t \le 4$ in	63	435	42	290	21
A500	Cold-formed structural tubing, round or shaped					
	Round, Grade A	45	310	33	228	25
	Round, Grade B	58	400	42	290	23
	Round, Grade C	62	427	46	317	21
	Shaped, Grade A	45	310	39	269	25
	Shaped, Grade B	58	400	46	317	23
	Shaped, Grade C	62	427	50	345	21
A501	Hot-formed structural tubing, round or shaped	58	400	36	250	23
A514	Quenched and tempered, $t \le 2\frac{1}{2}$ in	110–130	760–895	100	690	18%
A572	42, $t \le 6$ in	60	415	42	290	24
A572	50, $t \le 4$ in	65	450	50	345	21
A572	60, $t \le 1\frac{1}{4}$ in	75	520	60	415	18
A572	65, $t \le 1\frac{1}{4}$ in	80	550	65	450	17
A588	$t \le 4$ in	70	485	50	345	21
A992	W-shapes	65	450	50	345	21

Table B-2: Properties of ABS (Acrylonitrile Butadiene Styrene)

ABS Material Data Sheet

Physical Properties	**Metric**	**English**	**Comments**
Density	1.04 g/cc	0.0376 lb/in³	Grade Count = 3
Melt Flow	18 - 23 g/10 min	18 - 23 g/10 min	Average = 21.3 g/10 min; Grade Count = 3
Mechanical Properties			
Hardness, Rockwell R	103 - 112	103 - 112	Average = 110; Grade Count = 3
Tensile Strength, Yield	42.5 - 44.8 MPa	6160 - 6500 psi	Average = 44 MPa; Grade Count = 3
Elongation at Break	23 - 25 %	23 - 25 %	Average = 24.3%; Grade Count = 3
Flexural Modulus	2.25 - 2.28 GPa	326 - 331 ksi	Average = 2.3 GPa; Grade Count = 3
Flexural Yield Strength	60.6 - 73.1 MPa	8790 - 10600 psi	Average = 68.9 MPa; Grade Count = 3
Izod Impact, Notched	2.46 - 2.94 J/cm	4.61 - 5.51 ft-lb/in	Average = 2.8 J/cm; Grade Count = 3

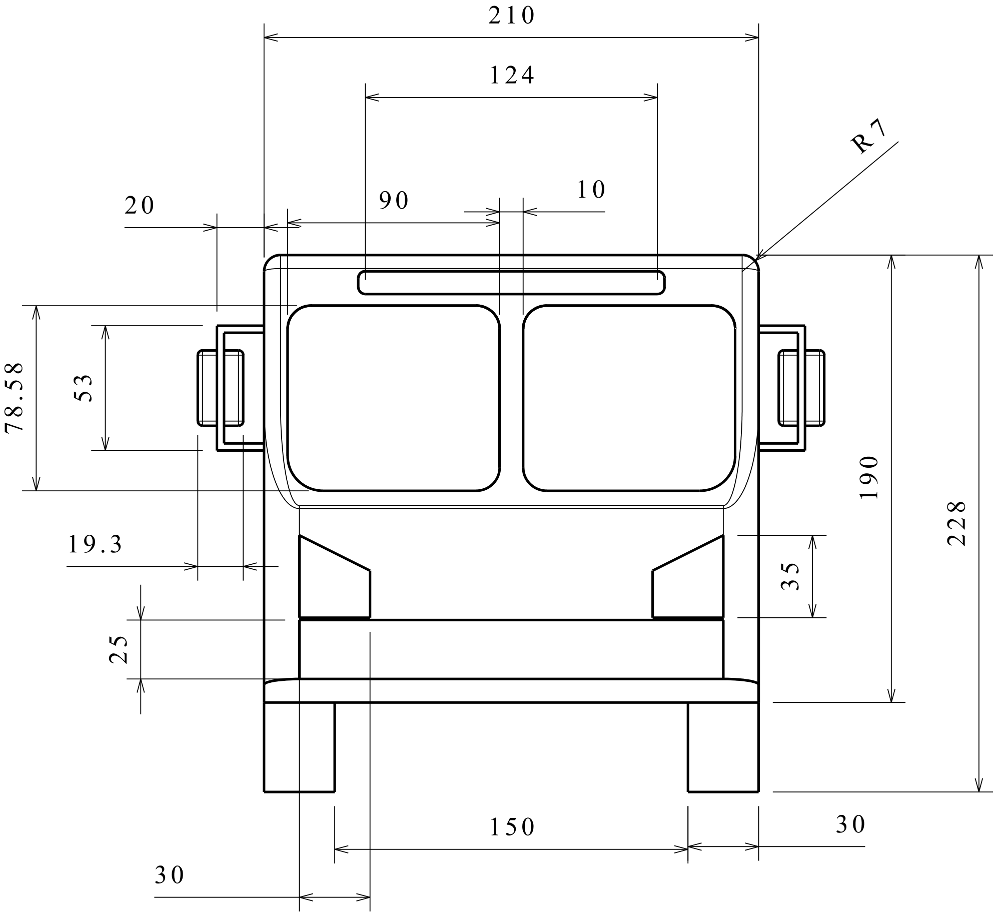

All Dimensions are given in **mm**.

Front View of the existing bus without roofrack

ASTU

Drawn By

Addis Tefera

Front View

Advisor

Dr. Addisu Bekele (Associate Professor)

Co-Advisor

Mr. Mekonnen Liben (Assistant Professor)

Size	Drawing Number
A4	1

Scale	1:10	Sheet	1/11

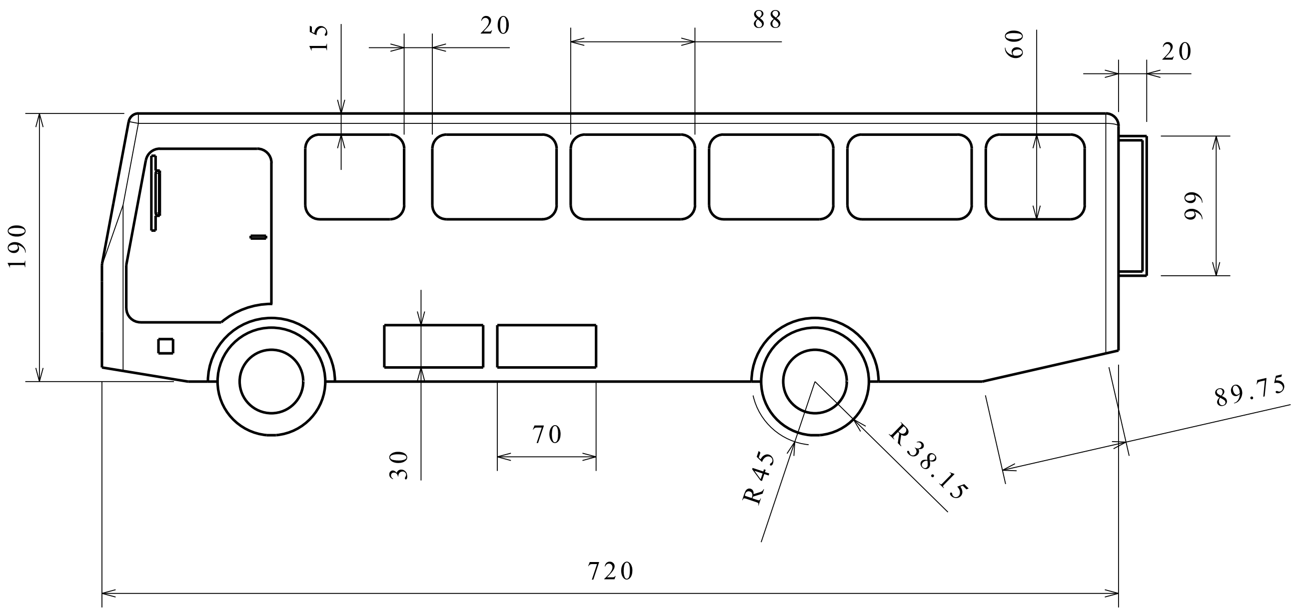

All Dimensions aer in **mm**.

Right Side View of the existing bus without roofrack	ASTU		
Drawn By Addis Tefera	Right Side View		
Advisor Dr. Addisu Bekele (Associate Professor)	Size A4	Drawing Number 2	
Co-Advisor Mr. Mekonnen Liben (Assistant Professor)	Scale 1:10	Sheet	2/11

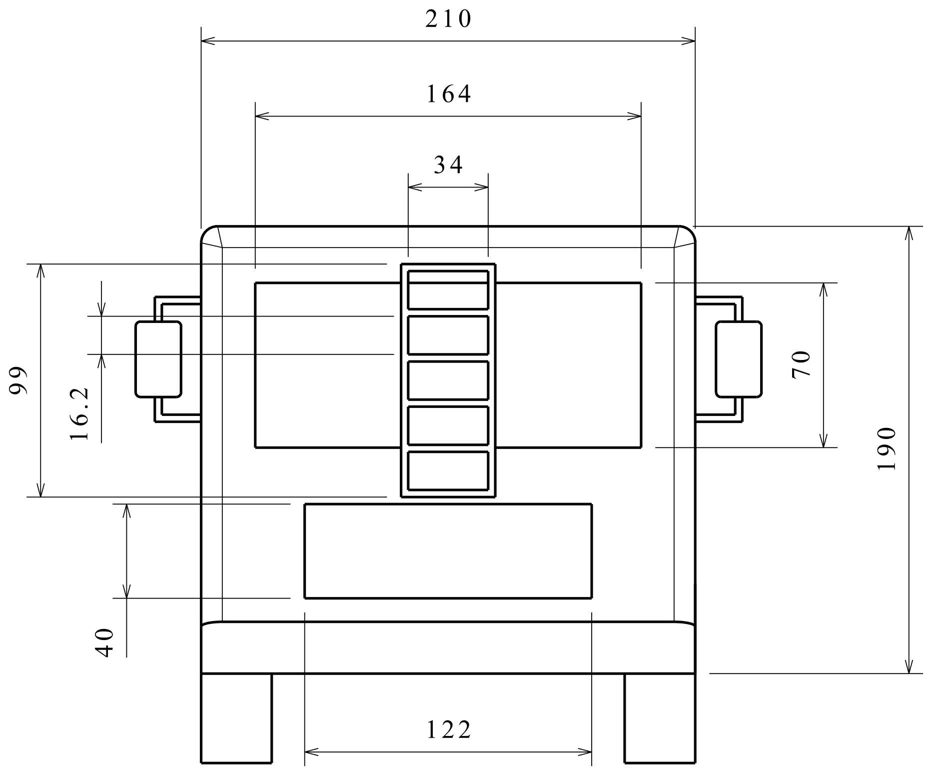

All Dimensions are in **mm**.

Rear View of the existing bus without roofrack	**ASTU**		
Drawn By Addis Tefera	Rear View		
Advisor Dr. Addisu Bekele (Associate Professor)	Size A4	Drawing Number 3	
Co-Advisor Mr. Mekonnen Liben (Assistant Professor)	Scale 1:10	Sheet 3/11	

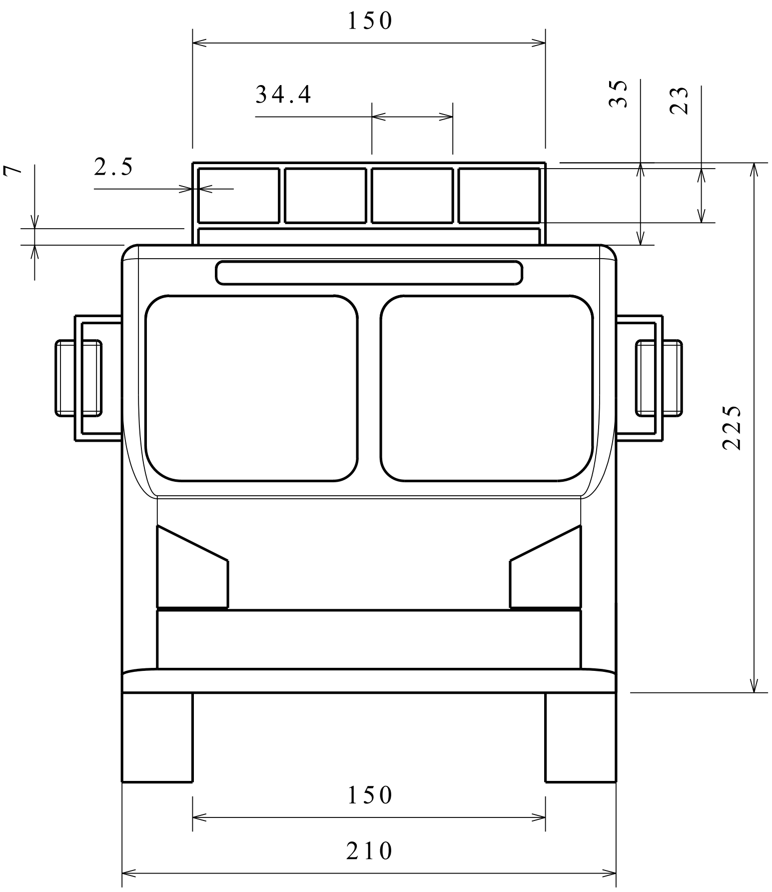

All Dimensions are given in **mm**.

Front View of the existing bus with roofrack	**ASTU**		
Drawn By Addis Tefera	Front View		
Advisor Dr. Addisu Bekele (Associate Professor)	Size A4	Drawing Number 4	
Co-Advisor Mr. Mekonnen Liben (Assistant Professor)	Scale 1:10		Sheet 4/11

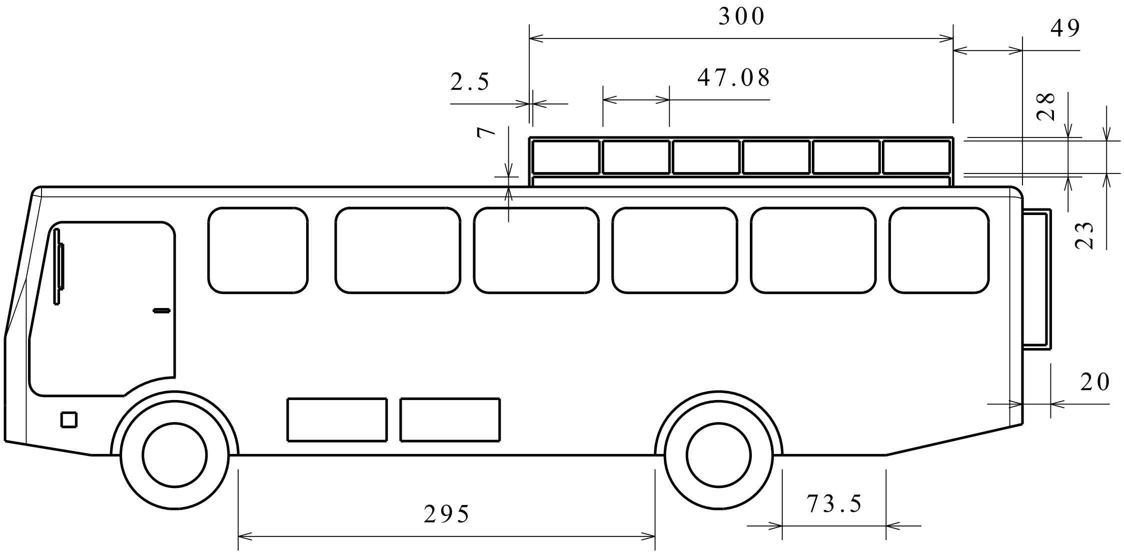

All Dimensions are given in **mm**.

Right Side View of the existing bus with roofrack	**ASTU**			
Drawn By Addis Tefera	Right Side View			
Advisor Dr. Addisu Bekele (Associate Professor)	Size A4	Drawing Number 5		
Co-Advisor Mr. Mekonnen Liben (Assistant Professor)	Scale	1:10	Sheet	5/11

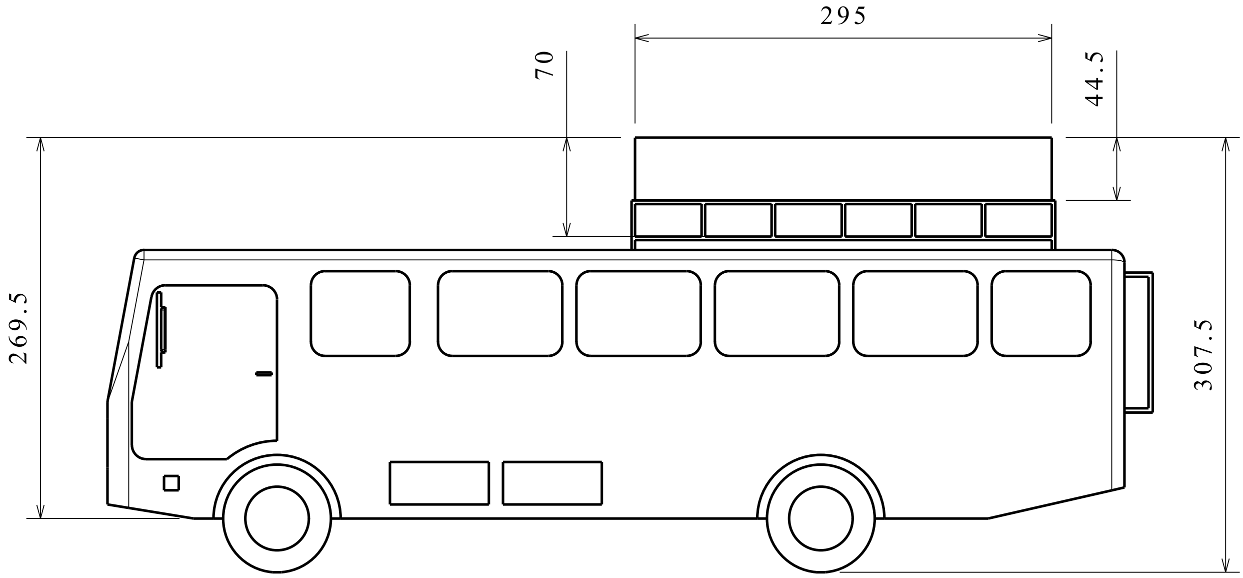

All Dimensions are given in **mm**.

Right Side View of the existing bus with Luggage	ASTU		
Drawn By Addis Tefera	Right Side View		
Advisor Dr. Addisu Bekele (Associate Professor)	Size A4	Drawing Number 6	
Co-Advisor Mr. Mekonnen Liben (Assistant Professor)	Scale 1:10	Sheet 6/11	

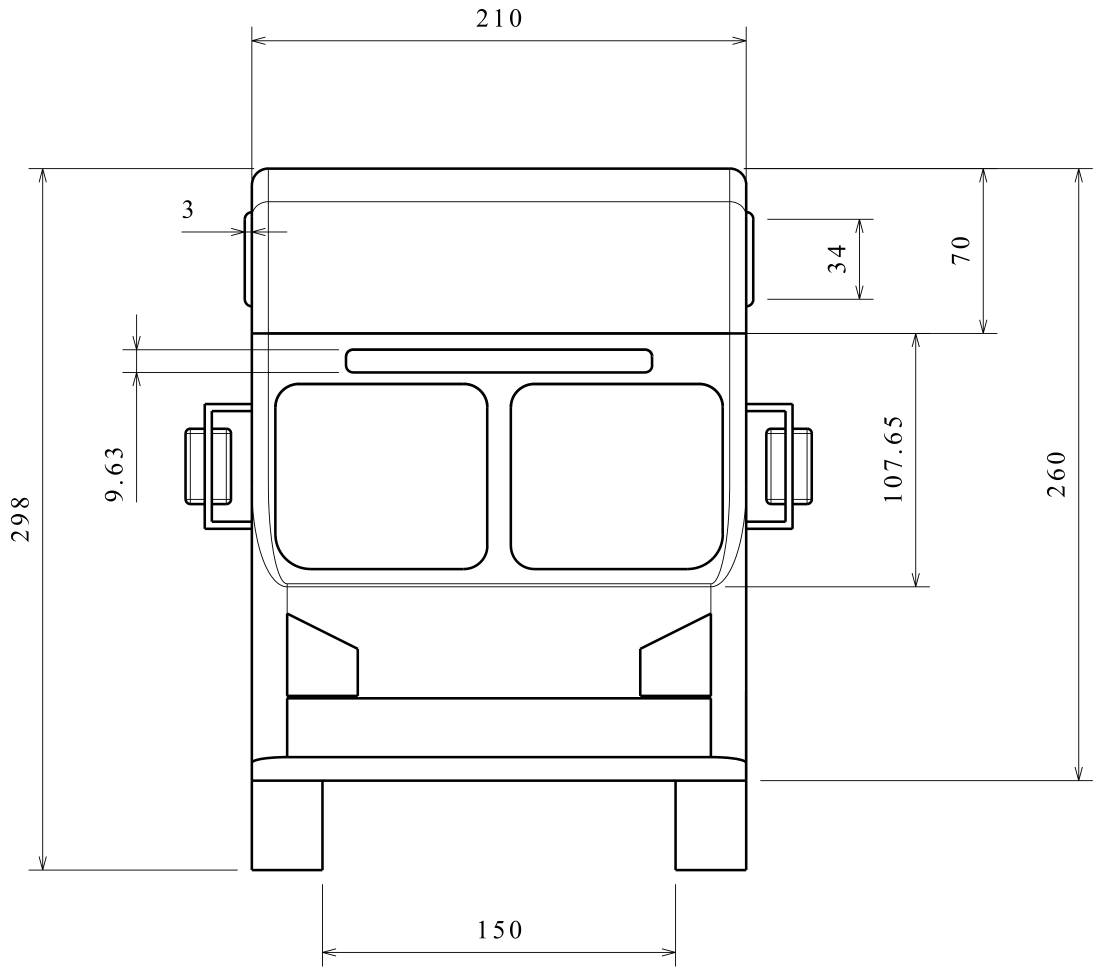

All Dimensions are given in **mm**.

Front View of the Modified bus	ASTU			
Drawn By Addis Tefera	Front View			
Advisor Dr. Addisu Bekele (Associate Professor)	Size A4	Drawing Number 7		
Co-Advisor Mr. Mekonnen Liben (Assistant Professor)	Scale	1:10	Sheet	7/11

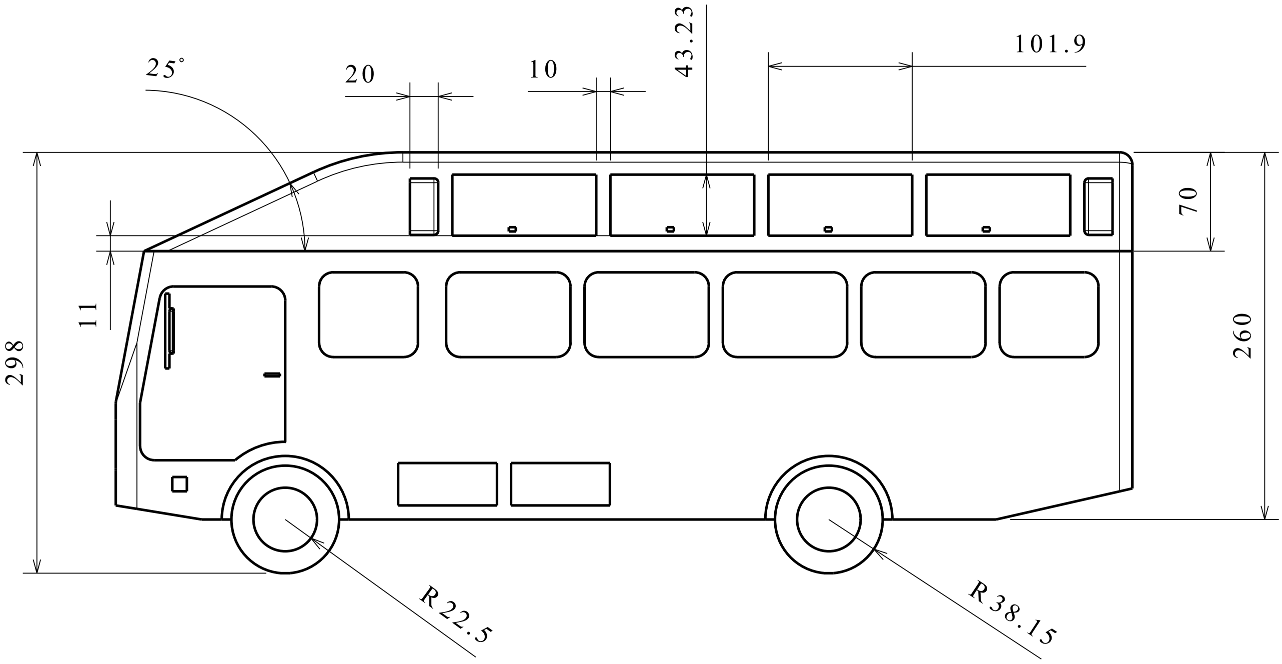

All Dimensions are given in **mm**.

Right Side View of the Modified bus	**ASTU**			
Drawn By Addis Tefera	Right Side View			
Advisor Dr. Addisu Bekele (Associate Professor)	Size A4	Drawing Number 8		
Co-Advisor Mr. Mekonnen Liben (Assistant Professor)	Scale	1:10	Sheet	8/11

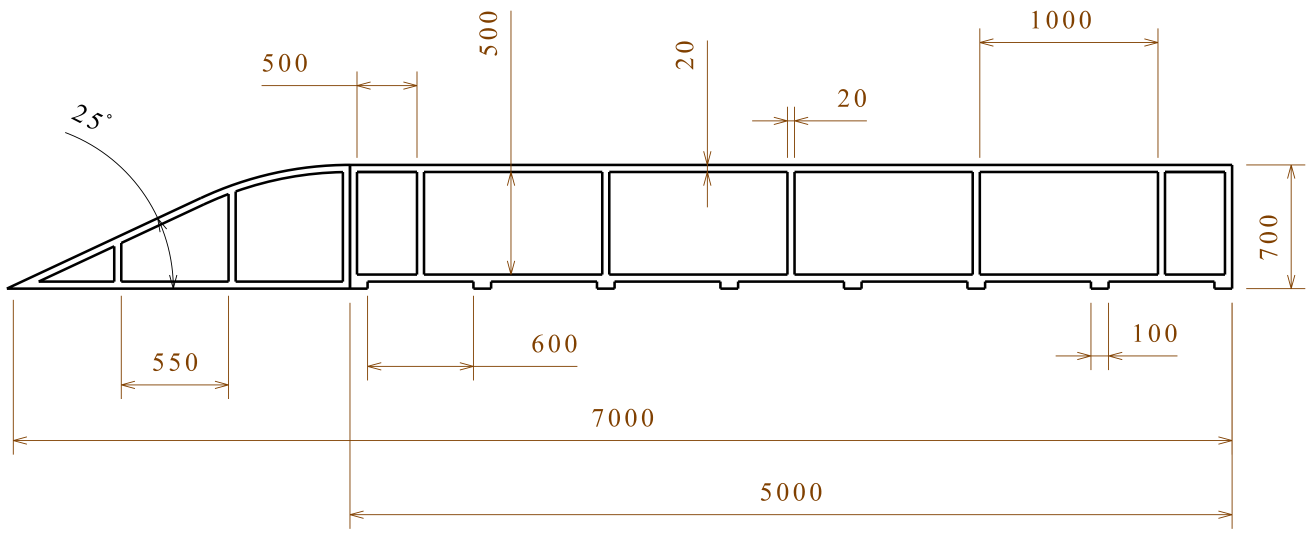

All Dimensions are given in **mm**.

Side View of the luggage compartment structure (it is constructed from 20 mm × 20 mm × 2 mm RHS Steel)	**ASTU**		
Drawn By Addis Tefera	Side View		
Advisor Dr. Addisu Bekele (Associate Professor)	Size A4	Drawing Number 9	
Co-Advisor Mr. Mekonnen Liben (Assistant Professor)	Scale 1:1	Sheet 9/11	

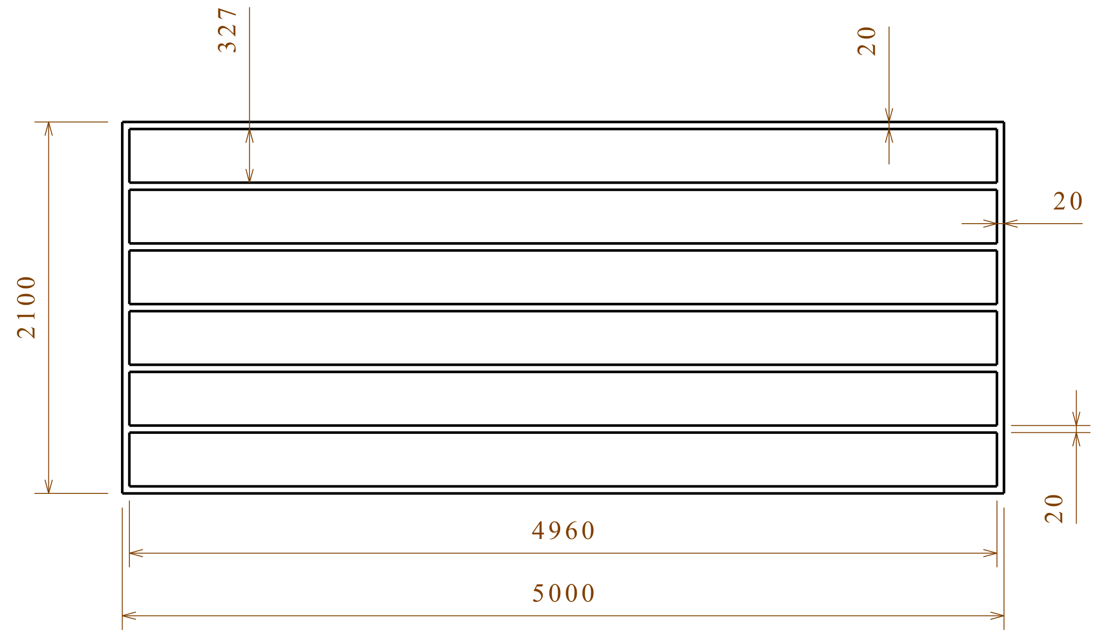

All Dimensions are given in **mm**.

Floor of the Luggage Carrier (it is constructed from 20 mm × 20 mm ×2 mm RHS Steel)	**ASTU**		
Drawn By Addis Tefera	Luggage Compartment Floor		
Advisor Dr. Addisu Bekele (Associate Professor)	Size A4	Drawing Number 10	
Co-Advisor Mr. Mekonnen Liben (Assistant Professor)	Scale 1:1	Sheet 10/11	

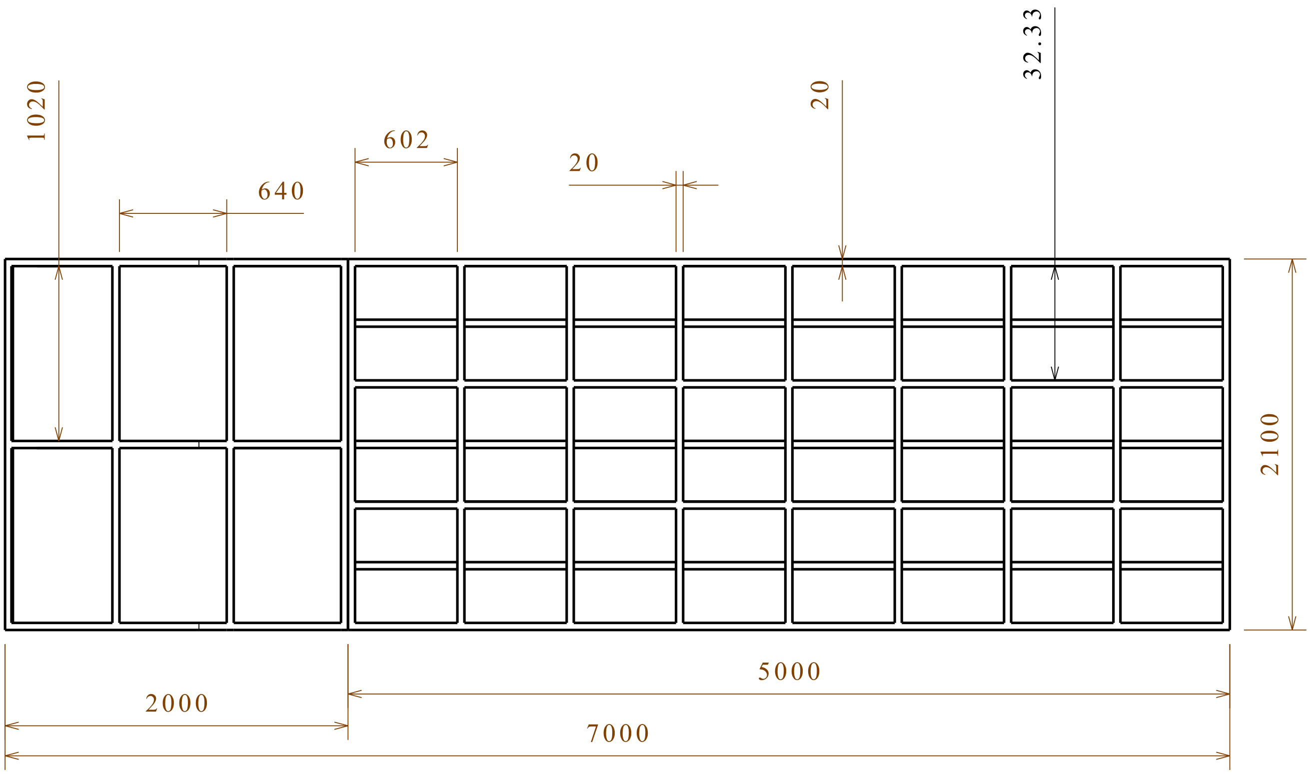

All Dimensions are given in **mm**.

Top View of the luggage compartment structure (it is constructed from 20 mm × 20 mm × 2 mm RHS Steel)	**ASTU**		
Drawn By Addis Tefera	Top View		
Advisor Dr. Addisu Bekele (Associate Professor)	Size A4	Drawing Number 11	
Co-Advisor Mr. Mekonnen Liben (Assistant Professor)	Scale 1:1	Sheet 11/11	